MICROMACHINED STIMULATING ELECTRODES

Final Report

Contract NIH-NINDS-N01-NS-2-2379

September 1992 --- September 1995

Submitted to the

Neural Prosthesis Program
National Institute of Neurological Disorders and Stroke
National Institutes of Health
Bethesda, MD 20892

by the

Center for Integrated Sensors and Circuits

October 1995

MICROMACHINED STIMULATING ELECTRODES

Final Report

Contract NIH-NINDS-N01-NS-2-2379

September 1992 --- September 1995

Submitted to the

Neural Prosthesis Program
National Institute of Neurological Disorders and Stroke
National Institutes of Health
Bethesda, MD 20892

by the

Center for Integrated Sensors and Circuits
Department of Electrical Engineering and Computer Science
University of Michigan
Ann Arbor, Michigan
48109-2122

October 1995

MICROMACHINED STIMULATING ELECTRODES

Summary

The goal of the contract reported here was to develop stimulating electrode arrays capable of delivering precisely controlled stimulation at multiple points in the central nervous system. Building on a technology base established during a previous contract, the results obtained during the past three year period have moved us significantly closer to that goal. The basic probe technology has been improved in a number of important ways. Continuing problems with the adhesion of iridium oxide sites to their underlying conductors were solved by modifying the site structure and introducing improved cleaning procedures for removing fluorocarbon residues left as the result of dry etching processes. The new site structures also allow the site to overlap adjacent conductors, decoupling the shank width from the size of the site. The use of a shallow boron diffusion was introduced to allow the formation of sharper tips on the probes than can be obtained using a deep diffusion; this process requires no additional process steps when used on chronic probes since the same diffusion is employed for ribbon cables. Preliminary work on the development of a low-resistance interconnect structure has shown that titanium silicide can be used to reduce lead resistances by a factor of from five to ten below those provided by polysilicon conductors. Such leads remain viable at temperatures up to 820°C, making them compatible for use with low-temperature oxide (LTO), PECVD silicon nitride, and LPCVD silicon nitride encapsulating dielectrics. During the past contract period, we have continued to develop both acute and chronic stimulating and recording probes for other investigators in the Neural Prosthesis Program. More than 1500 fully-tested probes of over 100 different designs have now been provided to investigators nationwide.

Work to characterize the probes in-vivo is underway both in-house and in the laboratories of our collaborating investigators. The feedback obtained is essential in continuing the optimization process and in understanding the limitations of the technology. During the past contract we have established automated facilities for iridium activation using cyclic voltammetry and for making in-vitro impedance measurements. In addition, we have established facilities for doing in-vivo measurements of site impedance and charge capacity for probes implanted chronically. Measurements on probes implanted for two weeks and then stimulated for four hours per day over five days with charge-balanced bipolar 50μA 100μsec/phase current pulses have shown the back voltages and site impedances for 1600μm^2 sites to be stable over time. The charge capacity measured for 400μm^2 sites gradually declined in-vivo, and this decline is not yet understood. No significant changes in current flow paths along probe shanks (between sites on the same shanks) or between shanks (sites on different shanks) have been observed during these measurements. In addition, sites produced using the new fabrication procedures have been pulsed in PBS solution using similar protocols (50μA, 100μsec/phase, 1000μm^2) for over 200 million pulses with no change in their impedance characteristics. We have also explored the ability of single- and multi-shank probes to penetrate pia arachnoid in guinea pig using probes fabricated with strain gauges on their shanks. Probes having tip angles that varied from 10° to 45° were used with both shallow- and deep-diffused tips. Pia dimpling is over 700μm for the larger tips and less than 300μm for the sharper ones. A significant observation in using the sharper tips is that penetrated blood vessels appear to

self-seal around them so that no detectable bleeding is observed, whereas the larger tips cause bleeding upon penetration. Preliminary experiments with 8x8-shank three-dimensional probe arrays have shown that these structures, which have shallow-diffused sharp tips, penetrate guinea pig pia quite readily. The 3D array technology was developed under a companion recording contract but is ready to apply to stimulating arrays.

During the past contract, considerable progress has been made in the development of active probes containing on-chip signal processing. At the beginning of the contract, a set of first-generation active stimulating probes had been realized and were undergoing test. Since that time, these tests were completed, the designs were iterated, and a set of second-generation probes were fabricated and tested. In order to complete these probes, a successful encapsulation/interconnect process was developed in which LPCVD silicon dioxide and silicon nitride are used over polysilicon conductors on the probe shanks and aluminum interconnects are used in circuit areas under an overcoat of LTO. Additional layers of PECVD silicon nitride, metal barriers, and polymers can be used for chronic structures. The three active probes implement monopolar, bipolar, and multipolar (8-channel) designs. The monopolar and bipolar probes offer one and two simultaneously active channels, respectively, selected from among 16 sites. The monopolar design routes an externally-generated current to the selected site, while on the bipolar probe the current and sites are both selected digitally and the current is generated on-chip over a biphasic range from -254μA to +254μA ±2μA. Both of these active probes have now been used in preliminary in-vivo tests and both developments are considered complete. The high-end second-generation probe, STIM-2, contains 64 sites on 8 or 16 shanks. A front-end selector allows the user to select 8 of these sites for simultaneous stimulation using currents generated on-chip over a biphasic range from -127μA to +127μA ±1μA. This probe offers seven different operating modes including the ability to test site impedances, externally measure stimulus currents, record from any selected site, ground unused sites, or anodically bias the sites between pulses. While this probe is also fully functional, several changes are planned for a coming iteration to improve electrical contacts, reduce sensitivity to process variations, and allow recording while the current flow patterns from the probe are changed. The development of a high-performance external circuit interface for the active probes has also been completed. This circuit interface will soon facilitate the testing of STIM-2 in-vivo in both acute and chronic situations.

These results will be extended under a new contract through work in several areas. An improved contact technology for active probe circuitry will be developed along with a low-resistance interconnect material for use on probe shanks and ribbon cables. In addition, studies of probe encapsulation and probe performance in chronic situations will be continued. The design of STIM-2 will be iterated and a new probe capable of steering externally-generated currents to four sites selected from among 64 available on the probe will be developed. One version of STIM-2 will be fabricated to be compatible with a 3D 16x16-shank array, and such arrays, consisting of 128 channels and 1024 sites, will be developed. It is our hope that this technology will be applied in prosthetic applications before the year 2000 and that 3D active probe arrays will set the stage for a new generation of neural prostheses by the beginning of the new millennium.

MICROMACHINED STIMULATING ELECTRODES

Table of Contents

Summary
Table of Contents

1. Introduction 1

2. Progress on Passive Stimulating Electrode Arrays 2

    2.1 Basic Probe Structure and Recent Fabrication Advances 4
    2.2 Ribbon Cable and Interconnect Developments 12
    2.3 Three-Dimensional Electrode Arrays 17
    2.4 External Distribution of Passive Probes 20

3. In-Vitrro and In-Vivo Characterization 24

    3.1 Electrode Site Verification and Testing 24
    3.2 Activation of Iridium Arrays 24
    3.3 Stimulation Implants 25
    3.4 Penetration Studies 33

4. Active Stimulating Arrays 34

    4.1 Active Probe Fabrication 36
    4.2 Active Stimulating Probe Designs 38
    4.3 Active Probe Performance 50
        STIM-1b 50
        STIM-1a 61
        STIM-1 62
        STIM-2 63
    4.4 External Electronics for Active Stimulating Probes 66

5. Future Research 72

6. Summary and Conclusions 75

7. References 77

Appendix: Recent Publications from the University of Michigan and from External Users on Micromachined Microelectrode Arrays 80

MICROMACHINED STIMULATING ELECTRODES

1. Introduction

This final report summarizes work performed under funding from the Neural Prosthesis Program of the National Institute of Neurological Diseases and Stroke between September 1992 and September 1995. The work was targeted at the development of dense high-performance arrays of micromachined stimulating electrodes for use in the central nervous system. These arrays are intended to allow highly selective chronic stimulation of neural systems in terms of stimulus amplitude and time and in terms of spatial location. Thus, these arrays should permit many small clusters of neurons to be stimulated independently, both to allow neural systems to be better explored at the circuit level and, especially, as a basis for future neural prostheses. The primary initial target here is intracortical microstimulation of the visual cortex as the basis for a possible visual prosthesis; however, the same techniques and many of the same structures should also be applicable to auditory, bladder, and motor prostheses.

The work performed under this contract was based technology developed with previous support from the Neural Prosthesis Program (NPP) and continued these efforts in several areas. A variety of passive stimulating electrodes, both acute and chronic, were fabricated and supplied to other investigators nationwide. During the past contract period, some of this activity shifted to a new Center at Michigan funded under the NIH Biomedical Research Resource Program; nevertheless, new passive probe designs also continue to be fabricated under NPP support expressly for other investigators in the Neural Prosthesis Program. Efforts were made to improve passive probe technology through studies of new interconnect materials, the introduction of shallow-boron-diffused probe tips, the use of low-temperature encapsulating dielectrics, and improved procedures to ensure iridium site adhesion to the underlying interconnect materials. Modified site structures were introduced to solve adhesion difficulties encountered during the contract period. The passive probes were also characterized both in-vitro and in-vivo to gain additional insight into their performance limitations.

For practical prostheses, electrode arrays having hundreds of sites will likely be needed, and this will require the use of multiplexing circuitry integrated directly in the probe substrate. At the beginning of the contract period, a first generation of active stimulating probes had been realized and were in test. These tests were completed, the designs were iterated, and a second generation of active stimulating probes was produced during the new contract. These new designs implement monopolar, bipolar, and multipolar probe structures. The monopolar and bipolar probes allow the user to select one and two simultaneously active channels, respectively, from among 16 possible sites. The multipolar probe offers eight simultaneously active channels selected from among 64 sites. All of these active second-generation probes have now been tested and found to operate satisfactorily. The monopolar and bipolar designs are considered complete, while several minor modifications to the multipolar probe are planned for a coming iteration. In addition, a four-channel 64-site active array is planned under a new contract from the Neural Prosthesis Program which will continue this work.

Our approach to the problems associated with array fabrication continues to be based on merging high-performance silicon micromachining technology with the broad array of techniques that have been developed for use in integrated circuits. Silicon, in thin

(<20μm) microstructures, is an extremely strong and flexible material that can be etched with a precision far greater than that of any other known material. In addition, when silicon is used as the supporting substrate for the probes, circuitry can be embedded directly in it to allow the control of many sites from very few input leads. No bonds or externally-exposed contacts need be used in connecting to a hybrid chip; in fact, the output leads themselves can be realized as multistrand multilead ribbon cables, hermetically sealed using the same dielectric coatings that are used for the probes themselves. These leads can be fabricated as an integral part of the probes, yielding a completely sealed structure in which the only bonds required are within the final percutaneous plug. This technology now permits stimulation or single-unit recording from neurons on a chronic basis for several months or more.

In developing such electrode arrays, we believe that a critical aspect is the yield of the associated process and its compatibility with eventual fabrication in a commercial foundry. The devices must be reliable and producible in reasonable volumes at reasonable cost. For this reason, we have tried to pay close attention to both the reproducibility and the practicality of the processes involved. Although the technology levels are high for a university facility, they are conservative relative to the levels now required of industrial VLSI circuits. (By the year 2000, such circuits are expected to realize up to one billion transistors per chip running 0.18μm features on 300mm-diameter wafers with six levels of interconnect.) The micromachining steps generally permit yields above 90 percent and are not a limiting factor in the overall process. These efforts on probe development at Michigan have, in fact, been a technology driver for sensor development not only at Michigan but worldwide [Wise 91-1, Wise 91-2, Wise 90], both in terms of technology and in terms of circuit interfaces. Extensions of this work have directly fueled microstructures for the measurement of flow, pressure, acceleration, tactile images, IR/thermal images, gas chemistry, and many other variables. Some of these devices are already beginning to appear as commercial products [Bernstein 93, Spangler 95], and we would hope that the probes will eventually emerge in this form as well. Also significant is the fact that with the addition of a single additional masking step, microchannels can be formed in the probe substrate to allow chemical drug delivery at the cellular level while simultaneously performing electrical recording and stimulation. This promises to open up significant neuropharmacological studies and perhaps eventually therapeutic procedures that have been impossible in the past [Chen 94].

Section 2 of this report summarizes the results of work under the past contract in the development of passive probe arrays (those not having on-chip circuitry). Section 3 then describes in-vitro and in-vivo performance tests on these probes, and Section 4 reviews the development of active probes (containing on-chip circuitry). Section 5 comments briefly on planned future activities, and Section 6 summarizes progress under the past contract. Finally, an appendix lists recent publications by our group in this area and publications by others as the result of their work with the probes.

2. *Progress on Passive Stimulating Electrode Arrays*

Our work on microelectrode arrays for recording and stimulation in the central nervous system began many years ago with early work at Stanford [Wise 70, Starr 73, Wise 75]; however, more recent efforts began in the early 80s with work on recording electrodes, later extending to stimulating arrays. From the beginning, this work was aimed at utilizing the broad base of process technology developed for silicon integrated circuits as closely as possible. The basic probe structure is shown in Fig. 1. A micromachined silicon substrate supports an array of thin-film conductors that are insulated above and

below by deposited dielectrics of silicon dioxide and silicon nitride. Openings in the upper dielectrics along the probe shank define stimulating or recording sites which are inlaid with iridium oxide for interfacing to the tissue. At the rear of the probe, integrated circuits provide a multiplexed interface to the output leads, which connect to a remote percutaneous plug.

Virtually all of the efforts directed at photoengraved microelectrode arrays during the past quarter century have had the structure in Fig. 1 in common; however, the various efforts have differed considerably in their choices of substrate materials, insulating dielectrics, and substrate shaping technologies. These choices have resulted in widely differing process yields and have sometimes compromised compatibility with batch processing. Only the silicon approaches have attempted to include electronics on-board, and it has only been recently that single-unit recording with on-board circuitry has been demonstrated [Lund 94]. In addition, until recently no satisfactory solution to the output lead problems had been found, preventing the realization of practical chronic assemblies. Thus, in approaching structures such as that shown in Fig. 1, the critical areas to be considered are the substrate material (and how to shape it), the insulating dielectrics and their compatibility with the interconnect materials used, the possibility for merging the structure with electronics to reduce the number of output leads, and finally, the structure and encapsulation of the output leads themselves.

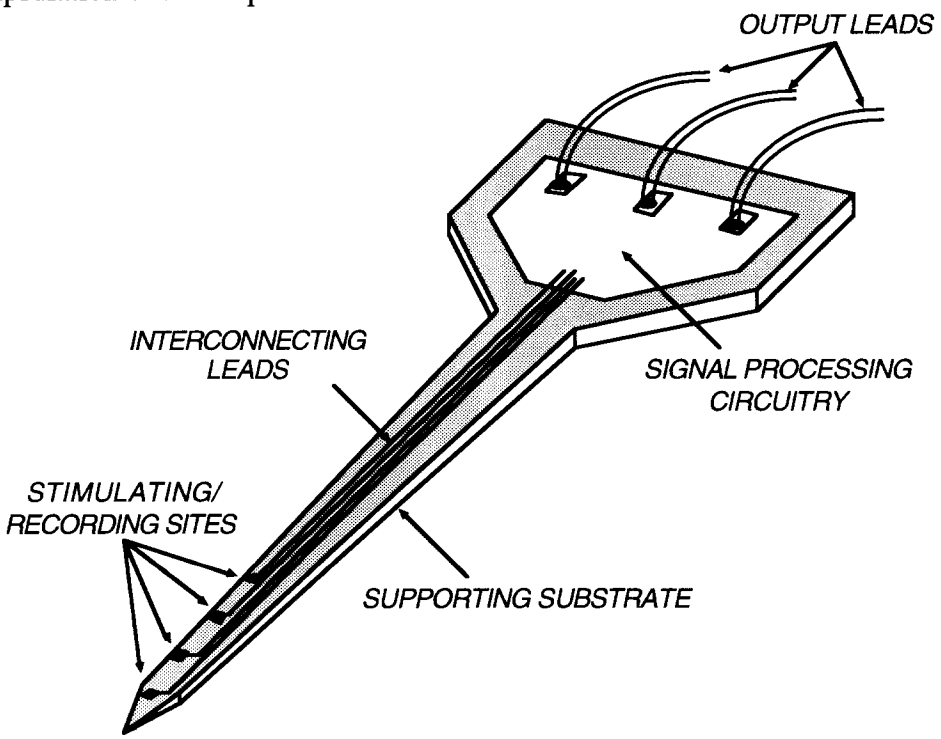

Fig. 1: Basic structure of a micromachined multielectrode probe for stimulating or recording in the central nervous system.

The most important single result from our work at Michigan has been the use of a diffused boron etch-stop for silicon substrate definition. This has allowed precise, reproducible substrate formation with a rounded probe cross-section, dimensional control to better than ±1μm, and a minimum shank width of 20μm or less [Najafi 90-1]. This is accomplished with a single-sided process using wafers of standard thickness. No other process we have considered has allowed this degree of control in a high-yield batch

process. We have shown that oxide/nitride stress-compensated dielectrics, in combination with interconnects of polysilicon and perhaps metal/polymeric barriers, are suitable for encapsulating the recording/stimulating sites, the probe shanks, and the circuitry for durations of at least one year and probably much longer [Hetke 94]. Site impedances, for example, have remained stable for over one year in-vivo in the range of a few megohms. We have also demonstrated the incorporation of high-performance CMOS circuitry in the probe substrates, both for recording and for stimulation [Ji 90, Tanghe 92, Lund 94]. This is the first time such circuitry has been integrated to form active probes that have recorded from single units in-vivo. Finally, we have demonstrated the use of the basic probe process to form multistrand multiconductor silicon ribbon cables for use in connecting the probes to the outside world [Hetke 94]. These cables offer minimal tethering forces, can be built directly into the probe itself, and can be completely surrounded by a conducting shield, protecting the dielectrics from the extracellular fluid. These cables now allow chronic probes to be fabricated and used in-vivo for periods of several months. The cables have been tested for over four years under bias in saline without any significant degradation.

2.1 Basic Probe Structure and Recent Fabrication Advances

As many as twenty different probe designs can be included on a single mask set as shown in Fig. 2, which shows several probe designs on the silicon wafer before final etching. Shank widths are as narrow as 30μm, with length-to-width aspect ratios of more than 100:1. Probe designs have been provided by both internal and external users following design rules that are detailed and explained in a User's Guide that is provided to investigators on request. Figure 3 shows several completed passive probes after etching from the wafer. More than 100 different designs have been produced for investigators nationwide during the last few years.

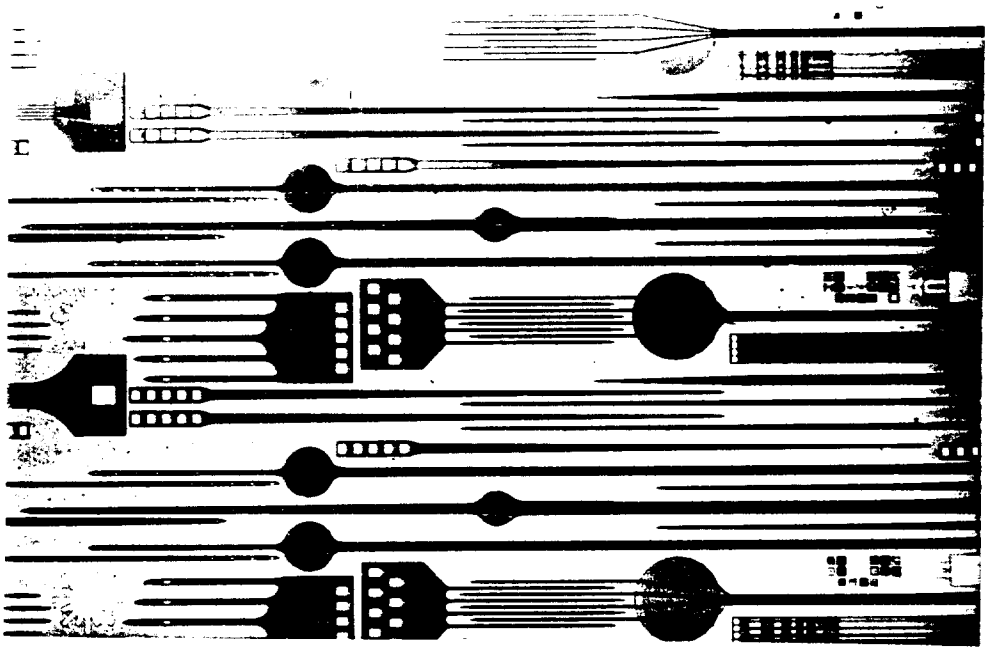

Fig. 2: One mask set of probes recently fabricated at Michigan. The probes are from 2mm to over 18mm in length, typically 15μm thick, and as narrow as 25μm. Ribbon cables, which are built into the probes, are as long as 5cm.

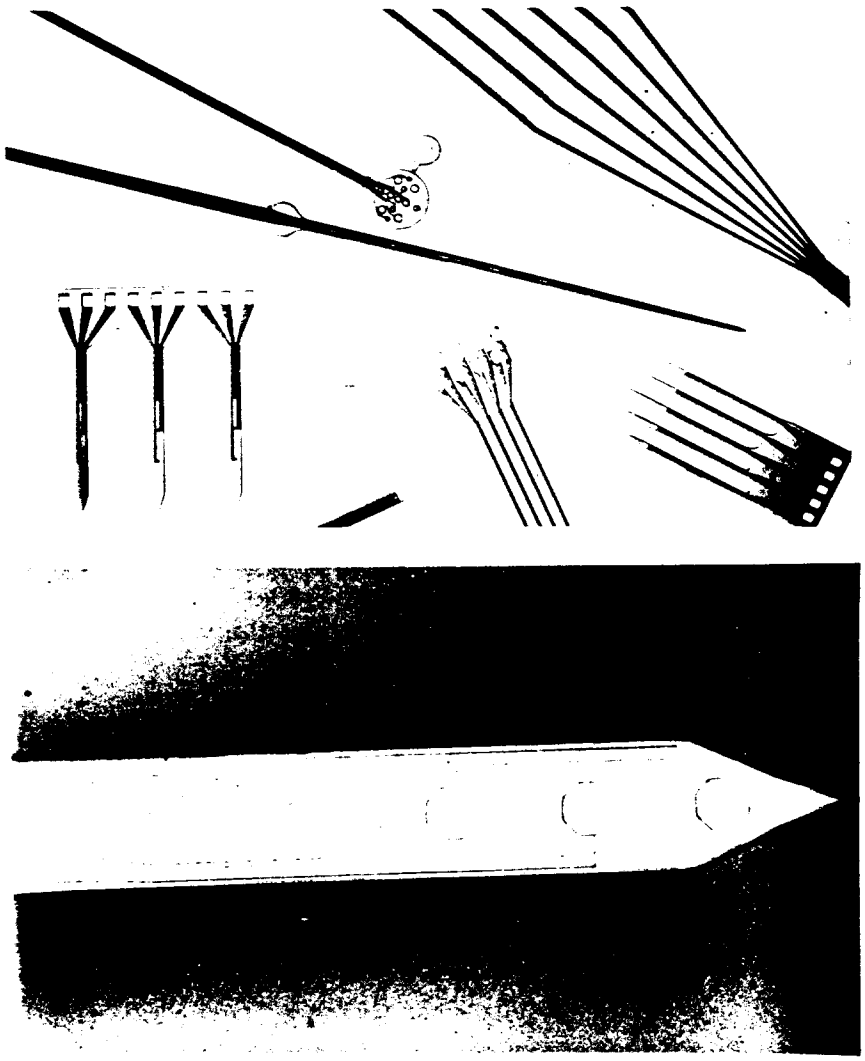

Fig. 3: Views of several different probe designs after etching from their host wafer. In the lower photo, a view of an early stimulating probe is given. The sites on this particular probe are 8000μm^2 in area.

The basic process flow for passive probes is shown in Fig. 4. Fabrication begins with a standard silicon wafer that is oxidized and patterned to define the intended probe shapes. These areas are subjected to a deep boron diffusion to heavily dope the probe substrate. The diffusion time and temperature are selected to produce a final probe thickness of about 15μm, although thicker substrates are possible depending on the demands of the application [Najafi 85]. The masking oxide is then stripped, and lower dielectric films are deposited using low-pressure chemical vapor deposition (LPCVD). These films consist of a layer of silicon nitride sandwiched between two layers of silicon dioxide. The thickness of each layer is selected so that the thermal expansion coefficient of the composite insulator approximately matches that of silicon to avoid warp in the final probes.

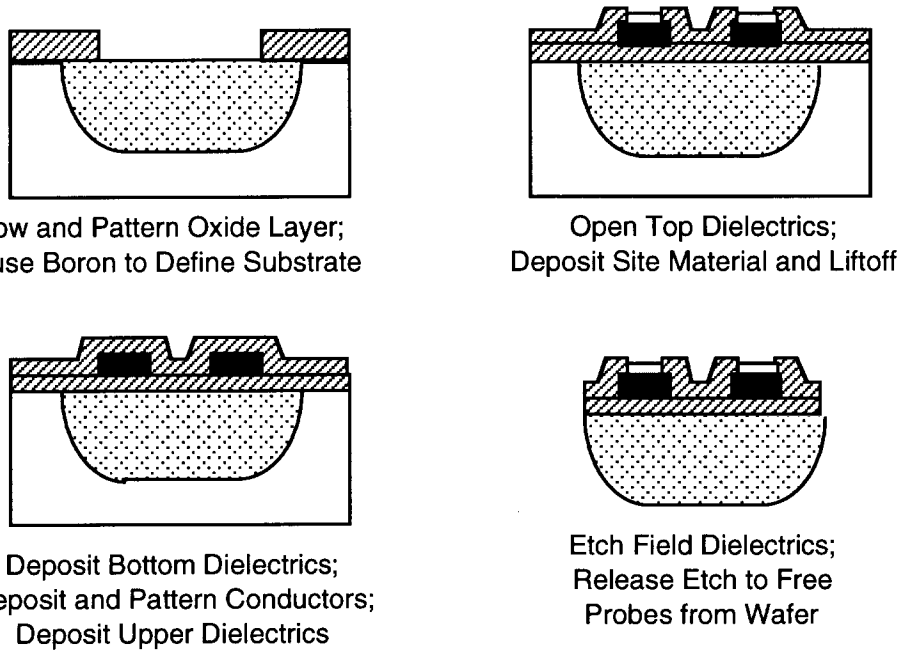

Fig. 4: Process flow for passive stimulating electrode arrays. The process is single-sided on wafers of normal thickness and requires only four masks when the site material is also used for the pads. The use of gold pads adds a fifth mask. A shallow boron diffusion for sharp tip formation and ribbon-cable definition adds a sixth.

Conductors of phosphorus-doped polysilicon are next deposited and patterned, followed by the deposition of upper dielectrics which are identical to those used for the lower composite film. These upper dielectrics are patterned using reactive ion etching (RIE) to open the stimulating sites and bonding areas. With the masking resist still in place, titanium (300Å) and then iridium (3000Å) are sputtered onto the wafer. The photoresist is then removed, lifting off the metal in all areas except where the upper dielectrics have been opened for the sites and bonding pads.

In forming the stimulating sites, care must be taken to ensure that the conductor surfaces in the opened site areas are free of surface contamination in order to ensure that the titanium-iridium site adheres tightly to the underlying conductor. This has not always been the case, and during the last three years many problems were experienced in our laboratory with metal adhesion. In addition, an electrical barrier was seen in many probes that prevented current flow for site potentials below a level that varied from tenths of volts to several tens of volts. Both of these problems were finally traced to the existence of a surface fluorocarbon residue on the polysilicon conductor surface left by the RIE process. The self-aligned site structure thus has a significant disadvantage in that it precludes thorough cleaning of this surface prior to metal deposition since the photoresist is still in place. The problem can be avoided by introducing a backsputtering step after contact formation and before metal deposition, by minimizing the RIE overetch and using a post-metallization anneal at 500°C for 30 seconds, or by going to a non-self-aligned metal process. Figure 5 compares the self-aligned and non-self-aligned site options. We have recently adopted a non-self-aligned site structure as shown in Figs. 5 and 6. This is particularly important for stimulating probes, where the site size may be relatively large. With a self-aligned site, the underlying conductor must be larger than the site, and other

shank conductors must detour around it, causing a site to expand the width of the shank considerably (Fig. 6). With non-self-aligned sites, not only is a thorough wet chemical cleaning possible before metallization but the site can overlap adjacent conductors to maintain a narrow shank. Thus, the site metal becomes an additional conductor level. Figure 7 shows recently-fabricated iridium sites. We have seen no problems with adhesion or interfacial barriers since going to the new site configuration.

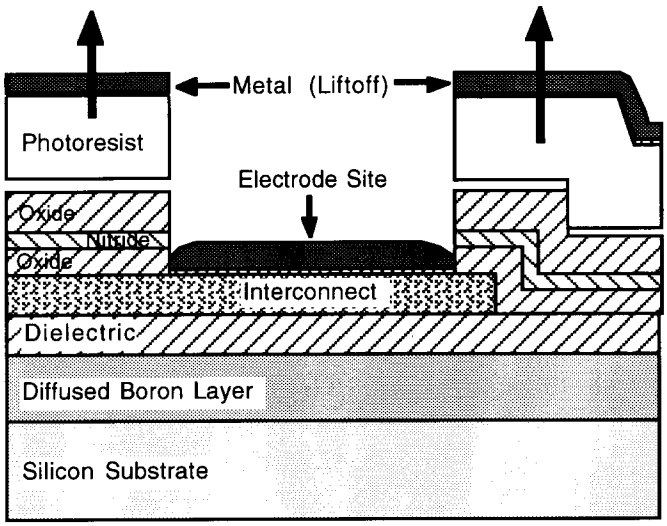

Self-Aligned Stimulating Site Produced by Lift-Off

The contact opening and metal are defined using the same photoresist layer.

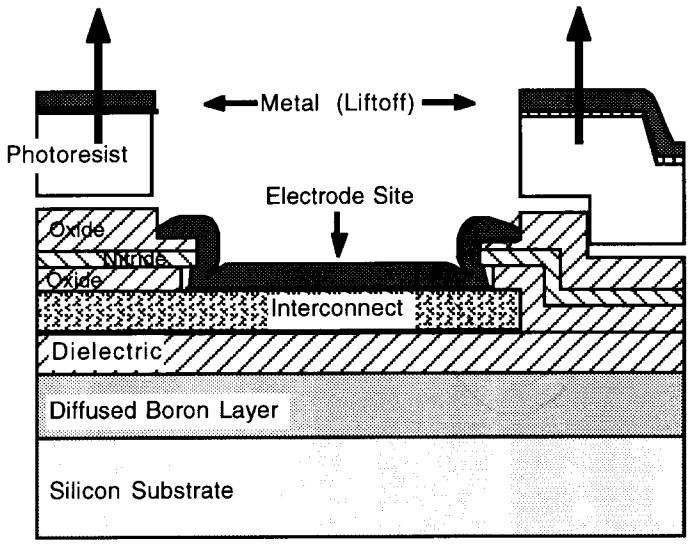

Non-Self-Aligned Stimulating Site Produced by Lift-Off

The dielectric opening and the metal are defined using different masking/photoresist layers.

Fig. 5: Comparison of a self-aligned site structure (above) with a non-self-aligned site structure (below). The upper structure requires backsputtering or a post-metallization anneal to ensure adequate iridium adhesion; the non-self-aligned structure allows premetallization cleaning to ensure high adhesion but requires an extra mask.

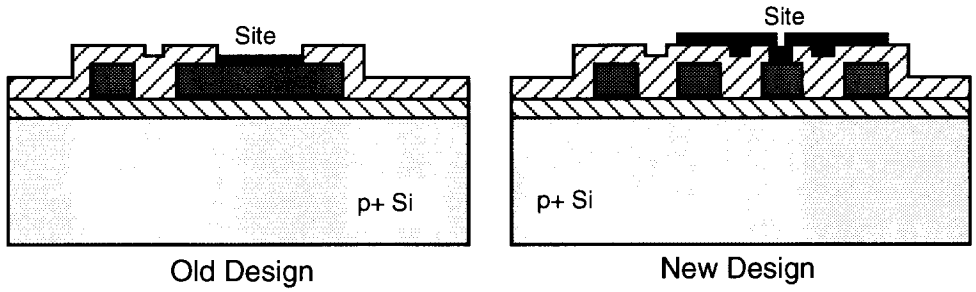

Fig. 6: Comparison of a self-aligned site structure (old design) with a non-self-aligned site that overlaps adjacent shank conductors. In the new design all contact vias can be the same size, simplifying the contact etch process.

After site formation using lift-off, gold is inlaid in the bonding sites to allow simple bonding to the probes with either gold or aluminum wire. The field dielectrics outside the intended probe areas are now removed using RIE. Finally, the wafer is thinned to about 100μm from the back in an isotropic etchant (10% hydroflouric, 90% nitric acid) and then subjected to an unmasked etch in ethylene diamine-pyrocatechol-water (EDP) [Bohg 71] to separate the individual probes. The EDP etches lightly-doped silicon but stops on the heavily-doped regions and does not attack the dielectrics or metals used. The completed probe chips are removed from the etch, ready for the lead attachment and mounting.

This simple four-mask process results in very small structures and requires only single-sided processing on standard silicon wafers. All etching steps are highly selective and self-stopping. Probe features can be controlled to ±1μm or better. The thicknesses of the finished probes can be varied in the range 1-40μm by varying the boron diffusion time and temperature and the final etching process [Najafi 90-1, Najafi 85]. The substrate can have any two-dimensional shape as defined by the mask. All probe materials are biocompatible and suitable for chronic applications [BeMent 86, Drake 88].

One final process option added during the past contract period should also be mentioned. In addition to the use of a deep boron diffusion for primary substrate definition, a shallow boron diffusion can be added to allow the formation of sharper probe tips. This diffusion can also be used to form the substrate for integrated ribbon cables as noted below. Figure 8 shows a deep-diffused probe having a 45° tip taper compared with a shallow-diffused tip having a tip taper of 10°, while Fig. 9 shows additional views of a shallow-diffused probe tip. Such probes enter tissue with very little force and minimal cortical dimpling. Penetration of blood vessels does not result in bleeding but appears to be self-sealing.

For acute experiments, the probe is mounted on a special printed circuit board connector. Electrical connections are made by wire-bonding from the pads on the probe to the connector. This assembly then plugs into a standard dual-in-line-package (DIP) socket to provide easy electrical access to the electrodes. For long-term (chronic) applications, the connections to the probe are made with a ribbon cable wire-bonded to the probe or fabricated as an integral part of it. Building the cable into the probe to realize a "long probe" eliminates any external connections between the probe and cable and adds one mask to the basic five-mask process. Figure 10 shows an example of a chronic probe assembly, with the probe, an integral silicon ribbon cable, and the percutaneous plug.

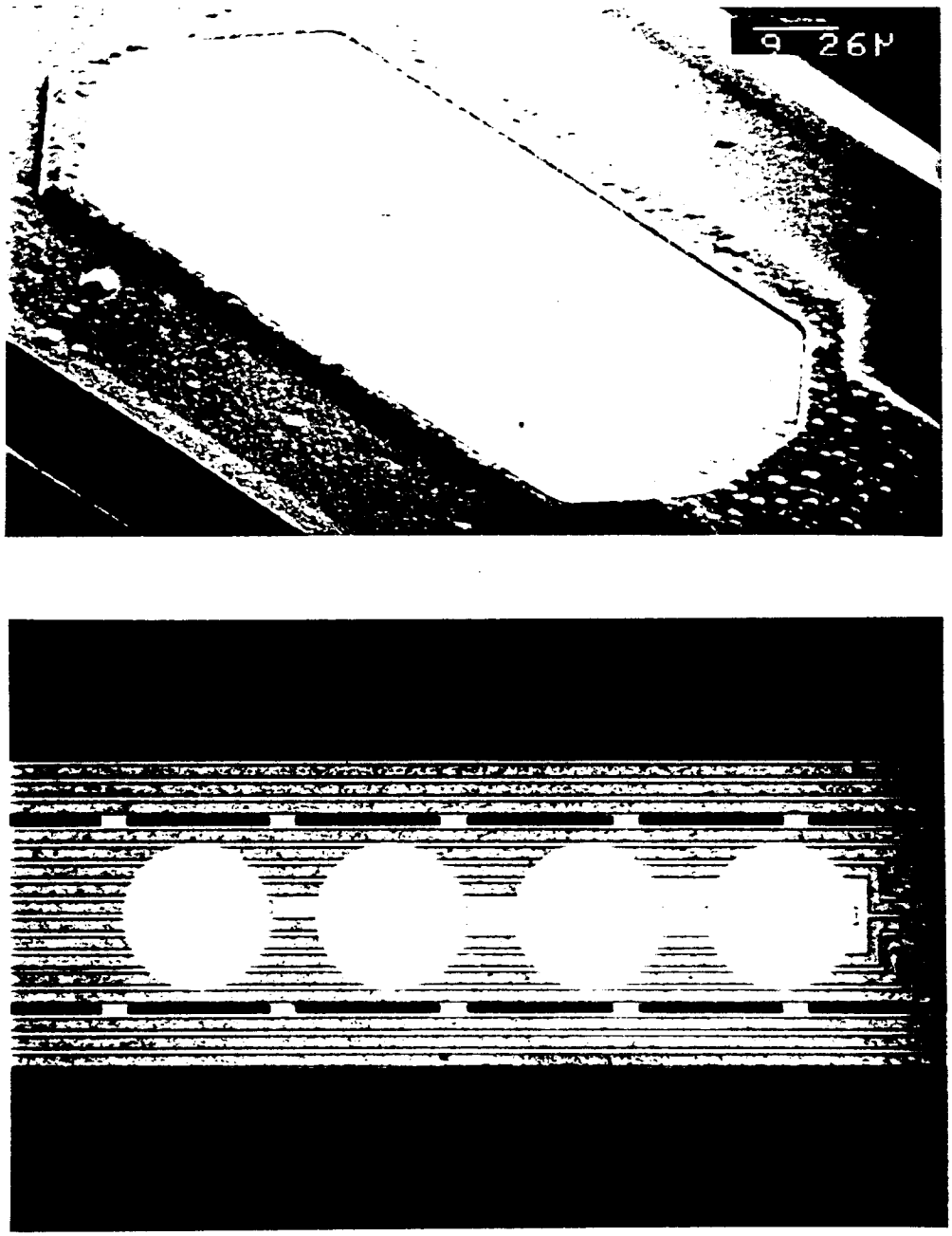

Fig. 7: Top view of recently-fabricated stimulating sites produced using the non-self-aligned process. The overlap of a large site over adjacent conductors is clearly seen in the lower photo.

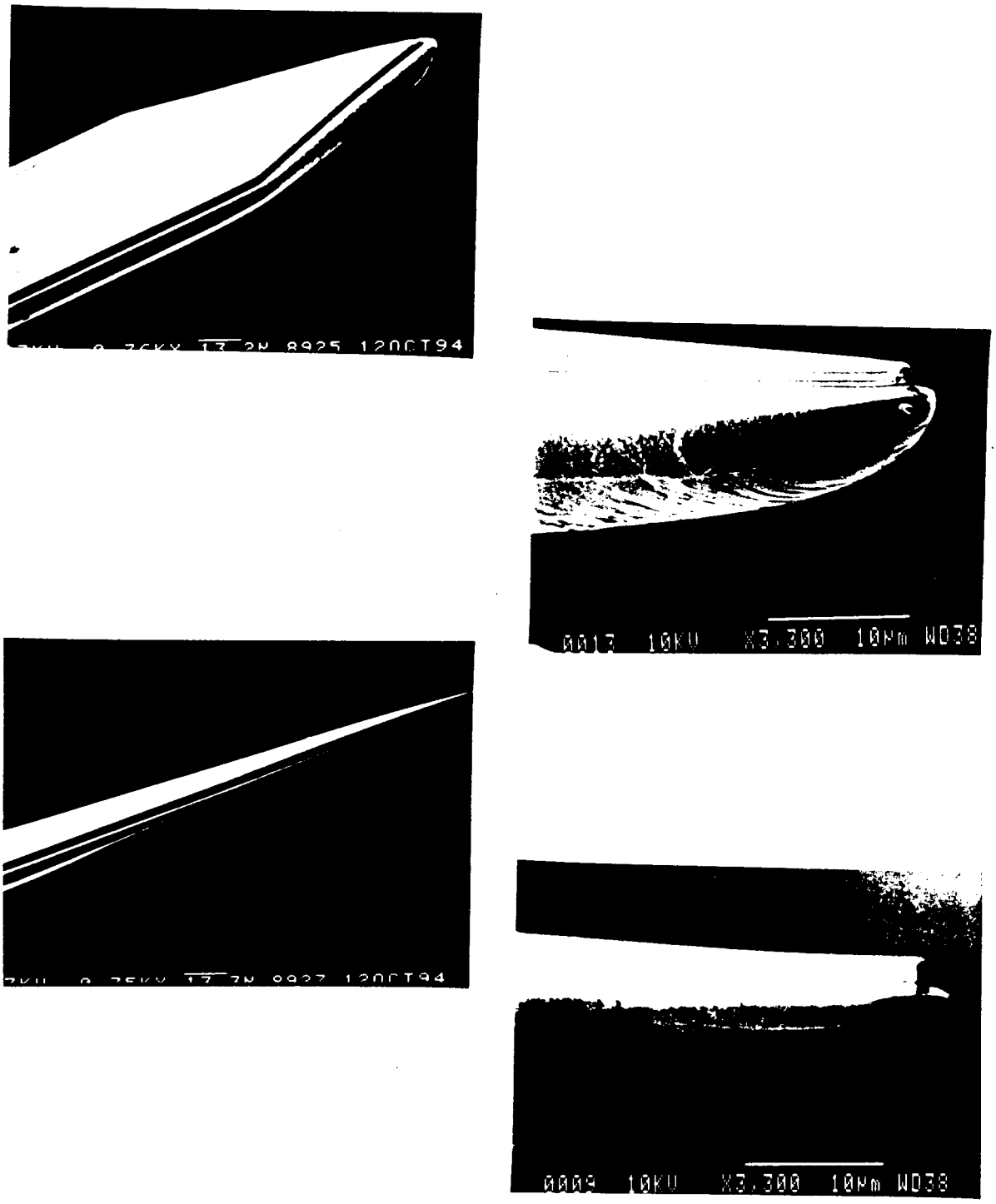

Fig. 8: Comparison of probe tip shapes possible with the usual probe process. A deep-diffused probe tip is shown above with a 45° tip taper. A shallow-diffused tip having a 10° taper is shown below.

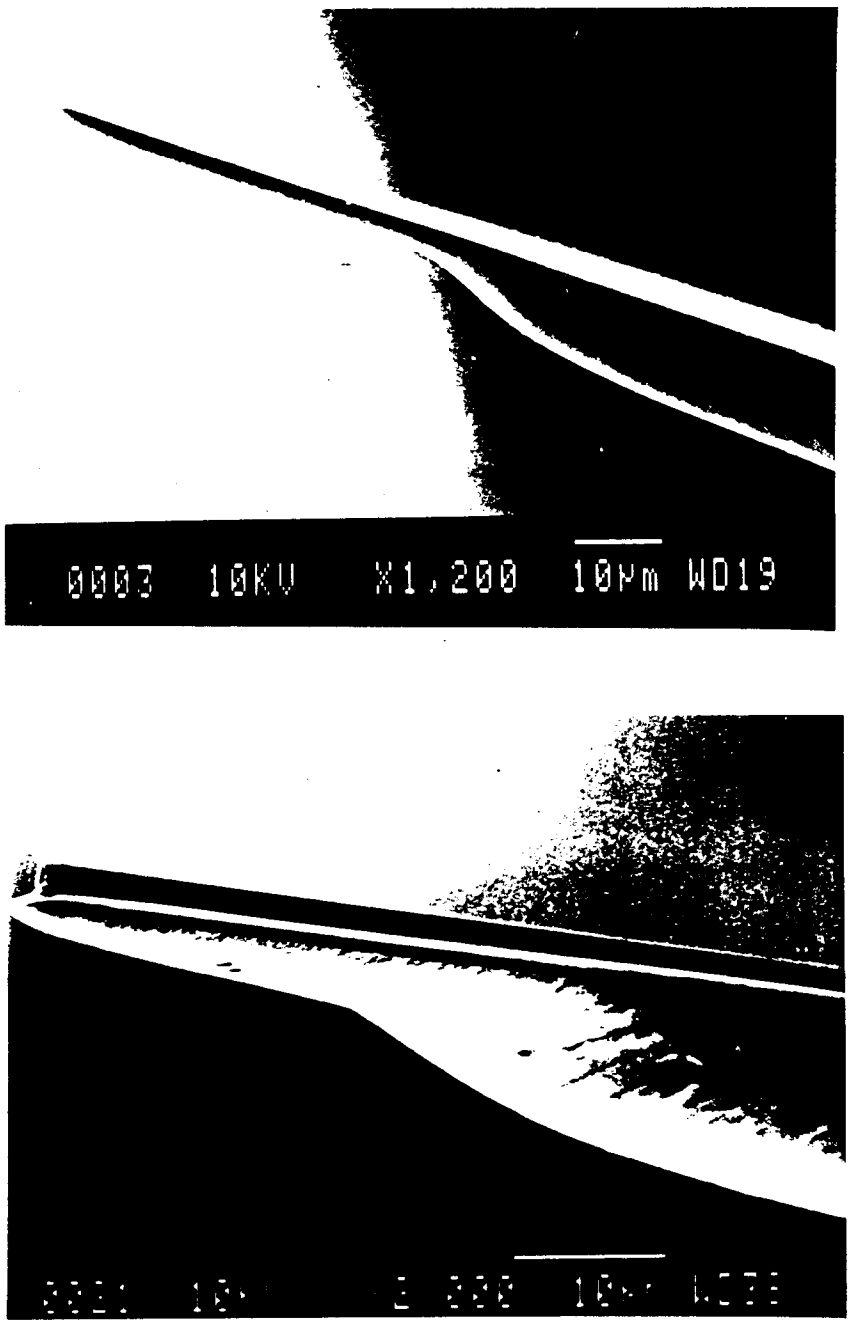

Fig. 9: SEM views of a shallow-diffused probe tip produced using a shallow boron diffusion to extend the deeper diffusion used for the main section of the shank. The boron diffusions flow together in the latter case to produce a nearly ideal taper that can be controlled within 1µm.

Fig. 10: Photograph of a complete passive stimulating probe assembly, including the probe itself, an integral silicon ribbon interconnect cable, and the percutaneous plug.

2.2 Ribbon Cable and Interconnect Developments

For many years, the biggest obstacle to using thin-film recording and stimulating electrode arrays (or any other electrode arrays) chronically was the lack of a stable, reliable interconnect system. The use of discrete leads with the probes using fine (25μm) gold, platinum-10% iridium (Pt-Ir), and pure platinum wires having Teflon coatings (5-7μm) has not been successful in our Laboratory. Problems have been experienced with wire flexibility and tethering, Teflon stripping, bonding, and Teflon integrity. Additionally, the construction of interconnect systems using discrete wires is very labor-intensive and cannot be done in batch. Most of our efforts on a chronic probe interconnect system over the past few years has focused on the use of silicon ribbon cables as mentioned above. Figure 11 shows the structure of such a cable. It consists of a long thin silicon substrate that supports multiple dielectrically-encapsulated leads. At either end of the cable is a thicker platform with exposed metal pads for bonding the cable to either a probe or to a percutaneous connector. The main cable itself is further passivated with a metal (typically gold) barrier layer over the upper dielectrics. This layer makes contact to the silicon substrate so that the leads are electrically as well as chemically shielded, making the cable in effect a multilead "coaxial" structure. The ribbon cables are fabricated in a five mask process which is fully compatible with the process used for passive probes. In fact, one of the greatest advantages of silicon ribbon cables is that they can be integrated into the probe itself, eliminating the need for any bonding, soldering, or additional encapsulation between the probe and the interconnect. Figure 12 shows two recently-fabricated ribbon cables. The cables are slotted to maximize rotational (in-plane) flexibility.

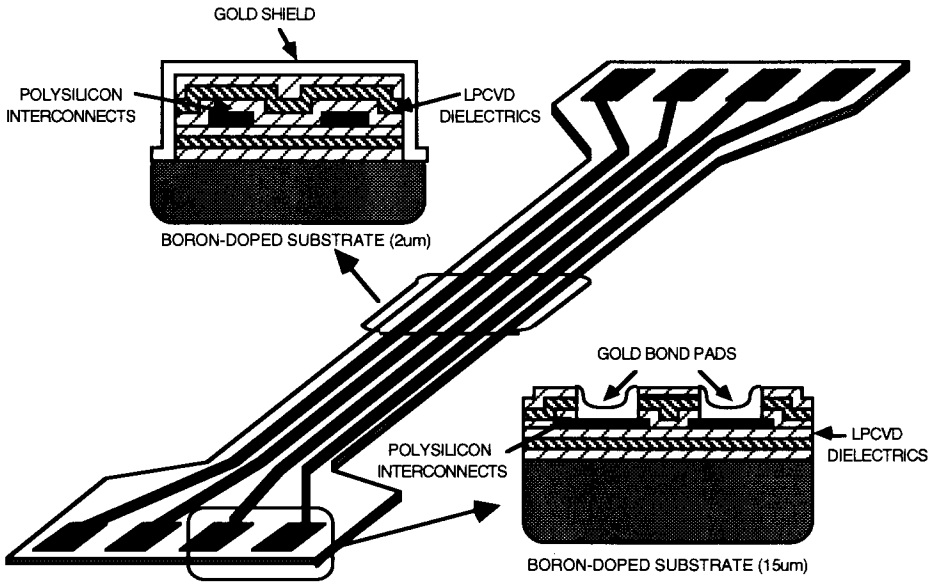

Fig. 11: Structure of a silicon ribbon cable. A flexible silicon substrate supports dielectric-encapsulated conducting leads. The substrate-defining boron diffusion can be masked to create slits in the cable to increase rotational flexibility.

In the first step of the fabrication sequence for the cables, an oxide layer is grown and patterned for deep boron diffusion (15μm) to form the cable bonding areas or the probe substrate. This procedure is then repeated for the cable itself, except that the diffusion is much shallower (2-3μm). The bottom dielectrics are deposited via low pressure chemical vapor deposition (LPCVD). Next, the conducting material is deposited and patterned. Present cables and passive probe-cable designs use phosphorus-doped (n-type) polysilicon, which has the advantage that it can be passivated with high-temperature LPCVD films. The disadvantages of and alternatives to this approach will be discussed shortly. After deposition of the top dielectrics, the field areas are etched clear so that the devices may be freed from the wafer in EDP. If a gold shield is desired, it is patterned using the same mask as the shallow boron diffusion. The final thickness of the cable is 4-5μm. These cables have excellent flexibility and can be tied in "knots" with radii of less than 400μm.

An important measure for the integrity of such an interconnect system is the amount of leakage current between leads or from the leads to the surrounding ambient fluid. While this is most critical for passive recording situations, where very low-level signals may be severely degraded by excessive leakage current, it is a potential problem in any chronic recording or stimulating application. We have done extensive in-vitro leakage testing on polysilicon-lead ribbon cables insulated with LPCVD dielectrics shielded with gold. The actual cable leakage is thought to be below our ability to measure it (<10fA). The measurements are quite sensitive to environmental factors, however, particularly room humidity and electromagnetic noise. After taking steps to eliminate these factors, the measured leakage currents are at most a few picoamperes, but are still strongly influenced by room humidity even when dessicators are used. This is thought to be due to the formation of condensed salt films near the small cable bonding areas when the connections are taken from the same end of the cable. A special ribbon cable designed specifically for testing purposes (with adjacent leads exiting from opposite ends of the cable) has allowed us to confirm that the observed leakage is indeed due to end effects. Leakage currents of a

few picoamperes are insignificant for passive and active probes so long as they are not symptomatic of cable degradation. Figure 13 shows the leakage current for an ongoing soak test with the shielded cable biased continuously at +5V with respect to the solution. The data is similar for cables soaked at -5V. The seasonal variations due to humidity artifacts are easily seen.

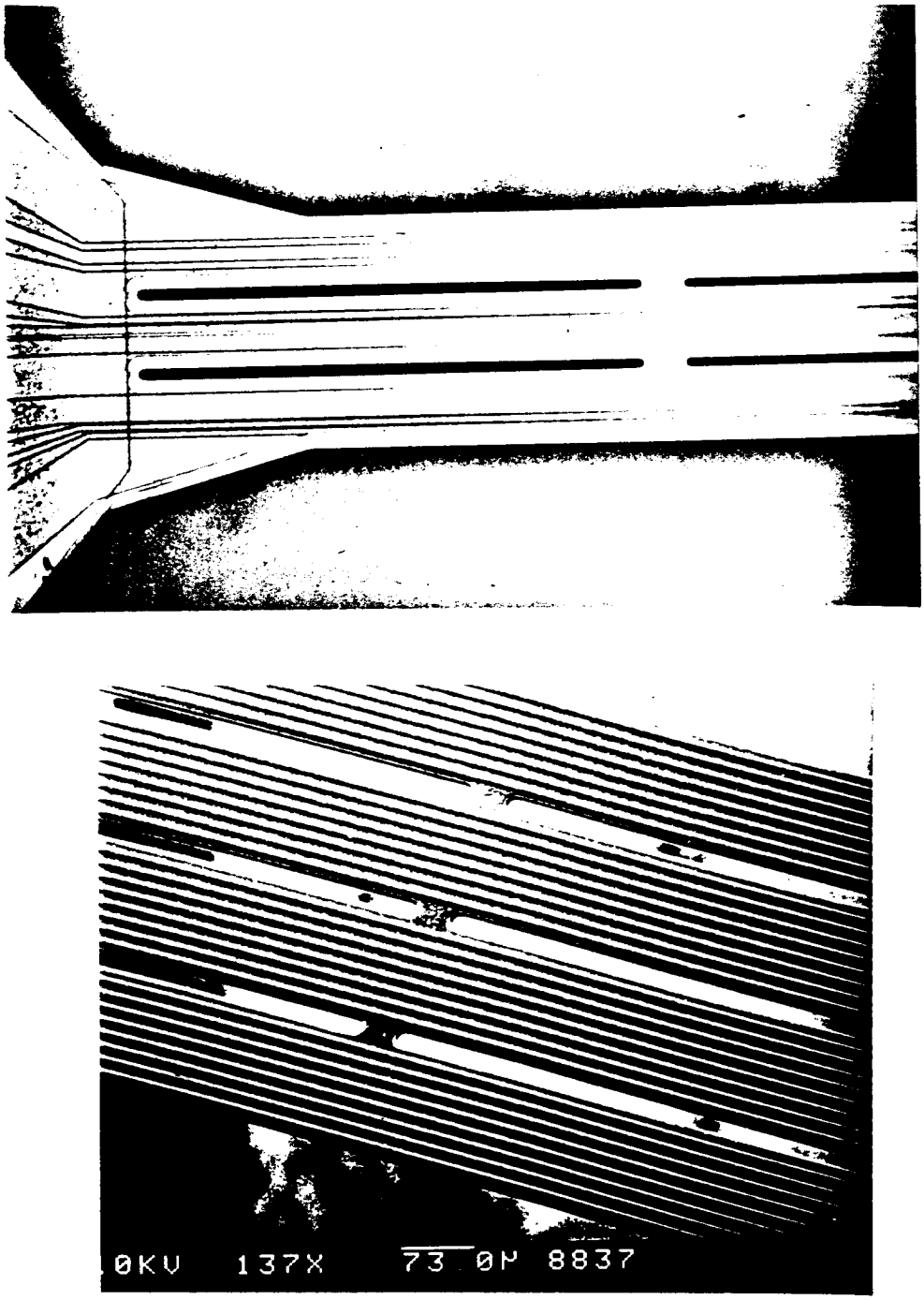

Fig. 12: Photographs of two slotted ribbon cables. The upper cable features two layers of polysilicon interconnect, while the lower cable has 32 leads in single-level polysilicon.

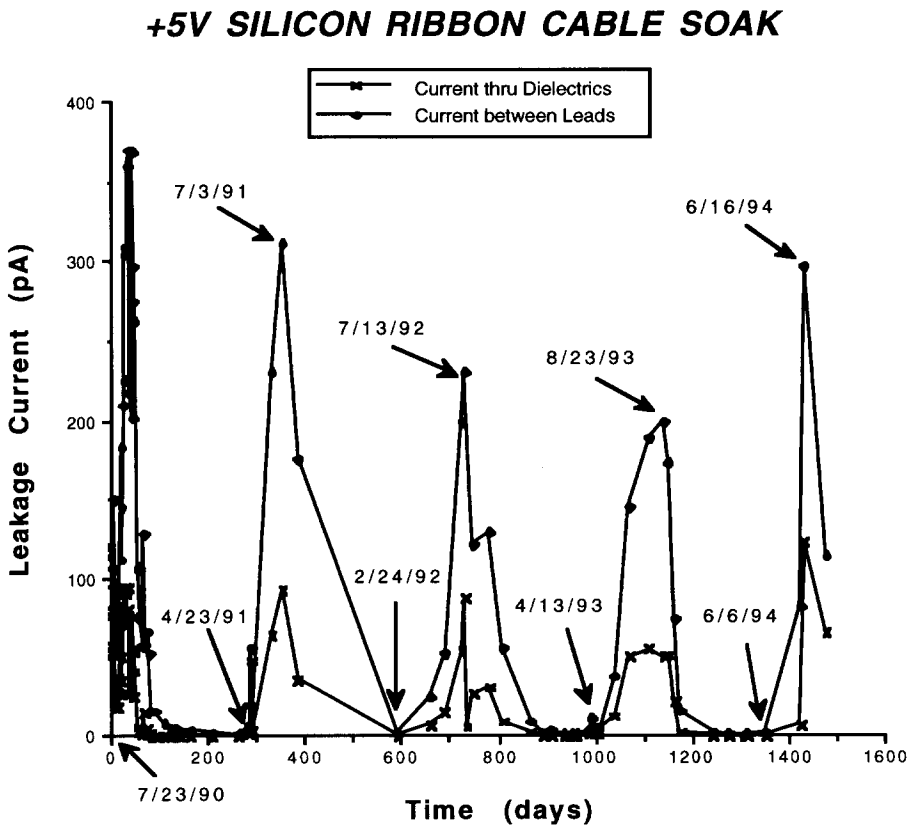

Fig. 13: Results of an ongoing silicon ribbon cable soak test. This shielded cable has been soaked in saline at +5V for over 1400 days without loss of integrity. The large fluctuations in leakage current have been traced to ambient humidity.

Silicon-based ribbon cables are probe process compatible, can be batch fabricated, and can be integrated directly into probe designs. They have greater flexibility and integrity of insulation than any of the discrete wires we have tested. Assembly of chronic implant structures using silicon ribbon cables is relatively easy compared to the task of making discrete wire assemblies. Ribbon cables with polysilicon leads do suffer from higher end-to-end resistances than their discrete wire counterparts, however, and for stimulating leads and active supply lines a lower resistance interconnect is needed. The interconnect metal used should have very low resistance ($\leq$ 1 ohm/square as compared to $\geq$10 ohms/square for polysilicon) so that reasonable voltages may be used to deliver the needed stimulation currents. The interconnect must be able to withstand the temperatures used for deposition of the final probe/cable dielectrics, which are 420°C for low-temperature oxide (LTO) and as high as 920°C for LPCVD oxide. The material must be easily etched to define narrow leads (the minimum feature size required is about 3μm). Additionally, it must have good adhesion to the dielectric layers used below and above it. If the same interconnect material is used for circuit metallization, it must also be able to provide ohmic contact to both the n+ and p+ regions of the circuit. Satisfying all of these criteria simultaneously is a very challenging task

We have worked to a limited extent on defining a better interconnect material in the past and plan to accelerate these efforts in the future. Refractory metal silicides have a sheet resistance of about 1 ohm/square and pure refractory metals can reach levels of 0.1 ohm/square. Thus, either group of metals could potentially serve as the desired material. For use on cables, the situation is simplified since the requirement of ohmic circuit contacts is removed; however, in both cases, there are potentially serious problems with adhesion and mechanical stress to be overcome. The most commonly used refractory metal silicides are $TiSi_2$, $TaSi_2$, $MoSi_2$, and WSi_2. Among these, $TiSi_2$ has the lowest resistivity, although it is the least stable of the group. Fine line patterning of titanium silicide can be achieved by direct patterning of polysilicon followed by the deposition of the titanium film and selective silicidization with the underlying polysilicon region. In this way, a difficult multi-layer polycide etch can be avoided. One of the major drawbacks of titanium silicide is that it is soluble in hydrofluoric acid (HF) and some other chemicals used for wafer cleaning. In order to overcome this restriction, titanium silicide can be covered by a thin layer of silicon nitride.

We have formed layers of titanium silicide by using phosphorus-doped polysilicon as a base material. This was patterned using RIE and titanium was deposited on the polysilicon to a thickness of about 0.1μm. The wafers were then annealed and sintered to form the silicide. Finally, the wafers were cleaned and were ready for high-temperature LPCVD dielectric passivation. Table 1 lists the sheet resistance of the titanium silicide after the deposition of different LPCVD dielectrics film at different temperatures. The initial sheet resistance was about 1 ohm/square. For 180nm of silicon nitride deposited at 820°C for 40 minutes (the total exposure time of the wafer to high temperature was about 90 minutes) the sheet resistance rose to about 2.5 ohms/square. Figure 14 shows a photomicrograph of patterned titanium silicide after passivation by LPCVD Si_3N_4. The finest line width in the pattern is 3μm. The films are visually good with no sign of the stress cracking and adhesion difficulties that have been a problem with some of our previous silicide films. For an additional 300nm of SiO_2 deposited at 920°C as an additional dielectric, the sheet resistance rose to 11 ohms/square, approximately equal to that of doped polysilicon. Thus, we conclude that titanium silicide is an adequate dielectric for use with LTO films and can even be used with LPCVD nitride films up to a deposition temperature of 820°C; however, above this temperature the films degrade badly. This does allow the possibility, however, of using LTO covered with LPCVD nitride as a passivation layer on future probes.

For chronic applications, a still lower interconnect resistance may be desirable. One option is to use aluminum not only for the circuit metal but on the shanks and ribbon cables as well. The aluminum could be passivated with LTO and possibly with an upper PECVD nitride layer as well. If it can be demonstrated that the leakage currents from these structures are comparable to those of ribbon cables passivated with LPCVD dielectrics, this option may well be the simplest implementation of low resistance interconnect for both passive and active arrays. Another option is to use a refractory metal. The major drawbacks to the refractory metals we have experimented with are instability on SiO_2, stress cracking due to thermal expansion mismatch during high temperature dielectric deposition, poor adhesion to the dielectric layers, and lack of resistance to post-processing chemicals. One approach which may be able to overcome all of these difficulties is to use a refractory metal core surrounded by n+ doped polysilicon (or a silicide). The polysilicon outer layer would adhere intimately to the surrounding dielectrics and furnish resistance to chemical reagents. The refractory metal core, on the other hand, would provide a very low (<0.1 ohm/square) resistance pathway for stimulation currents. Both the aluminum-LTO and the refractory core approaches will be explored under the coming contract for future stimulating probes.

Dielectric Layer Deposited	Deposition Time	Deposition Temperature (at outer-middle-inner zone of the furnace)	Sheet Resistance of $TiSi_2$ (after high-temp. LPCVD deposition)
Si_3N_4 (180nm)	40 min.	810°C-820°C-830°C	2.5 ohms/square
Si_3N_4/SiO_2 (180nm/300nm)	40 min./30 min.	810°C-820°C-830°C/ 910°C-920°C-930°C	11 ohms/square
Si_3N_4/SiO_2 (180nm/280nm)	40 min./40 min.	810°C-820°C-830°C/ 840°C-850°C-860°C	9.5 ohms/square

Table 1: Sheet resistance of deposited $TiSi_2$ as a function of subsequent high-temperature dielectric deposition at the indicated processing temperatures. The sheet resistance before high-temperature processing was 1 ohm/square.

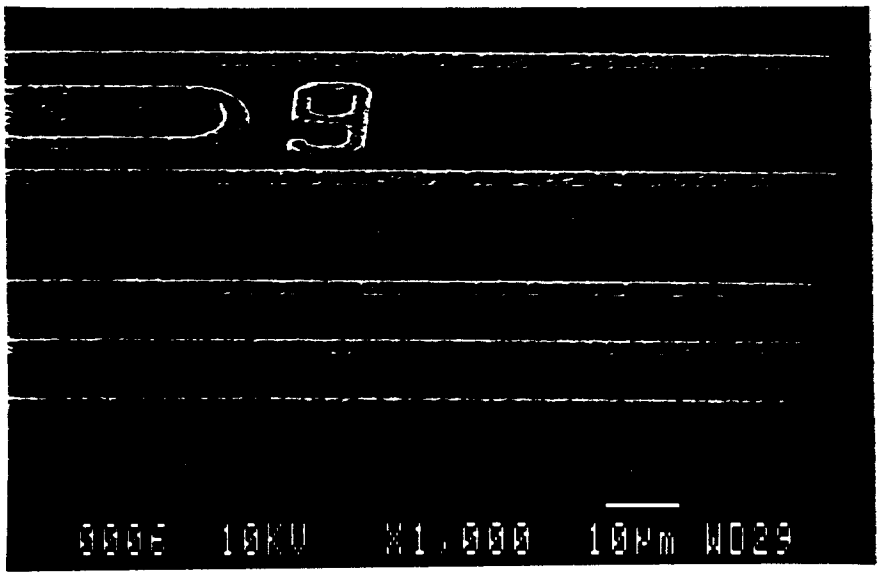

Fig. 14: Photomicrograph of a patterned $TiSi_2$ film after passivation by LPCVD Si_3N_4, deposited at 820°C. The line width is 3µm.

2.3 *Three-Dimensional Electrode Arrays*

Since the structure and process used for our electrode arrays is inherently planar, one- and two-dimensional arrays are easily realized; however, neural systems are three-dimensional, and thus for any practical prosthetic device it is of interest to be able to define three-dimensional stimulating arrays in order to fully instrument the target tissue volume. This requires a method for assembling several planar probes to create the needed structure [Hoogerwerf 94].

Since many of our efforts in this area have been supported under a separate recording contract, we will not give a complete account of this work here but will simply indicate the status of efforts in ths area, which are critical to the realization of the large stimulating arrays that are needed to test the feasibility of full neural prostheses. The development of a technique for assembling 3D arrays of planar probes is now essentially complete. Figure 15 shows the approach taken, which uses electroplated beam leads on the probes to form the lead transfers. These gold tabs are bent at right angles and attached to the platform using conventional thermocompression or ultrasonic bonding. The lead transfers are made via small low-profile "wings" on the sides of the probes. These wings permit the platform to be supported firmly by a simple fixture during the bonding process and allow the bonding wedge to enter between probes on 200μm centers. Micromachined spacers hold the individual probes parallel in the array and fit in slots in the rear of the probes.

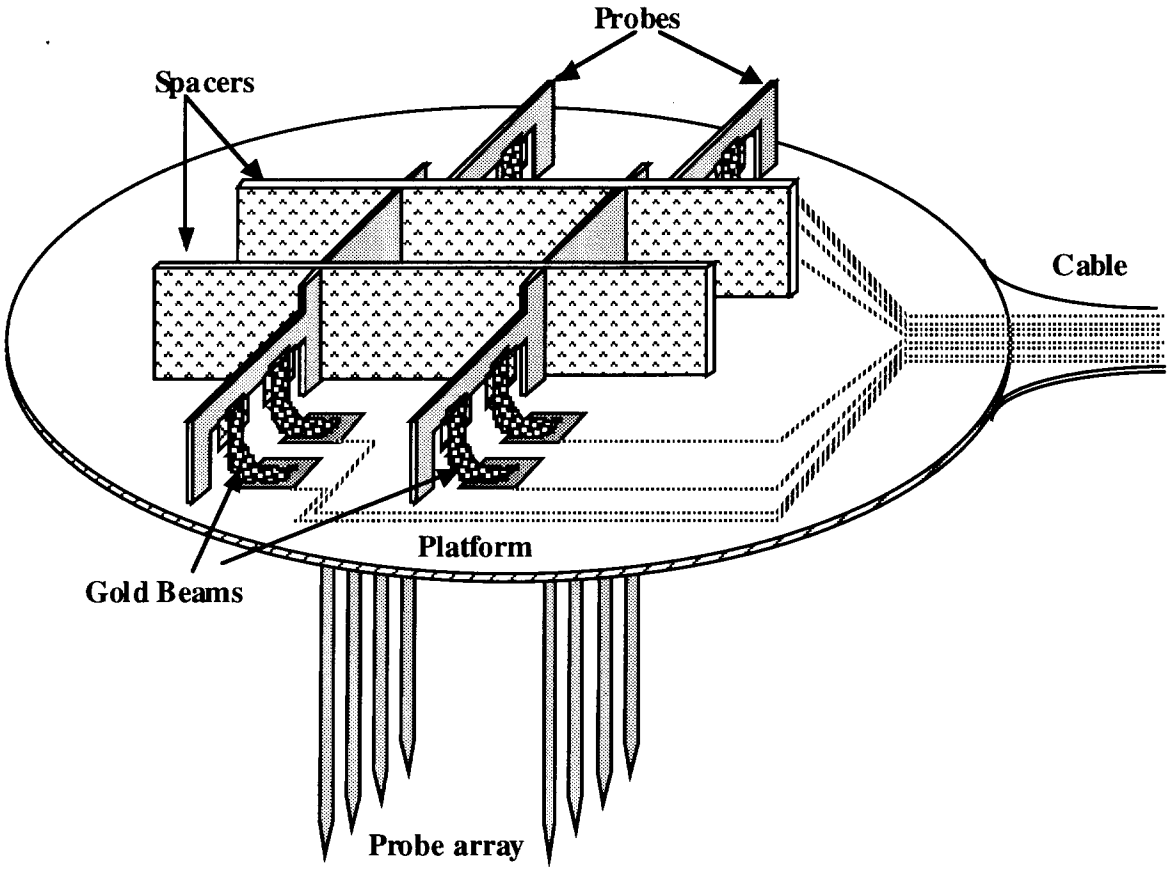

Fig. 15: Basic structure of a 3D microassembly of two-dimensional probes. The lead transfers are via gold-plated tabs that are bent at right angles and bonded ultrasonically to gold pads on the platform.

The bonding areas are finally covered with silastic to provide good insulation over the lead transfers. Figure 16 shows two views of a fully-assembled 3D probe array of eight 16-shank probes and 128 total shanks (an 8x16-shank array). The shanks are on 200μm centers, which is approximately half (double the density) that thought to be needed for a stimulating prosthesis. The cortical platform uses a slotted ribbon cable to connect to a percutaneous plug, where conventional wire bonding is used to connect to the connector pins. We are just now beginning to study the insertion characteristics of these arrays.

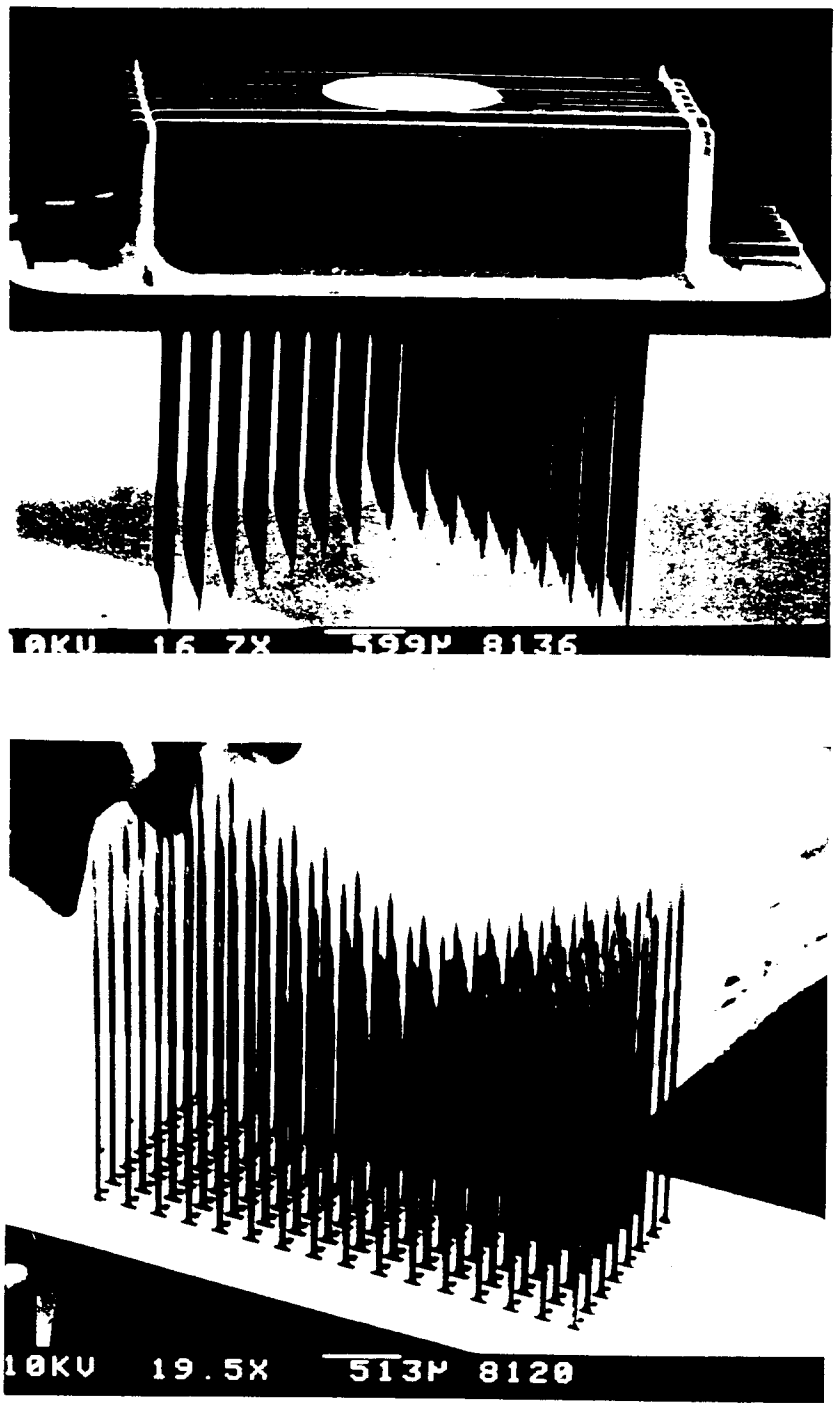

Fig. 16: SEM views of a fully-assembled and bonded 8x16 shank array consisting of 8 16-shank probes. The shanks are on 200µm centers.

2.4 *External Distribution of Passive Probes*

The distribution of passive probes to users external to the University of Michigan has been an ongoing effort since 1988. Since that time, over 1500 devices have been supplied to interested investigators for use in such areas as cortex (motor, auditory, visual), deep brain structures (hippocampus, inferior colliculus, cochlear nucleus), nerve (peripheral, cranial), and even heart muscle. The original impetus to this distribution effort was to obtain feedback on the functionality of the probes in a variety of applications, and so the distribution was carried out under recording and stimulating probe contracts from the Neural Prosthesis Program. The increasing demand for probes and customization of designs for various research projects, however, led to the need for greater resources. Many of the probes are now being provided through support from the Center for Neural Communication Technology, funded by the NIH-NCRR in May 1994, while passive and active probe technology development is still funded through the NINDS Neural Prosthesis Program.

During the past three years, three new mask sets were processed based on designs from external investigators. Some of the more active probe users who have submitted custom designs include Drs. William Agnew and Douglas McCreery of Huntington Medical Research Institutes, Dr. Steven Goldstein of the University of Michigan, Dr. Steven Highstein of Washington University, and Dr. J. A. Hoffer of Simon Fraser University.

Seven custom designs have been fabricated for the Huntington group for their NPP project to study safe stimulation of cortex and peripheral nerve. Mr. Leo Bullara of Huntington visited our laboratory during the last contract period to learn more about the design and fabrication processes and to exchange ideas on custom designs. Two new designs submitted by the Huntington group (one for cortical and the other for spinal cord stimulation) are currently in fabrication. We look forward to extended collaboration with Huntington and the House Ear Institute on electrodes for stimulation of the auditory brainstem.

One of the more unusual probes designed for an external investigator is shown in Fig. 17. This probe was designed by Dr. Steven Goldstein and colleagues for stimulation of chick embryo leg muscle. The round protrusion is a handling tab to aid in insertion. A strip of shallow boron-doped silicon at the neck of this tab permits it to be easily snapped off once the probe is in place. The longest shank, designed to be inserted completely through the leg, has holes to accommodate insertion an anchoring pin once the probe has been placed. This probe has successfully produced contractions of the leg muscle, and a second iteration of the design is currently in process.

Dr. Highstein, an external collaborator on the Center grant, is applying passive probe technology to vestibular nerve in the toadfish. We have fabricated four "sieve" electrode designs for him, the most recent of which is shown in Fig. 18. This electrode is designed to be placed into a severed nerve and has holes through which the nerve fibers can regenerate. Nine of the holes on the design shown are outfitted with recording sites. Dr. Highstein is working with PI Medical of Portland, Oregon, to develop a hybrid system which will make use of their cable technology to obtain the longer, more robust interconnect needed in his preparation.

Fig. 17: Probe designed by Drs. Steven Goldstein and John Germiller. The round protrusion (800μm in diameter) is a break-off handling tab. This probe is used to stimulate chick embryo leg muscle.

Three designs have been fabricated for Dr. Hoffer's group for recording and stimulation of peripheral nerve in the behaving cat. The newest design (Fig. 19) is an iteration based on experience with the first design. It has a slotted cable for increased flexibility in the radial direction, sharper barbs for improved positional stability, a "hook" to aid in insertion and as a possible location for a suture tie, and holes through the bonding pads so that lead-out wires can be passed through and held during application of conductive epoxy.

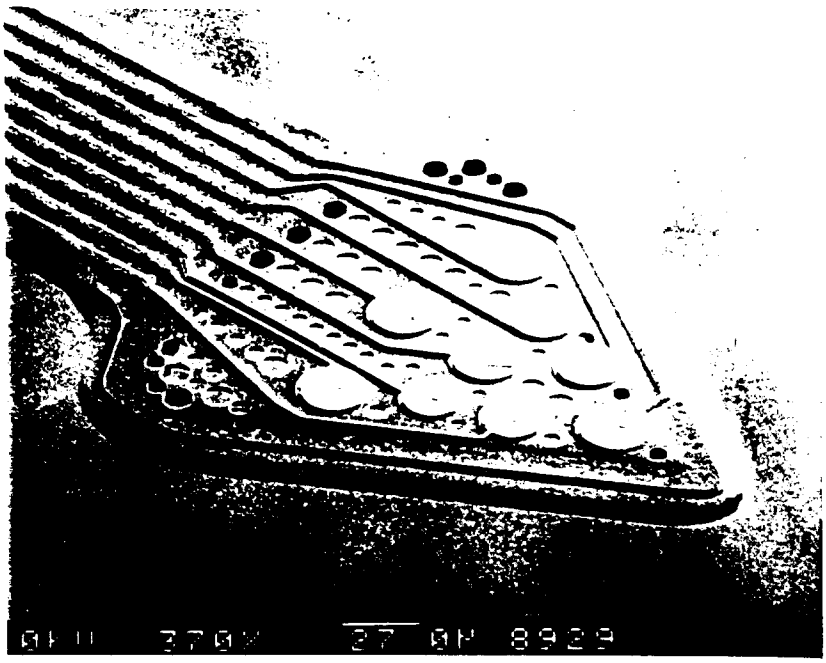

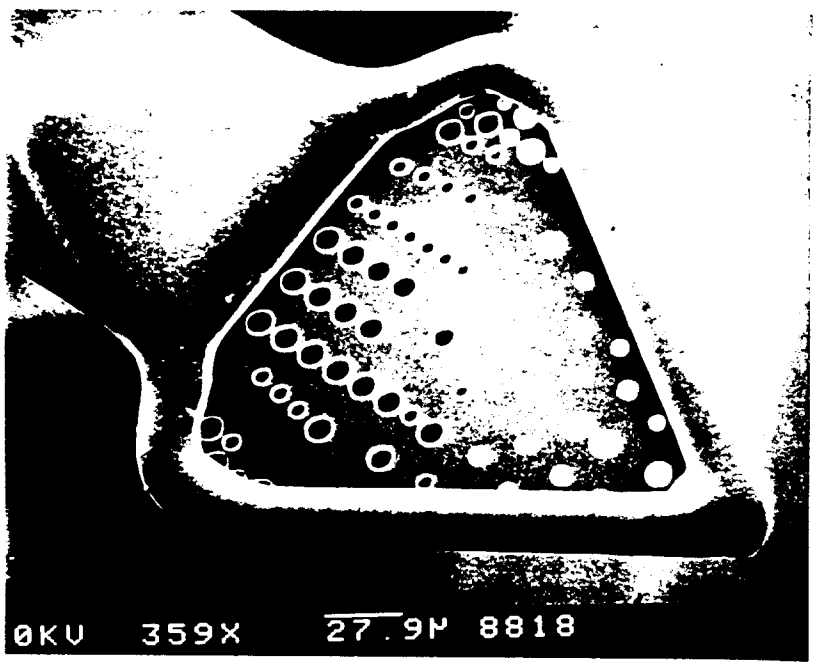

Fig. 18: Sieve electrode designed for Dr. Steven Highstein. Nine of the holes (5µm and 8µm in diameter) have annular recording sites so that recordings can be obtained from regenerated nerve fibers. The sites reside on a dielectric membrane, as is illustrated by the photo on the lower right. A boron-doped silicon ring acts as a support structure for this membrane.

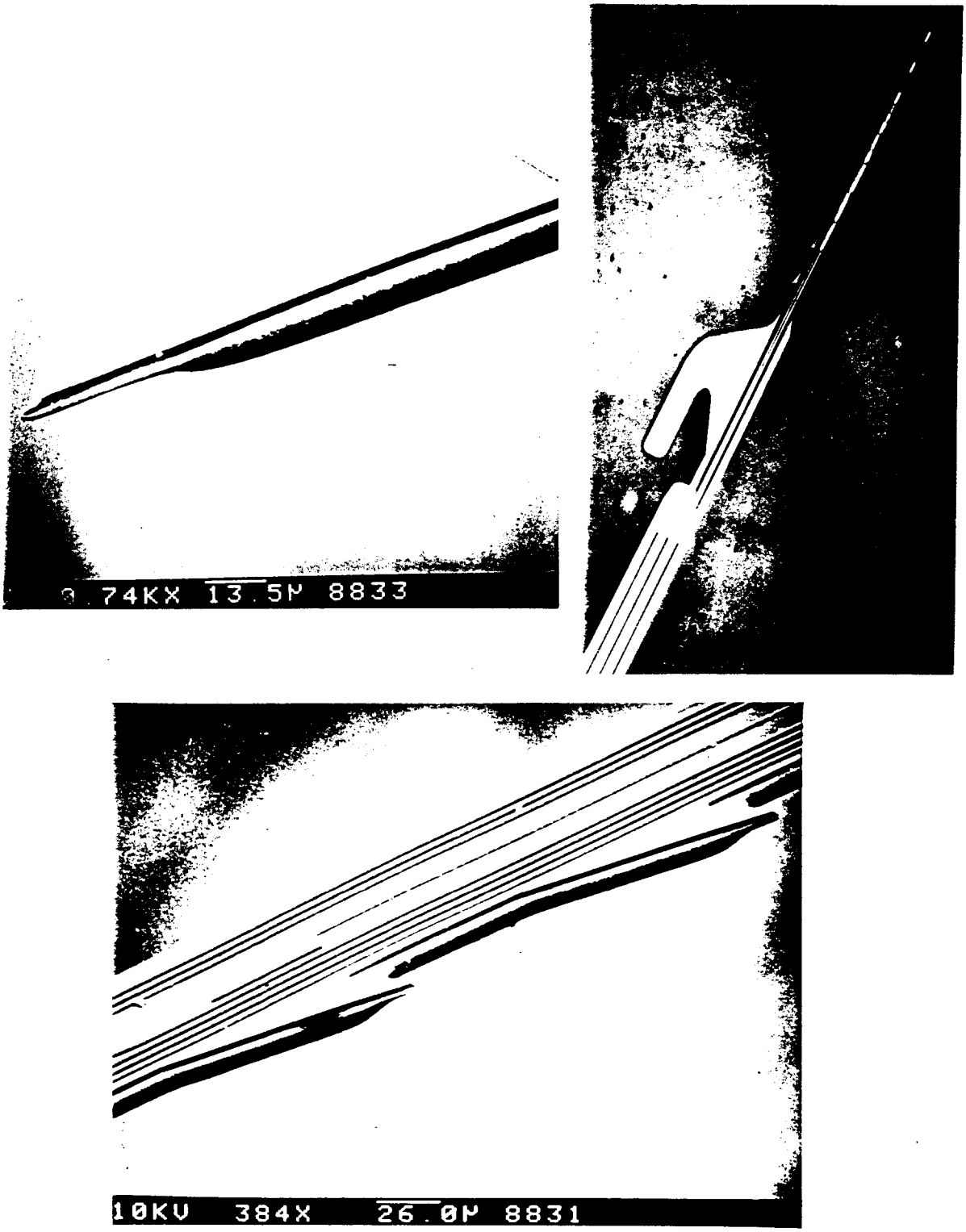

Fig. 19: A new probe design fabricated for Dr. J. A. Hoffer. Several new features were incorporated into this design based on experiences with a previous design: a slotted cable, sharper barbs, a suture/handling hook, and holes through the bonding pads. The sites are on 125µm centers. The shallow-boron formed. sharpened tip permits penetration into the nerve.

3. *In-Vitro and In-Vivo Characterization*

3.1 *Electrode site verification and testing*

Short- and long-term *in-vitro*, short- and long-term *in-vivo*, and model testing are critical to understanding the relationships among site design, maintenance of sites, flow of current between sites, tissue volume specificity for activation, and tissue damage. We have developed test cells and experiments which can address these issues in terms of short-term tests. Long-term soak tests of stimulating electrodes and long-term tests tissue compatibility are also needed, and some of these studies are being carried out by other participants in the NPP, and especially by the Huntington Medical Research Institute. The following paragraphs outline the methods which we currently have for the testing of electrode sites and small systems of electrodes.

3.2 *Activation of Iridium Arrays*

Before using these electrode arrays, iridium oxide is grown on the electrode sites to increase the amount of charge density that can be safely delivered by the site to tissue [Anderson 89]. We have developed a second-generation automated test facility that allows electrochemical activation of the iridium (oxide growth), charge-balanced current-pulse testing, and electrode site impedance monitoring. The current technology in use for this system consists of an IBM-compatible PC equipped with National Instruments D/A and A/D cards and running LabView software. This system is shown in Fig. 20. The object is to make an activation instrument which can be purchased by a user of the Michigan probes with a minimum of custom electronics. The automated system, through the use of a relay multiplexer, has the ability to move from one site to another in performing activation without the need for manually changing the external probe connections. The system can also be operated as a single-channel system. All procedures are controlled by interactive software that collects all the desired information and sets the test protocols accordingly. Results from the experiments are sent back to the host computer and displayed on a monitor. They can also be printed to provide a permanent record for each probe fabricated. Electrode activation is carried out in phosphate-buffered solutions. Recently, following the advice of EIC Laboratories, we have begun using a square voltage waveform applied to the electrode in a standard three-electrode cell configuration. The automated equipment allows a wide range of parameter choices but we have obtained good results when the applied voltage is varied from -0.85V to +0.75V versus a saturated calomel electrode (SCE). The electrode attains a charge capacity (total amount of charge delivered per unit geometric area in one voltage cycle during activation) of 30mC/cm^2 after 300-400 cycles. Previously, we activated to 100mC/cm^2 but have now reduced this level for better mechanical stability of the oxide and a shorter activation time.

When the electrodes are used for current pulsing, they can only deliver a small percentage of their total charge capacity before the potential on the electrode exceeds the water window and oxygen or hydrogen is evolved through the electrolysis of water [Beebe 88]. The maximum charge delivery is defined as the amount of charge that can be delivered in a pulse test before the potential on the electrode is high enough to cause gassing (although the gassing may not show up as discrete bubbles). When using short pulses, about 1.5 of the 30mC/cm^2 can be used without gassing [Tanghe 92-1]. For a 100μsec pulse from a 1000μm^2 site, this corresponds to 150μA. This current is comparable to that needed in a realistic system delivering a maximum current of 100 to 300μA [McCreery 86]. We have experimented with using an anodic bias of 0.6V on the sites and have found a

much lower back voltage (see Fig. 21). EIC has shown that using an anodic bias can significantly increase the amount of stored charge that can be delivered to tissue [Robblee 90-1]. While this increases the efficiency of the system, the danger here is that the bias moves the operating point of the electrode much closer to the water window.

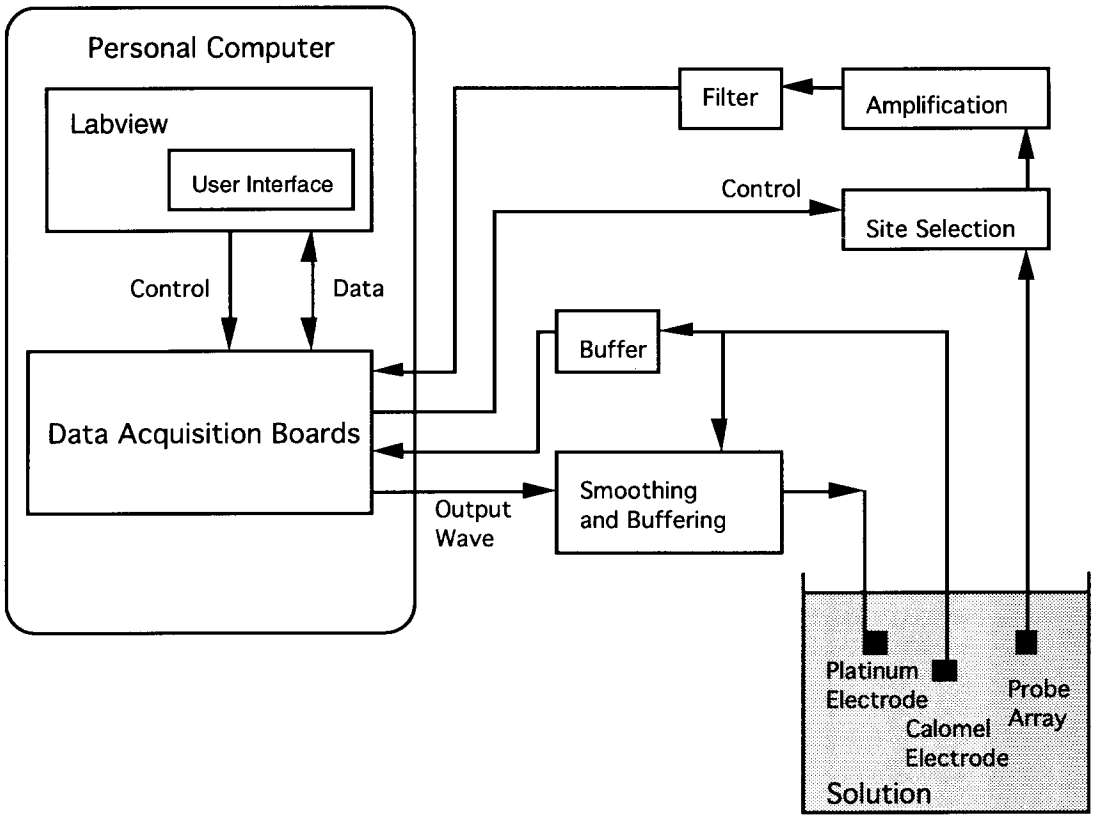

Fig. 20: Block diagram showing the LABView-based automated test station for electrode site activation and characterization.

3.3 Stimulation Implants

The effectiveness of the above electrode conditioning strategy is demonstrated by an automated in-vivo testing system. As in the activation system described above, the electronics are an IBM-PC computer, National Instruments data acquisition boards, voltage to current electronics, a multiplexer, and LABView software (Fig. 22). The animal test chamber is arranged such that, for a four hour testing period, the animal can roam in a small cage tethered by electrical connections passed through a swivel interconnect. The software can deliver charge-balanced pulses between a single site and ground or between two sites, can record the source voltage, and any evoked potential which arises can be recorded from a third electrode. A day-long experiment can be preprogrammed to deliver several hours of stimulation with data stored about the state of the electrode and animal response at intermediate times over the experiment period. Over the course of a week of testing, the condition of the electrode sites and the tissue are tracked. Impedance measures, access voltage waveforms, evoked responses, and cyclic voltammetry curves are collected by the system for all the experimental conditions. A summary of the experimental protocol is given in Fig. 23.

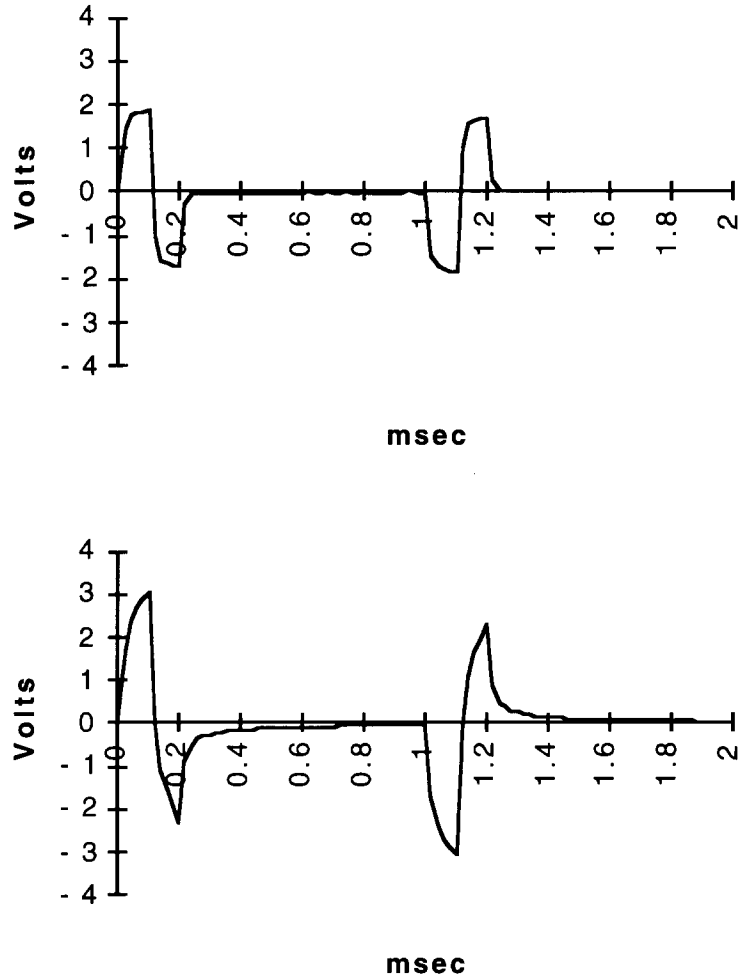

Fig. 21: Comparision of the back-voltage generated *in vitro* on a 1000μm^2 site due to current flow when an interpulse anodic bias of 0.6V is used (above) versus no interpulse bias (below).

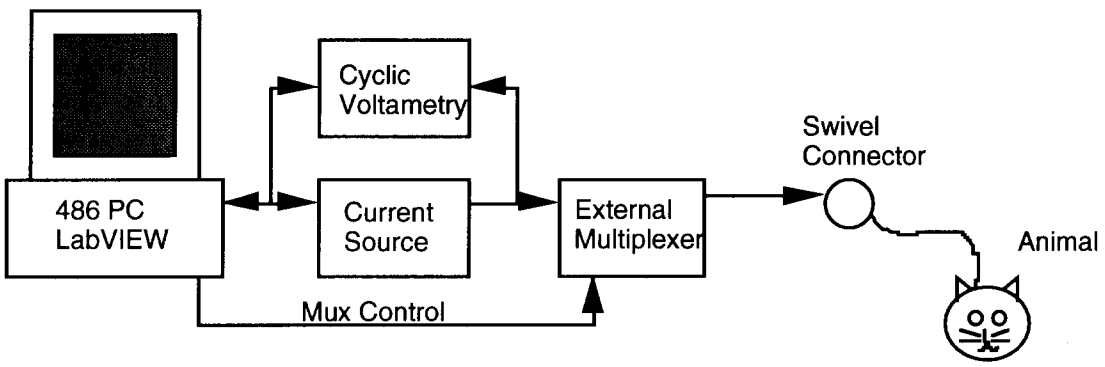

Fig. 22: Block diagram of the chronic stimulation test system

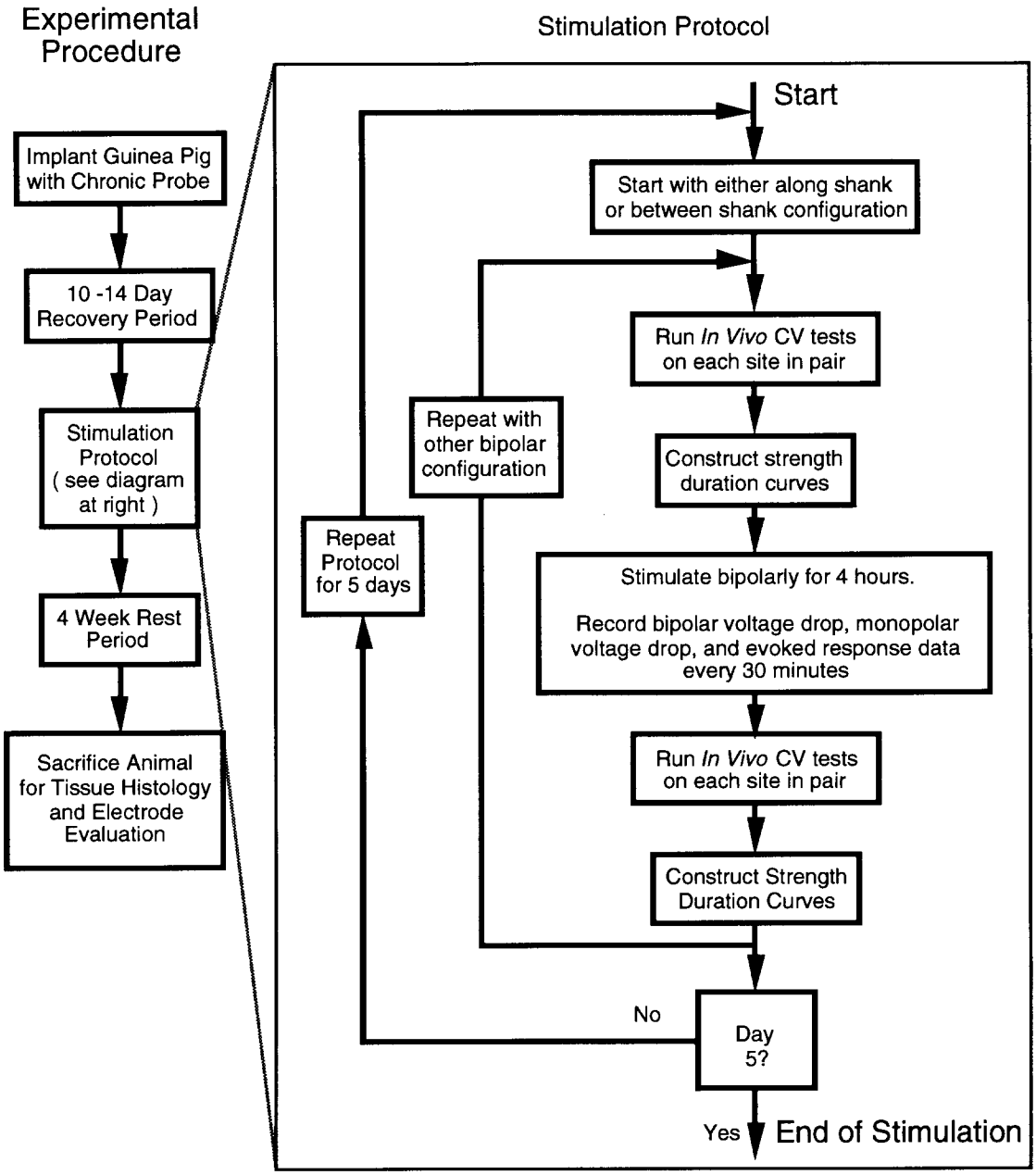

Fig. 23: Stimulation protocol used for chronic implant experiments.

The purpose of these experiments is to compare two types of bipolar stimulation. With a two-dimensional electrode array, a bipolar pair can be formed from electrodes on different shanks or from electrodes on the same shank. While the site size and site spacing may be the same for these two bipolar configurations, the current path between the two electrodes will be different. When passing current between sites on different shanks ("between shank" stimulation), the current is forced to flow through tissue. However, when sites on the same shank form a bipolar pair ("along shank" stimulation), the presence of the shank and a fluid filled encapsulating sheath may result in an altermate current flow path.

Plots of impedance, access resistance, anodic voltage, and cathodic voltage are shown below for a typical experiment (Figs. 24-31). Impedance data was acquired using a 1kHz sinusoidal, 10μA current signal. The access resistance was calculated by dividing the initial voltage drop (in response to a current pulse) by the initial current. Although most of the access resistance is due to current flow through tissue near the site, the bipolar current path will concentrate current between the two sites and may result in a different resistance than the sum of the two monopolar resistances. The difference in impedance and access resistance (Figs. 26, 29) for bipolar vs. monopolar stimulation was calculated as the bipolar impedance or resistance minus the monopolar impedance or resistance for each site. A positive value indicates that the bipolar site-to-site current path has a higher resistance than the sum of the two monopolar site-to-ground paths. Changes in this difference measurement may indicate a change in the tissue between the sites or in the current path. The anodic and cathodic voltages (Figs. 30, 31) were calculated by taking the maximum voltage developed due to an anodic/cathodic current pulse and subtracting off the voltage drop due to access resistance. The source is the site which receives a cathodic-first biphasic pulse. The magnitude of the pulse was 50μA and the duration was 0.1msec/phase. The sink receives a pulse of equal magnitude but opposite polarity.

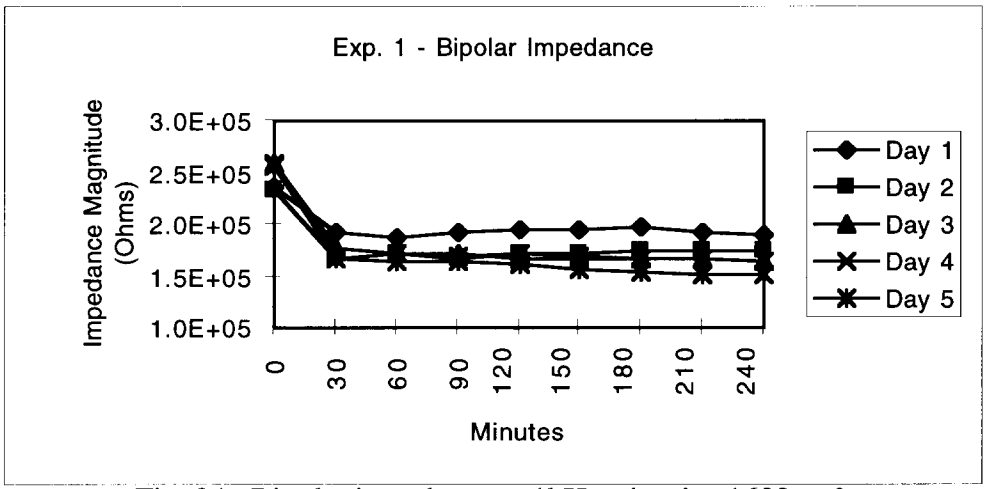

Fig. 24: Bipolar impedance at 1kHz, site size 1600μm².

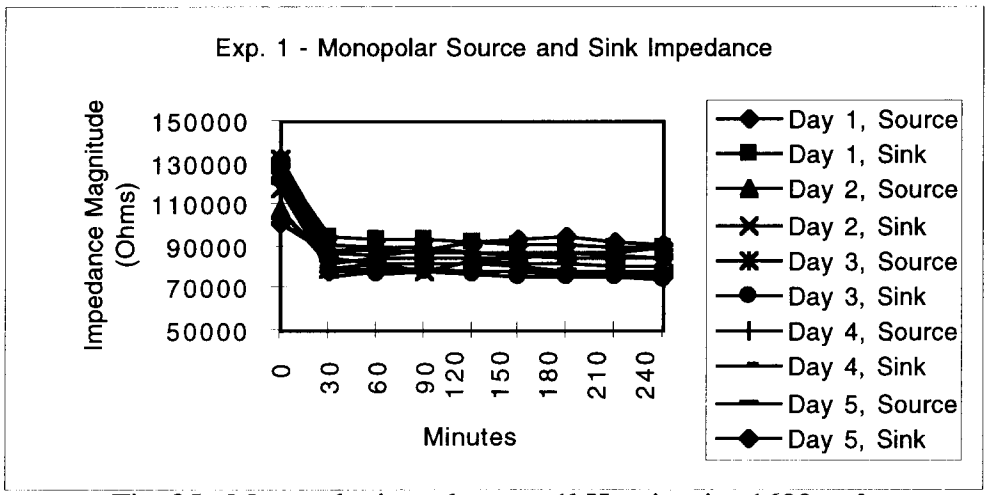

Fig. 25: Monopolar impedance at 1kHz, site size 1600μm².

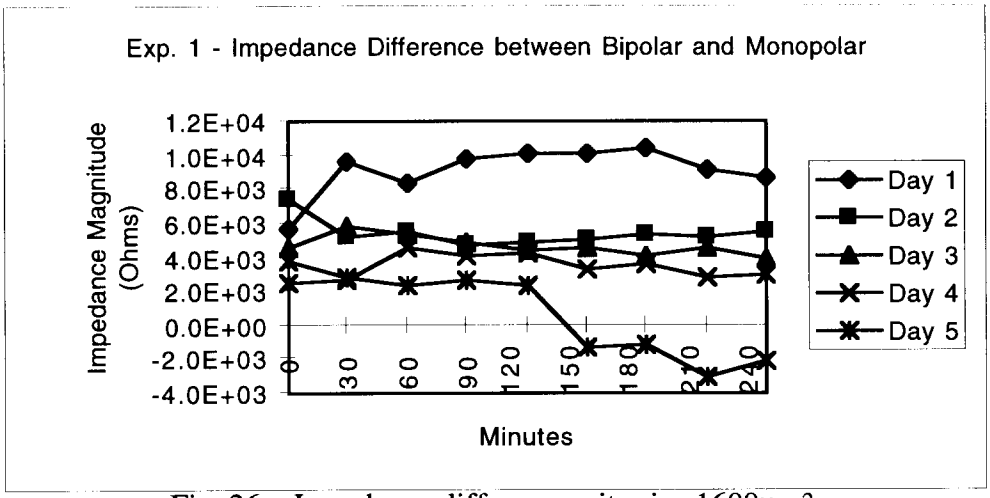

Fig. 26: Impedance difference, site size 1600μm².

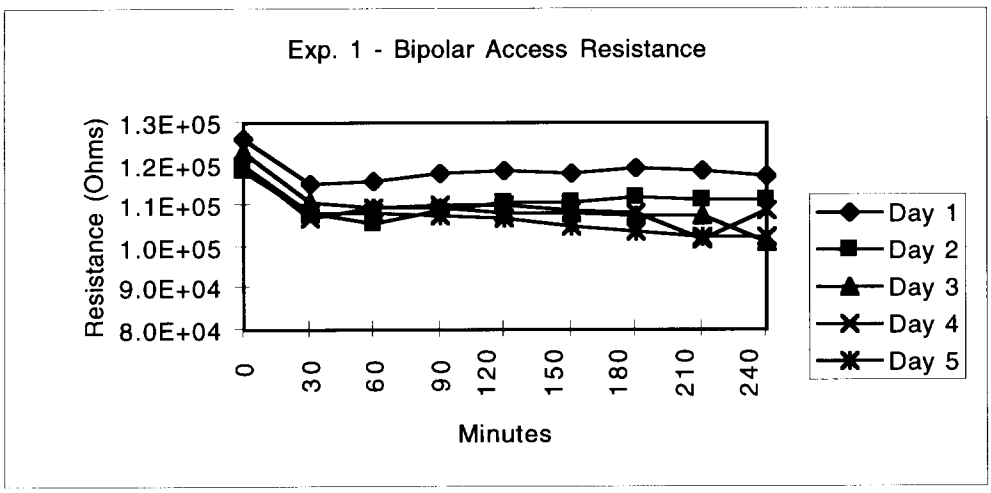

Fig. 27: Bipolar access resistance, site size 1600μm².

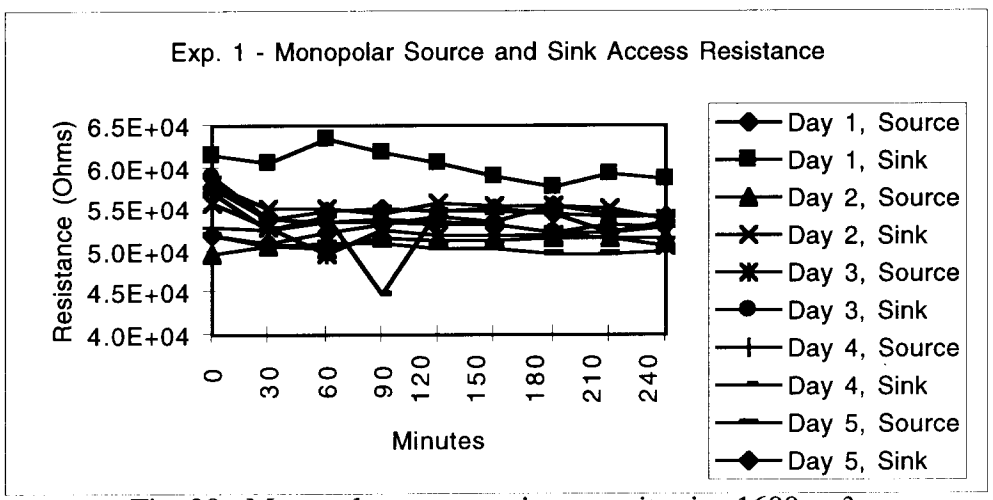

Fig. 28: Monopolar access resistance, site size 1600μm².

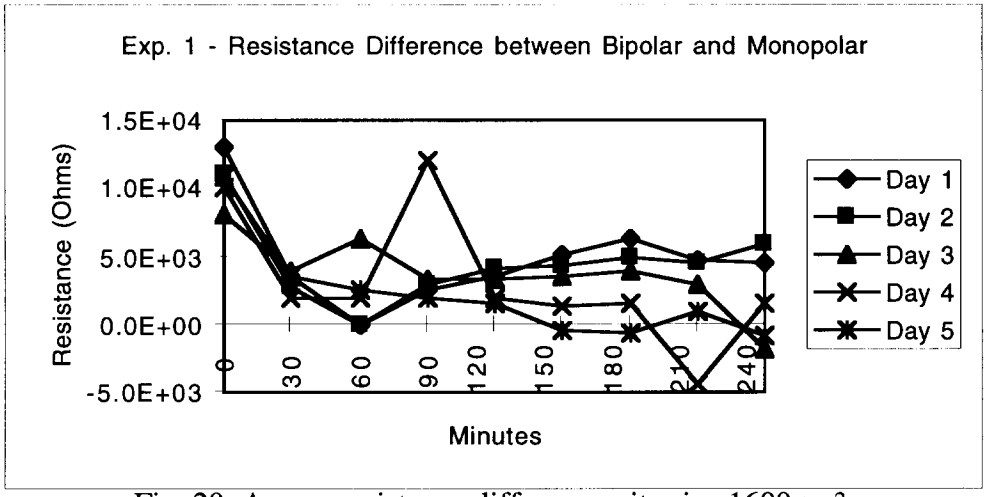

Fig. 29: Access resistance difference, site size 1600μm².

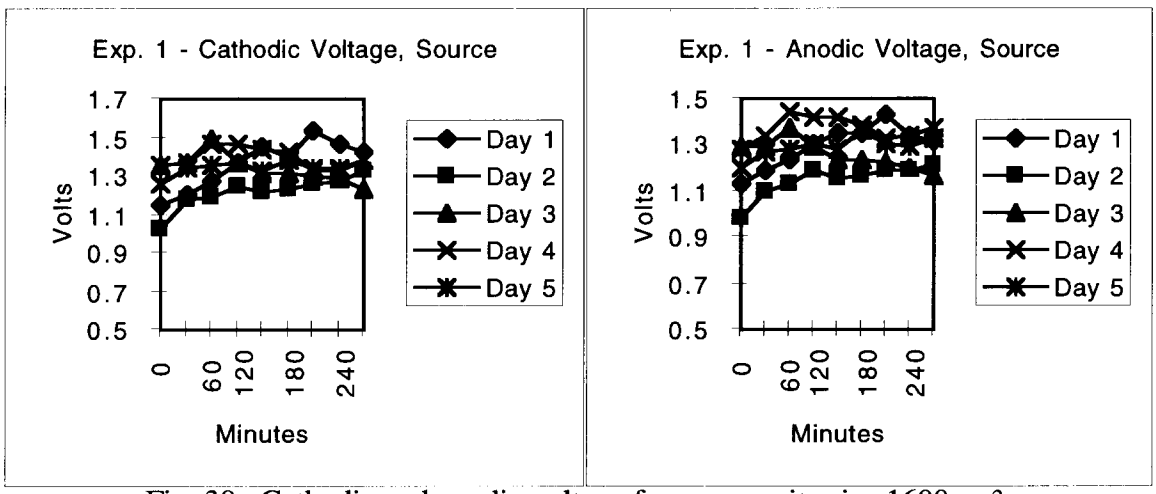

Fig. 30: Cathodic and anodic voltage for source, site size 1600μm².

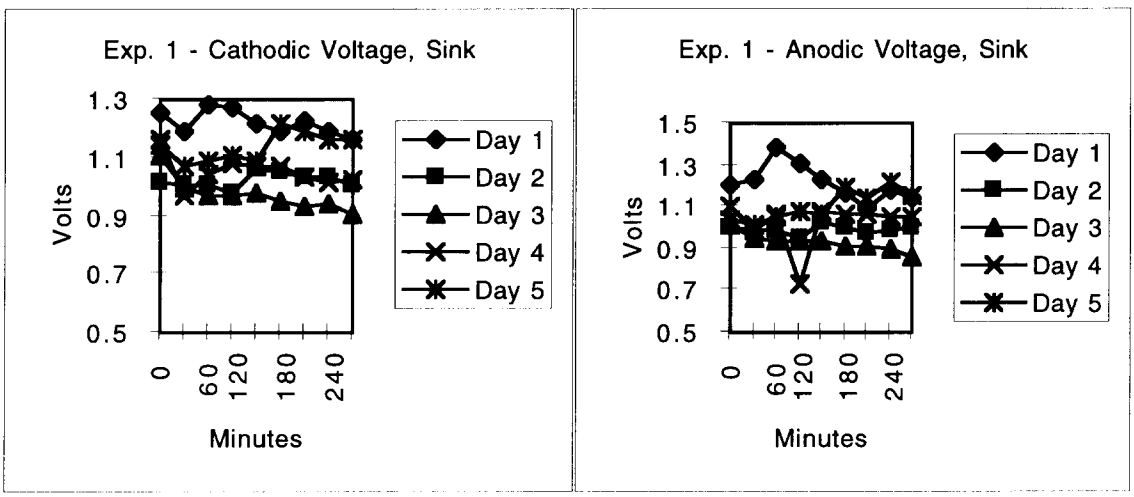

Fig. 31: Cathodic and anodic voltage for sink, site size 1600μm².

Overall, these data show that the electrical parameters of the electrode-tissue system were fairly constant over a week of stimulation and are representative of measurements taken for most of the experiments. Along-shank and between-shank stimulation were compared in several experiments and no difference in electrical parameters was noticed between the two configurations. A total of fifteen experiments were run, most of them showing stable electrical characteristics.

In-vivo cyclic voltammagrams were also recorded during the week of stimulation. A series of these data is shown below (Fig. 32). The CV curves appeared to be affected by implantation and by pulsing. The top waveform exhibits well defined current peaks typical of iridium oxide. After two weeks of implantation, the current peaks are gone and the charge storage has diminished. It is unclear what causes this change. One possible explanation is that the encapsulating glial sheath is limiting the flow of ions to the interface. However, impedance measurements taken immediately post-op and after two weeks of implantation show little change. Another possible cause is our measurement technique. What is shown above is data from an initial, single voltage sweep. We have recently learned that it may be better to use two sweeps: the first to condition the oxide and the second to record the measurement.

It was further noted that the CV curves tended to shift after pulsing. Before pulsing, the current flow at the most negative potential was low. After pulsing, this same potential resulted in a relatively high current flow, indicative of gas evolution. Again, it is uncertain why this is happening. Possible causes include a change in the resistance of the tissue near the site (which would increase the uncompensated resistance in the CV measurement) or a change in pH which may affect the potentials at which Faradaic reactions proceed.

A long term *in vitro* pulse experiment was also run. This test followed a similar stimulation protocol as the in-vivo test except that the electrode was placed in PBS. The probe used in this test was fabricated with the new metalization protocol. Pulsing was performed to validate the adhesion of the iridium. A total of 200 million pulses were applied to the electrode sites. After an initial drop in impedance during the first day of testing, no subsequent changes were seen. The bipolar impedances for five separate days are plotted below in Fig. 33.

Tissue and site damage analysis

The assessment of tissue damage is made postmortem using measurements of glial sheath and the numbers of remaining normal neurons in the area. It is of particular interest to correlate patterns of tissue damage with the magnitude and path of current flow and with the design of the electrode site and substrate. We are attempting to understand if the current flow pattern changes under conditions of damage by these physiological and histopathological correlations. Quantitative neural histology and three-dimensional analysis of the tissue using confocal microscopy are being conducted with the help of the Center for Neural Communication Technology at the University of Michigan using facilities located in the Kresge Hearing Research Institute and the Department of Anatomy and Cell Biology. Sites are tested for the presence of biological material and are visually inspected for morphological changes. Elemental analysis and visualization of the site and electrode substrate are carried out using the electron microscopy facilities located in the Department of Anatomy and Cell Biology and the Department of Material Science and Engineering. Hypotheses about impedance changes and tissue damage can be tested by tissue volume models computed for the experimental conditions. This work has just recently been undertaken and will be continued under the new contract.

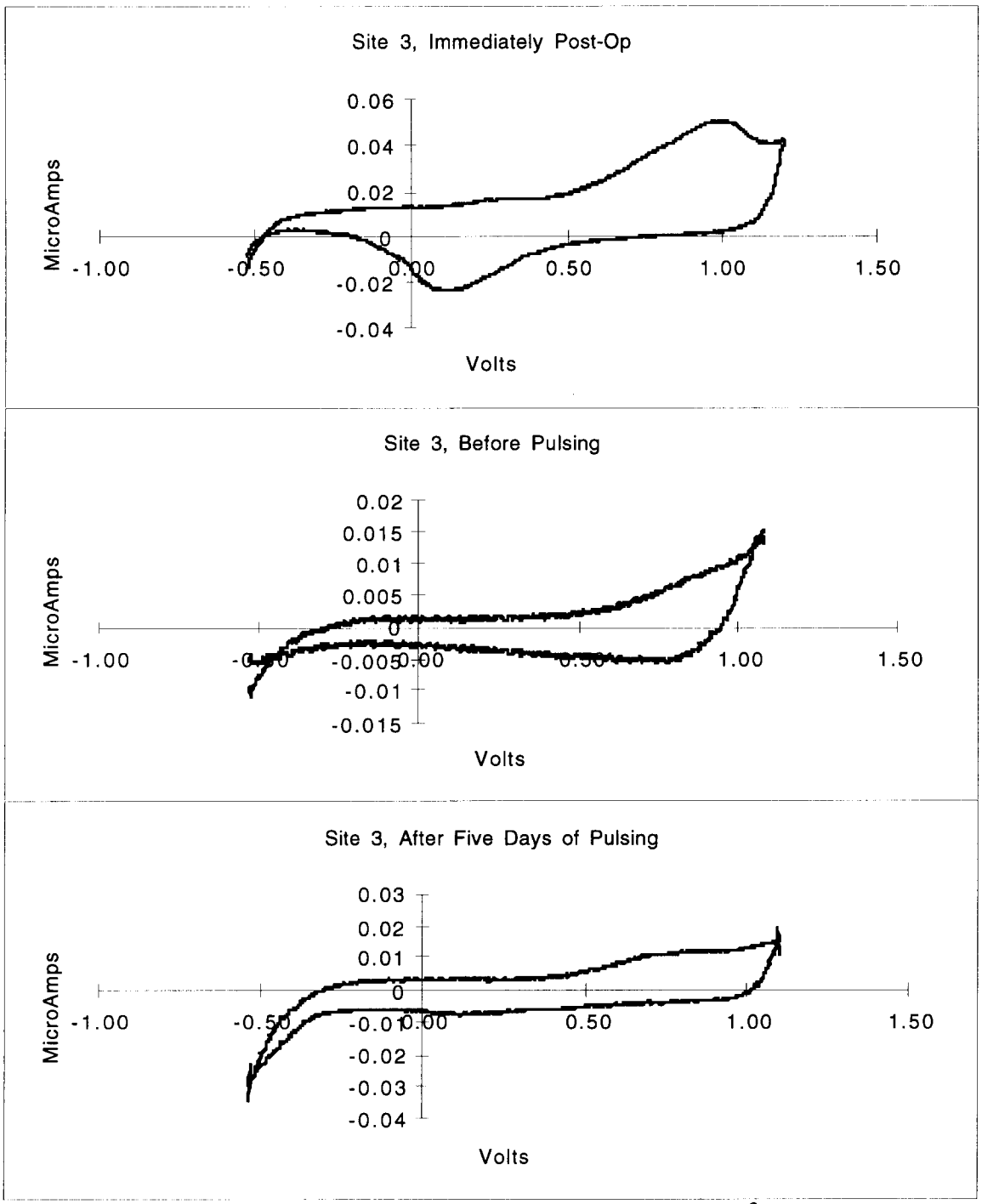

Fig. 32: In vivo cyclic voltammagrams for a 400μm^2 site.

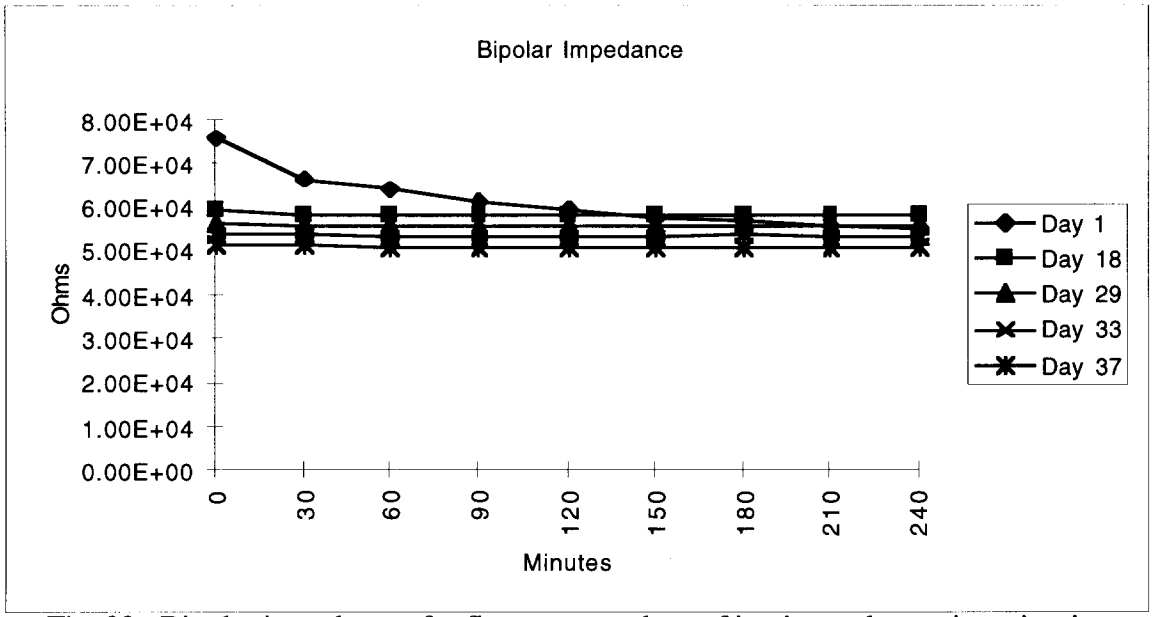

Fig. 33: Bipolar impedances for five separate days of in vitro pulse testing, site size 1000μm^2.

3.4 Penetration Studies

The development of three-dimensional probe arrays and a desire to scale probe cross-sections to still smaller dimensions reinforces the need to understand the physics of pia arachnoid penetration and the need to develop optimum methods for introducing the probes into tissue. The forces required to penetrate the pia result in cortical compression and possible damage to and/or ischemia in the underlying tissue. This can initiate severe edema, leading to the displacement of the array or an inability to stimulate the tissue. We have done considerable work during the past few years to understand the strength of these probe structures as a function of their dimensions and the requirements for penetrating both pia and dura mater [Najafi 90-2] and have recently begun a number of experiments using a computer-controlled microdrive to characterize the penetration characteristics of the probes as a function of tip shape. Single-shank and multi-shank probes have been used with tip structures spanning the range shown in Fig. 8 (tip tapers, 10° to 45°, deep and shallow-diffused). For the shallow-diffused 10° tips, the dimpling of the pia is quite small and probes with up to 10 shanks have been seen to penetrate quite easily. In 2D arrays, it appears better to use shanks all of the same length or even structures where the outer shanks are longer for easier penetration, as shown in Fig. 16. The intuitive structure having a longer central shank and decreasing lengths on the outer shanks does not penetrate as cleanly and produces greater dimpling. All of the test probes used in these studies have had integrated strain gauges built into their shanks, allowing force to be monitored as a function of probe displacement during penetration. Figure 34 shows a comparison between a sharp tip and a more blunt deep-diffused tip in penetrating the pia arachnoid in guinea pig. Pia dimpling is over 700μm for the larger tip and less than 300μm for the sharper one. A significant observation in using the sharper tips is that penetrated blood vessels self-seal around them so that there is no detectable bleeding observed. We have repeatedly penetrated small and large surface vessels with the sharper tips and seen this result, whereas the larger tips induce bleeding upon penetration. Preliminary experiments with 8x8-shank versions of the 3D structure shown in Fig. 16 have shown that these structures, which have shallow-diffused sharp tips, penetrate guinea pig pia quite readily.

We are still studying penetration forces and dimpling as a function of insertion speed. Past experiments have been performed with insertion speeds between 0.1mm/sec and 5mm/sec. Work in this area will continue under the new contract.

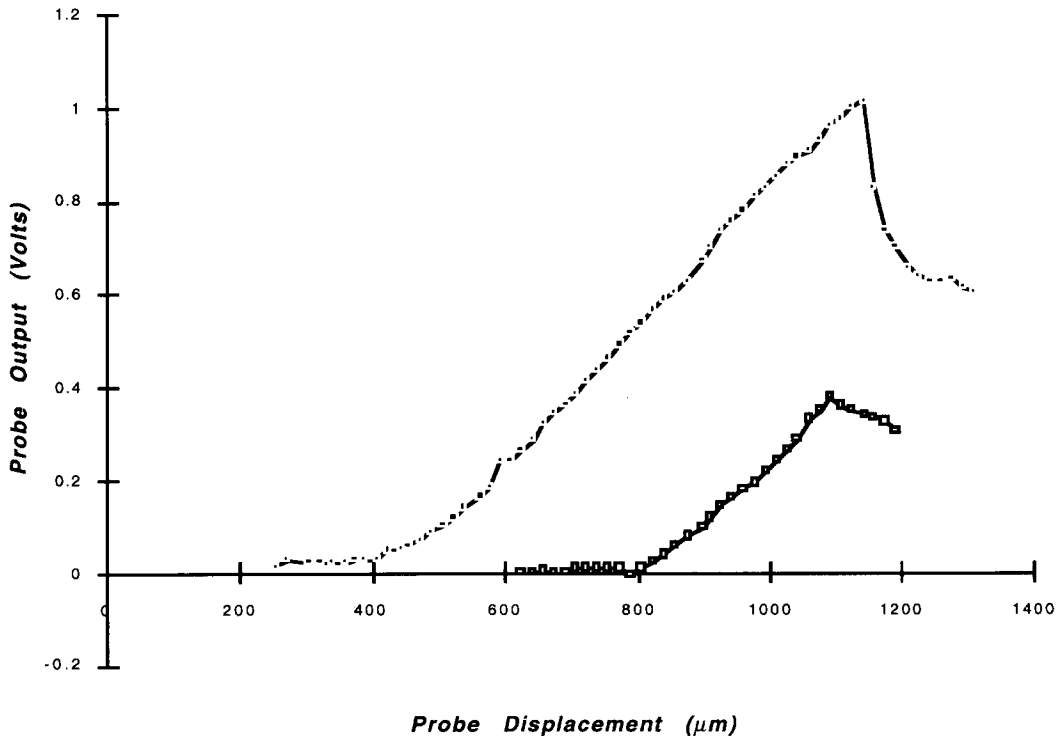

Fig. 34: Output from integrated probe strain gauges as a function of probe displacement during penetrations of the pia arachnoid in guinea pig using 45° deep-diffused probe tips and 10° shallow-diffused tips. The strain gauge output can be taken as indicative of force. The inserting microdrive was computer controlled and computer monitored. The insertion speed here was 1mm/sec.

4. Active Stimulating Arrays

The driving force behind the integration of electronics on the probe substrate is the desire to limit the number of output leads to a small number (e.g., five) while permitting the use of many different sites for high spatial selectivity. A small number of external leads is essential for two reasons. First, it is difficult to attach very many leads to a probe only a few millimeters across, and this part of the process is a one-at-a-time enterprise that is labor intensive. Second, when attached, the leads impose a stiffness and tethering on the probe that makes implantation difficult and can induce migration in long-term implant situations. For a stimulating probe, the goal is a circuit block that can accept serial data from the outside world and will then generate, on-chip, the required currents for each of the addressed sites. This implies a digital-to-analog converter (DAC) per active site, and that converter must be capable of biphasic current drive. It is generally felt that such a device should have 8-bit biphasic resolution over a current range of at least ±100μA and perhaps as great as ±254μA. We have elected to keep virtually all timing external in order to minimize the complexity of the probe itself, i.e., currents are started and stopped on external command with no timing performed on the probe. It is also clear, however, that

there must be a variety of safety checks on the probe to protect against malfunctions that could damage the surrounding tissue.

Figure 35 shows a general block diagram of the active probe electronics. An external system maintains a buffer memory loaded with the code sequences needed to launch the intended current patterns from the probe at the proper times. The control system writes this data to the probe over a serial data line. Synchronization is maintained using a separate clock line, and since the probe is to deliver biphasic currents, positive (VDD) and negative (VSS) supplies are required. This implies a five-line system. The data word consists of an address followed by data which sets the amplitude of the intended current pulse. The address and data are latched, and the new current pattern from the probe is initiated. This current pattern, in principle, will be maintained until altered by the external control.

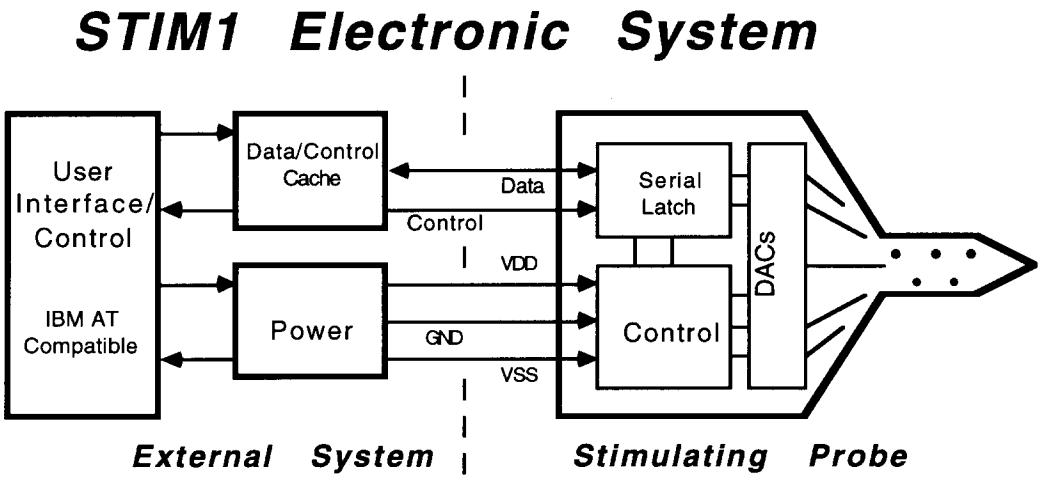

Fig. 35: Overall block diagram of the first-generation active stimulating probe.

In the first-generation series of probes, we designed a family of three probes, staggered in complexity and capability. All three are compatible with the same external drive circuitry, and all three offer 8-bits of biphasic current control across 16 sites. The simplest design (STIM-1b) is a monopolar probe (only one site active at any given time) which routes an externally-produced drive current to the addressed site. The next design (STIM-1a) [Kim 94] is a bipolar probe which accepts two site addresses and a single data word and which then generates positive and negative currents of the indicated amplitude for the selected sites. Only one site pair can be active at a time. Finally, the largest and most complex of the first-generation probes (STIM-1) [Tanghe 92-1] is a full 16-channel multipolar probe which allows any or all of the 16 sites to be active in parallel with drive currents that are set independently. This probe has a number of safety features and operating modes as mentioned below. As stated above, when the present contract began, prototypes of the first three designs had just been fabricated, at least in wafer form. The technology for encapsulating the circuit areas against EDP and against the extracellular fluid was not yet completely worked out. During this contract, we tested the first-generated probes and iterated the designs to correct problems with the first prototypes. In addition, a second-generation probe (STIM-2) [Kim 93] was developed. This probe has eight channels that can be routed via a front-end site selector to 64 different sites. Eight of these sites can be driven simultaneously to provide multipolar stimulation with 8 bits of current amplitude accuracy. A process for successfully merging CMOS electronics with the

passive probe process has now been demonstrated [Ji 92, Kim 93, Lund 94] and working versions of the various probes have been etched from the wafer and demonstrated in-vitro and in-vivo. The following sections summarize the present status of these probe designs.

4.1 Active Probe Fabrication

Figure 36 shows a perspective view of the active probe structure. It is very similar to the passive structure except that it contains CMOS circuitry, which performs signal demultiplexing and other functions. The probe shanks are typically 15μm thick and are defined using a diffused boron etch-stop, just as in the passive devices. Since these shanks are in direct contact with the tissue, they must be grounded. The CMOS circuitry, however, runs at elevated voltages. To provide electrical isolation between the circuitry and the tissue, an n/p p-well epi-CMOS technology is used. The cross-section of this structure is shown in Fig. 37. A p-tub is formed around the circuit areas using a combination of the deep-boron areas (p++) and the p-type substrate under the circuitry. The probe shank and p-tub are grounded, providing the necessary electrical isolation from the n-bulk region, which operates at +5V when the circuit is turned on. Note that the use of an electrochemical etch-stop on n-type material is probably precluded here since the exposed substrate must be p-type and must be grounded.

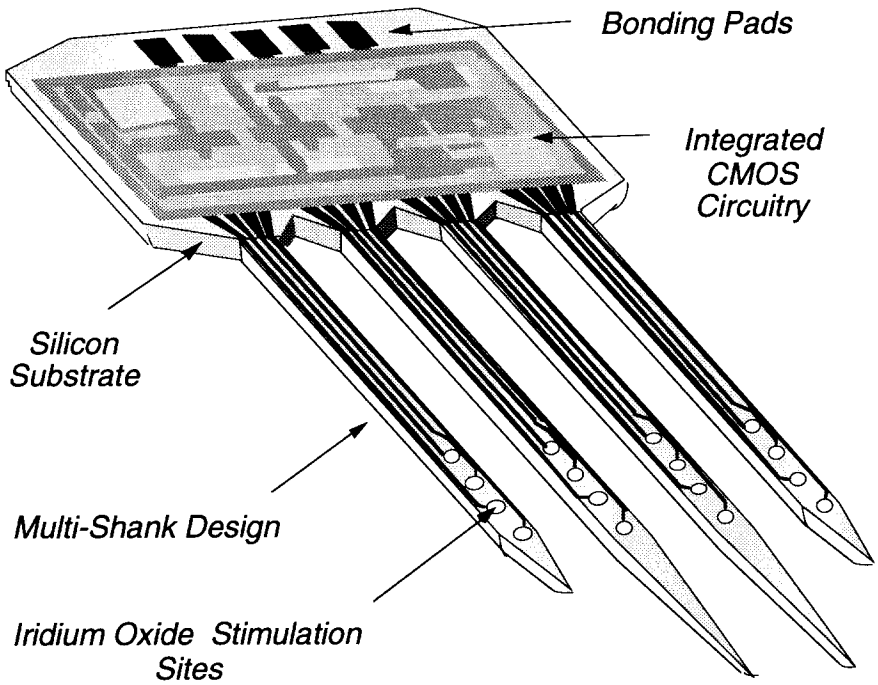

Fig. 36: Perspective view of an active stimulating probe structure.

The fabrication procedure is very similar to a standard CMOS integrated circuit fabrication sequence with steps added to form the probe and the electrode sites. The general process flow is illustrated in Fig. 38. Fabrication starts with a standard p-type silicon wafer that has an n-type epitaxial layer on the surface that is 15μm thick. Next, the p-wells for the circuitry are implanted, followed by the deep boron diffusion to form the intended probe shapes. During this diffusion, the p-wells are driven in to a depth that is

compatible with the circuit process. Next, standard CMOS circuit fabrication takes place through metallization to form the electronics integrated on the probe. Upper dielectrics are deposited to provide insulation for the circuitry and are opened in the areas where the sites and bonding pads are located. These sites and pads are formed by depositing and lifting off iridium, just as in the passive process. Finally, the wafers are thinned from the back and etched in EDP to separate the completed probes.

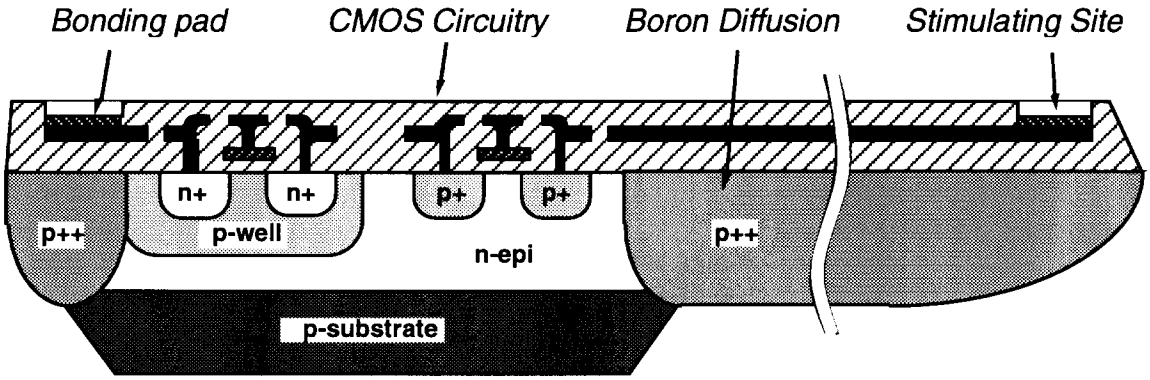

Fig. 37: Cross-section of an active probe, illustrating the p-well epi-CMOS structure. The p-type shank and substrate are grounded and are in contact with the tissue. The circuitry is formed in the n-type epitaxial region.

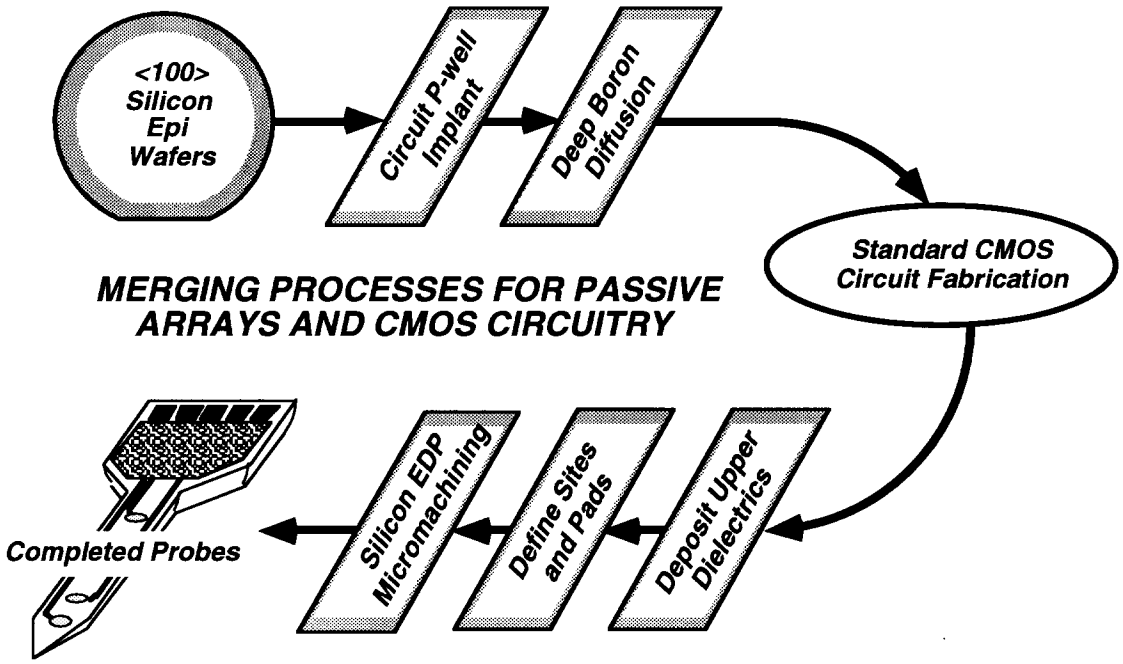

Fig. 38: Process flow for the fabrication of active probes. Standard CMOS fabrication techniques are used with steps added at the front-end and back-end of the process to realize the etch-stops and special metal-dielectric layers.

There are three main differences in the circuit fabrication part of this device that are not standard in CMOS circuit fabrication [Ji 90, Lund 94]. First, the p-well drive-in and at least a portion of the deep boron etch-stop diffusion are performed simultaneously. This requires adjustment of the p-well implant dose and energy to compensate for the additional masking oxide needed to protect the p-well from the deep boron diffusion and for segregation of the implanted boron into this oxide. Performing a portion of the deep boron drive-in prior to the p-well implant allows independent optimization of the p-well junction depth and the shank thickness. Secondly, the pad oxide and nitride layers used for the local oxidation of silicon (LOCOS) during circuit fabrication are also used for the lower dielectrics under the shank conductors. In a standard CMOS process, these layers are sacrificial, serving only temporary masking duties, and are stripped after use. The third alteration from the normal CMOS process flow is in the metallization and upper dielectric system used. We explored a number of alternatives here during the past contract.

The upper dielectrics are the final barrier between the probe electronics and the shank interconnect lines and the extracellular fluid. They must permit stable site impedances with no lifting around the site over time and must not degrade to permit significant electrical leakage currents to flow in-vivo. Over the circuit area, they, along with the metallization, must permit high-quality electrical contacts to both n- and p-type silicon. Many techniques are available for depositing films of silicon nitride and silicon dioxide. These include sputtering, low-pressure chemical vapor deposition (LPCVD), and a variety of techniques to enhance CVD such as plasma-enhanced CVD (PECVD). The quality of sputtered films is generally unacceptable, and PECVD films do not easily provide adequate coverage over surface steps. They are also susceptible to pinholes. Among the LPCVD approaches, film quality is generally proportional to deposition temperature. "High-temperature" films are deposited at 800-900°C, while "low-temperature" films are put down at about 400°C. As noted earlier in section 2.2, we need the highest possible quality in the upper dielectrics and yet must maintain compatibility with the circuitry in place on the probe and with the interconnect materials used there.

For the active probes now being fabricated, the structure shown in Fig. 39 is used. Here, aluminum interconnects are used over the circuit area and are covered with low-temperature CVD oxide (LTO). These materials are deposited after high-temperature LPCVD dielectrics are deposited on the shanks over polysilicon interconnects. This allows high quality dielectrics on the shanks but maintains a standard interconnect-dielectric sequence over the circuit block. A PECVD nitride layer can be added over the LTO as an option. After the sites are opened and the pads have been inlaid, a metal barrier can be added over the circuit area along with a polymeric film. Thus, the LTO is not directly exposed to the external fluid and the circuit area, which is segregated at the rear of the probe, can be coated with additional barriers to prevent degradation in-vivo. Using this arrangement, active probes can be realized with high yield and a relatively standard circuit process block. This was done for the first time during the present contract. Figure 40 shows the probe surface after etching from the wafer when encapsulated by a blanket LTO deposition. The properties of LTO are also compared in Table 2 with those of other dielectrics.

4.2 Active Stimulating Probe Designs

This section describes the circuit designs used for the active first- and second-generation stimulating probes. As noted above, four different probe types have been designed, varying in complexity and function. These are labeled STIM-1b (monopolar),

STIM-1a (bipolar), STIM-1 (16-site, 16-channel multipolar), and STIM-2 (64-site, 8-channel multipolar) in increasing complexity. They all offer the following features:

- Five input pads designated VDD, VSS, GND, DATA, and CLK.
- Sixteen selectable stimulating sites (64 on STIM-2)
- Capable of sourcing or sinking stimulus currents.
- Stimulus pulse timing is controlled off-chip.
- A special mode, turned on at chip power-up, allows site activation via an external signal applied at the data pad.

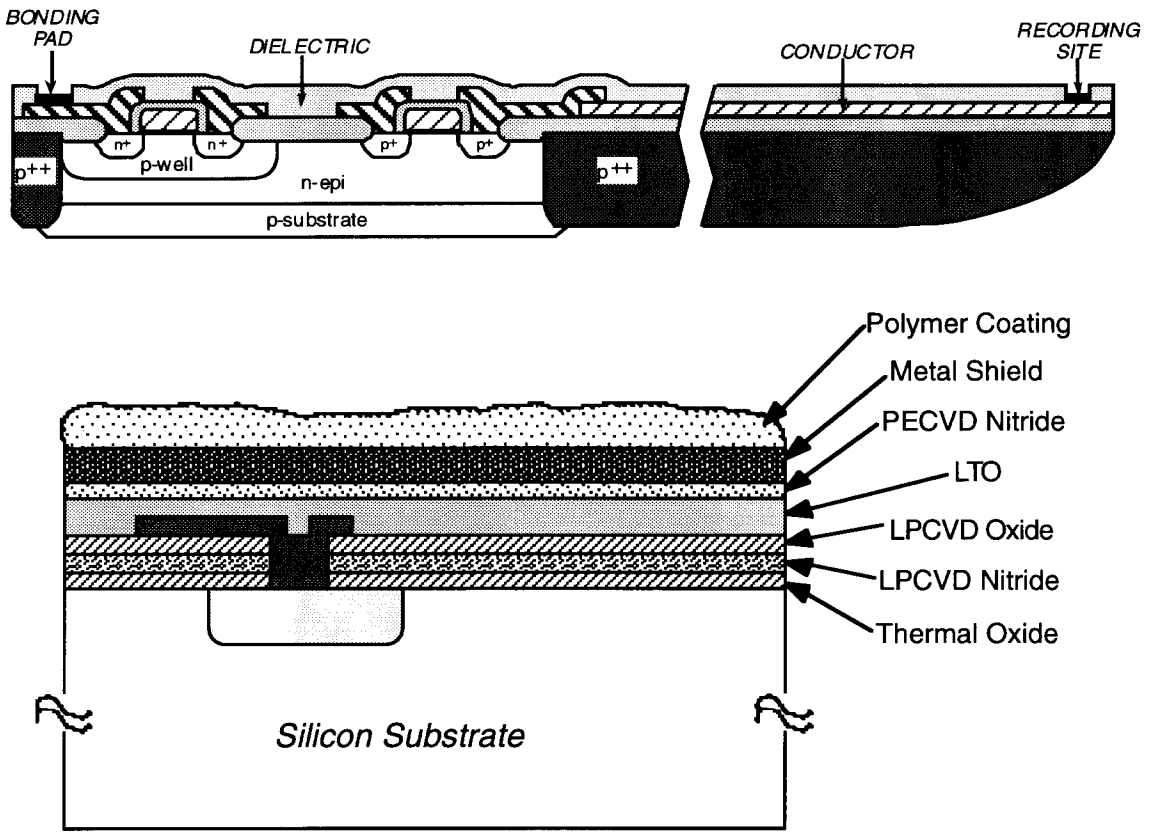

Fig. 39: Cross-section of an active probe and the upper dielectric layers. Polysilicon interconnect is used on the probe shank buried under high-temperature dielectrics. Aluminum interconnects are used over the circuit area (lower figure) covered by LTO, PECVD nitride, a metal shield, and a polymer.

The simplest design, STIM-1b, receives an analog stimulus current from off-chip and routes it to one of the 16 sites. The site is selected based on the count from an incoming serial pulse stream representing the address. This probe is a monopolar design in that only one site can source or sink current at any given time. The block diagram for this simple circuit is shown in Fig. 41. The advantages of STIM-1b are that it is simple, small, and can operate at reduced voltage levels of ±2.5V if desired.

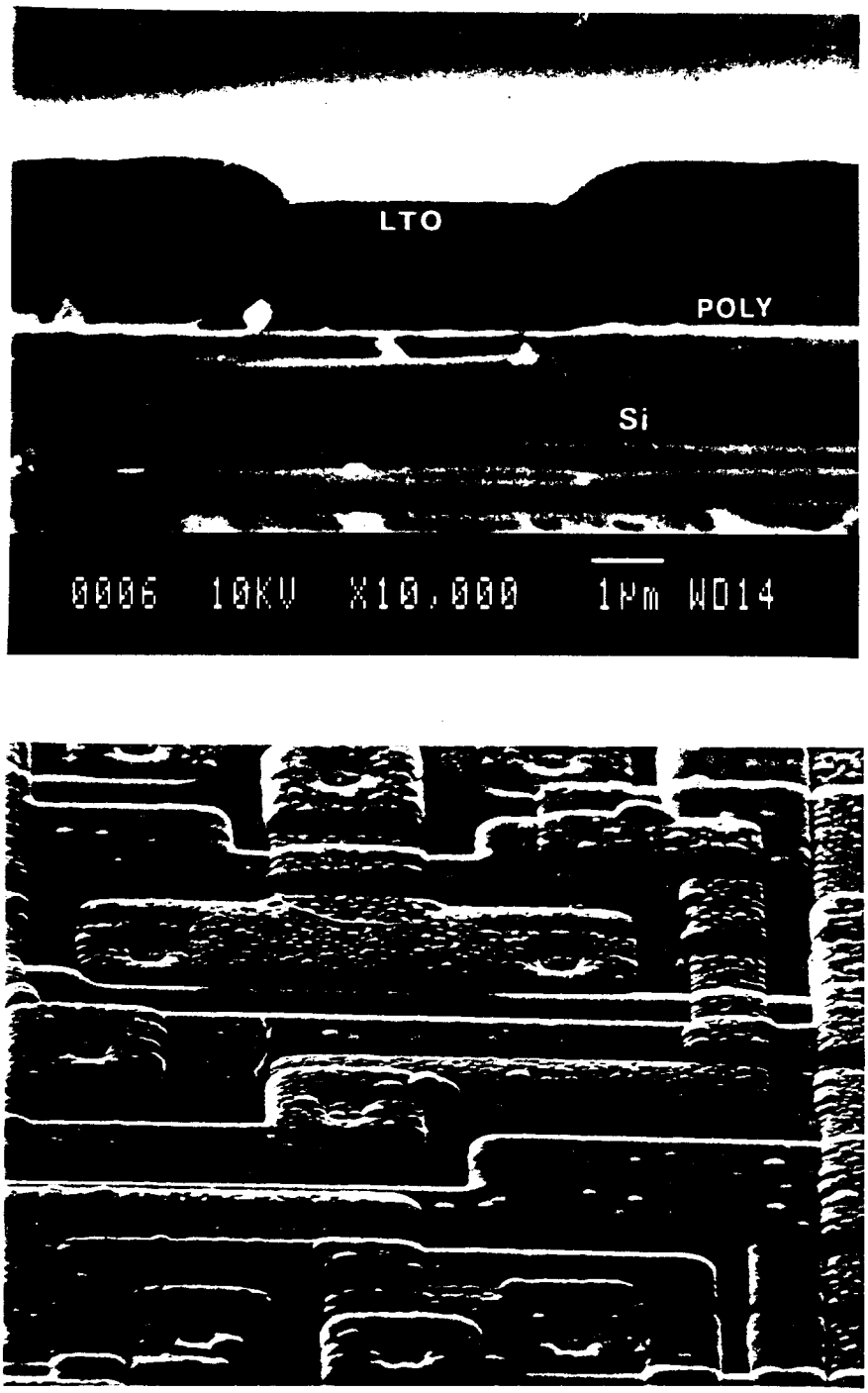

Fig. 40: Photographs of a probe shank (above) with LTO dielectric deposited over LPCVD nitride and oxide lower dielectrics and polysilicon interconnect. The step coverage is excellent and the total upper dielectric thickness is about 1.8µm. In the lower photo, a photo of the circuitry on an active probe is shown after encapsulation with LTO and etching from the wafer.

Film Type	Temp. [°C]	N_f	Stress [MPa]	BHF Etch Rate [Å/min]	EDP Etch Rate [Å/hr]
LPCVD SiO_2	920	1.460	-320	1570	300
LPCVD Si_3N_4	820	2.010	1440	<50	400
PECVD SiO_x	300	1.463	-220	3125	N/A
PECVD Si_xN_y	350	1.890	-100	280	550
LTO	450	1.455	-130	4070	485

Table 2: Comparisons of various dielectrics for probe encapsulation.

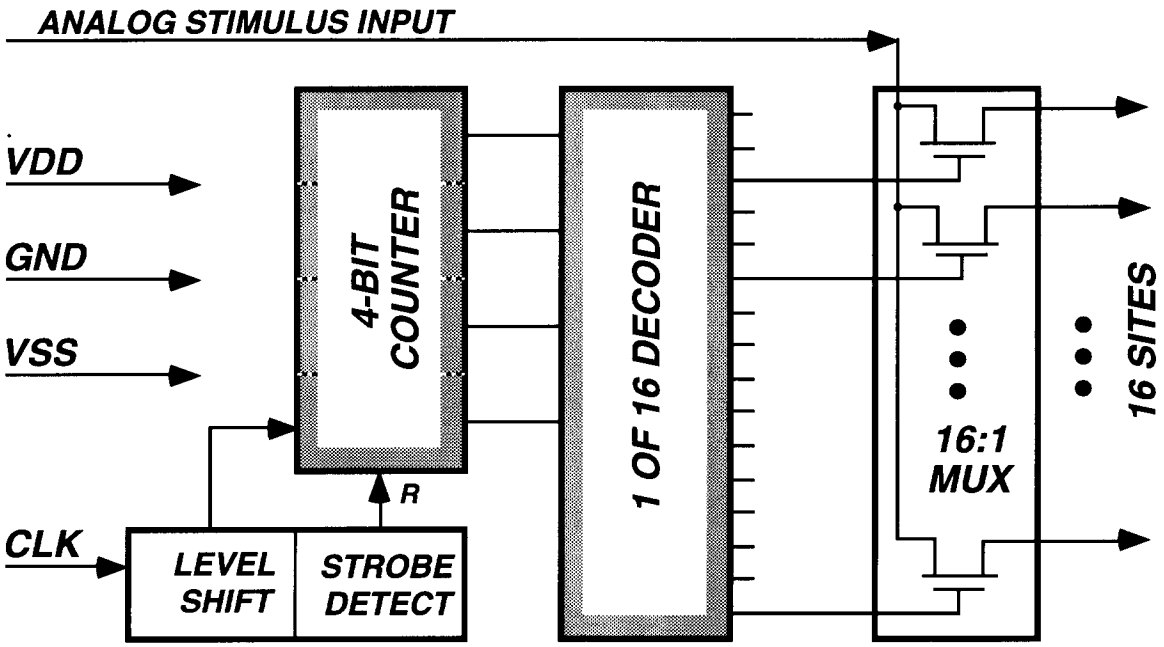

Fig. 41: Block diagram of the active monopolar probe, STIM-1b.

STIM-1a has an on-chip digital-to-analog converter (DAC) that delivers analog sourcing and sinking currents of equal magnitude to two selected sites out of the sixteen. The block diagram for this bipolar design is illustrated in Fig. 42. A 16-bit word is loaded into the shift register with the clock signal. The first eight bits represent the addresses of the two electrodes chosen to be the anode and cathode. The next seven-bit word sets the current magnitude from these sites. The last bit is reserved for a clock strobe that latches the incoming data stream. The advantages of STIM-1a are that it is a truly bipolar device (two sites on, one sourcing current and the other sinking the same current), it can deliver precise current stimuli (digital-to-analog conversion is done on-chip), and it has a small area layout compared to STIM-1 or STIM-2.

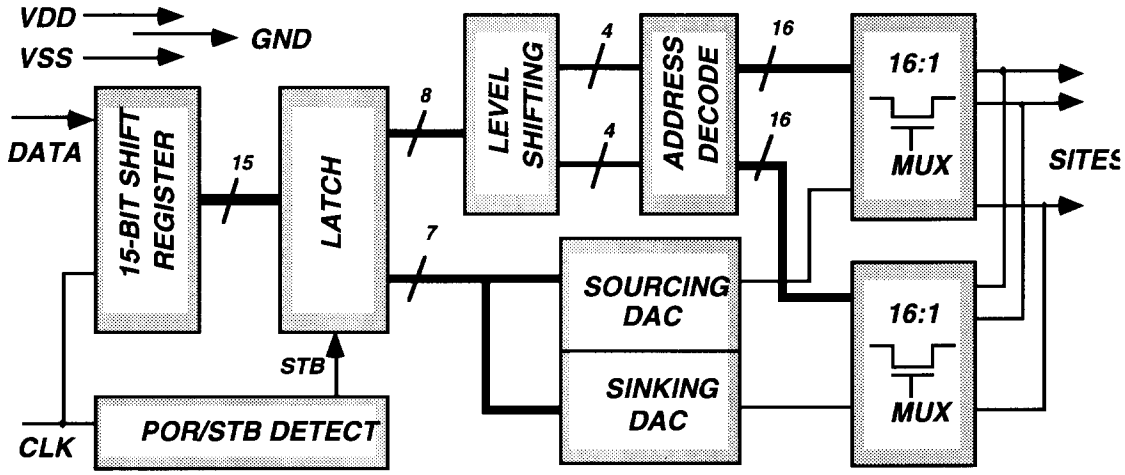

Fig. 42: Block diagram of the active bipolar probe, STIM-1a.

The most advanced of the first-generation of active probes is STIM-1. The block diagram for this chip is shown in Fig. 43. This device has a DAC for every channel, allowing all sixteen channels to be active at any given time, with individual control over the current amplitudes. The circuit receives 16-bit data words that are shifted into the data pad using a 4MHz clock. Four bits represent the site address, two are mode bits, eight set the current amplitude, and two are used for strobing and status. In the normal mode of operation, the specified current is set up on the addressed channel and remains on until the channel is accessed again to alter it. Other channels are set up sequentially to source or sink current as desired. At a clock rate of 4MHz, the time resolution between any two changes in the probe current pattern is 4μs, which is effectively simultaneous to the tissue. A second mode of operation grounds the associated stimulus channel, allowing the DAC currents to be calibrated externally without stimulating the tissue. A third mode of operation allows the analog voltage developed in response to stimulus current to be observed externally to check site integrity at any time. Finally, a fourth mode of operation biases the electrode anodically above ground between pulses to increase the charge delivery of the iridium oxide electrode sites [Beebe 88, Robblee 90-2].

Other important circuit features of STIM-1 include analog access through the data pad to all sites in parallel when the circuit is first powered up. This allows the growth of iridium oxide on all of the sites simultaneously. As a safety feature, the probe also includes per-channel timeouts which guard against overstimulation by shutting off the current on any channel that has not been accessed in more than one millisecond. In addition, the last bit in the data input stream is used to allow the probe to signal the outside world if any of the probe input signals are out of their proper range. Thus, probe function is checked with every input frame. The probe circuitry has an idle power dissipation of 80μW and operates at clock rates as high as 10MHz. The output currents are linear to 8 bits with sourcing and sinking currents matched within ±1/2 LSB, ensuring adequate charge balancing at the stimulating sites. The circuitry requires 7100 transistors and an area of 11mm^2 using a 3μm, 1-poly, 1-metal CMOS process. The specifications for STIM-1 are summarized in Table 3.

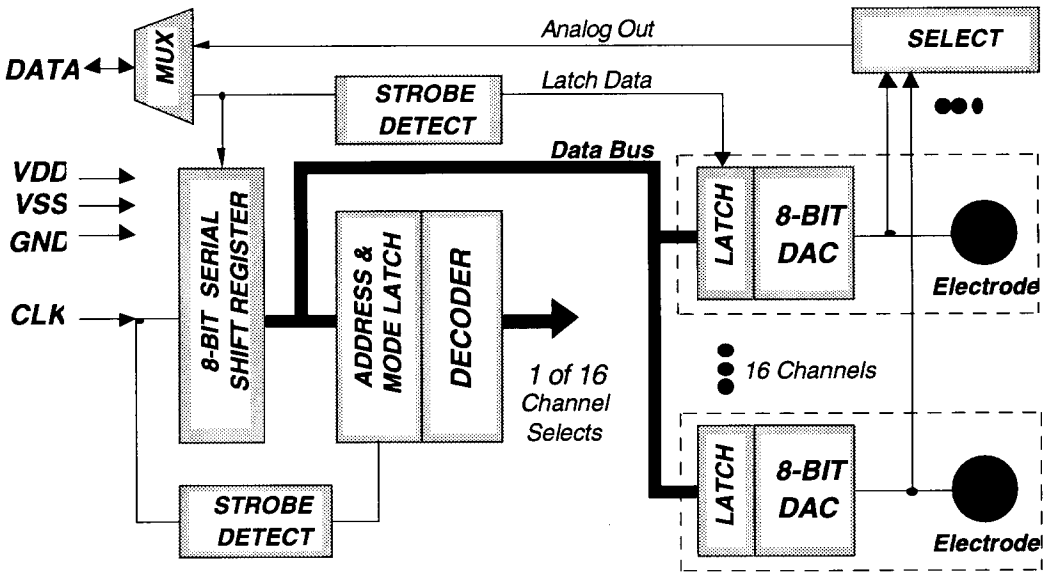

Fig. 43: Block diagram of the active multipolar stimulating probe, STIM-1.

Table 3 : STIM-1 Characteristics

No. of Bonding Pads	5
Voltage Supplies	VDD, VSS, GND
No. of Output Channels	16
Current Range per Channel	-254 to 254 μA
Current Resolution	2 μA
Operation Frequency	4 MHz *
Event Time Resolution	4 μs
Idle Power Consumption	80 μW
Modes of Operation	Normal
	Current Calibrate
	Impedance Check
	Electrode Anodic Bias
	Activation
Safety Features	Per-channel time out
	Status Check
	Site voltage monitor
Transistor Count	7100
Layout Area	11 mm^2

* Tested up to 10MHz.

At the high end of the active probes developed thus far is the second-generation active multishank probe STIM-2. This probe features improved on-chip circuitry and is extendable to multiprobe 3D assemblies. The electronic system designed for this probe will support 64 stimulating sites, simultaneously selecting any one of the 64 sites in both normal and special modes for either stimulation or recording. This selection scheme is globally multipolar since the time delay of 4μsec to select the next site is negligible at the clock frequency of 4.5MHz, appearing effectively simultaneous to the tissue. The probe allows stimulation through eight sites simultaneously, and any one of these sites can be monitored (recorded from) at any time. Table 4 gives a brief summary of the specifications and special features for this second-generation stimulating probe.

Table 4: Specifications of STIM-2

Process technology	3 μm, p-substrate, n-epi, p-well single poly, double metal two-step diffusion micromachined CMOS technology
Supply voltage	Vcc = 5.0V, Vss = -5.0V, GND = 0V
Control signals	DATA and CLOCK
Current range	-127 to +127 μA
Current resolution	1 μA
Power dissipation	Standby ≤50 μW, Operating ≤10mW
Clock frequency	4.5 MHz (~222 nsec)
Time delay to select any site	4 μsec
Total external pads	5 pads (VDD, GND, VSS, DATA, and CLOCK)
Electrode site size	1000 μm^2 (optional for 400 μm^2)
Probe shanks	8 and 16
Total stimulating sites	64
Chip area with boundary	11.2 mm^2
Circuit features	• low-impedance shunt mode for idle sites • anodic-bias mode for high current delivery • electrode-impedance monitoring mode • electrode recording mode • self-test and trouble flag modes • electrode-activation mode • simple level-shifter, no static power dissipation • clock-controlled address decoder • low power current source (DAC)

The STIM-2 system is configured as shown in Fig. 44. Each group of eight electrodes, placed on a micromachined silicon probe shank, is connected to a front-end site selector (an 8-to-1 multiplexing array) and is controlled by a DAC. Up to one site from each group can be selected for stimulation. As special options, several different modes are implemented, including a site-activation mode, a site-impedance test mode, a neural recording mode, a low-impedance shunt mode for unselected sites, a trouble flag mode, a current calibration mode, an anodic bias mode for high current delivery, and a platform address mode for use in three-dimensional arrays. The operations performed in these various modes are tabulated in Table 5.

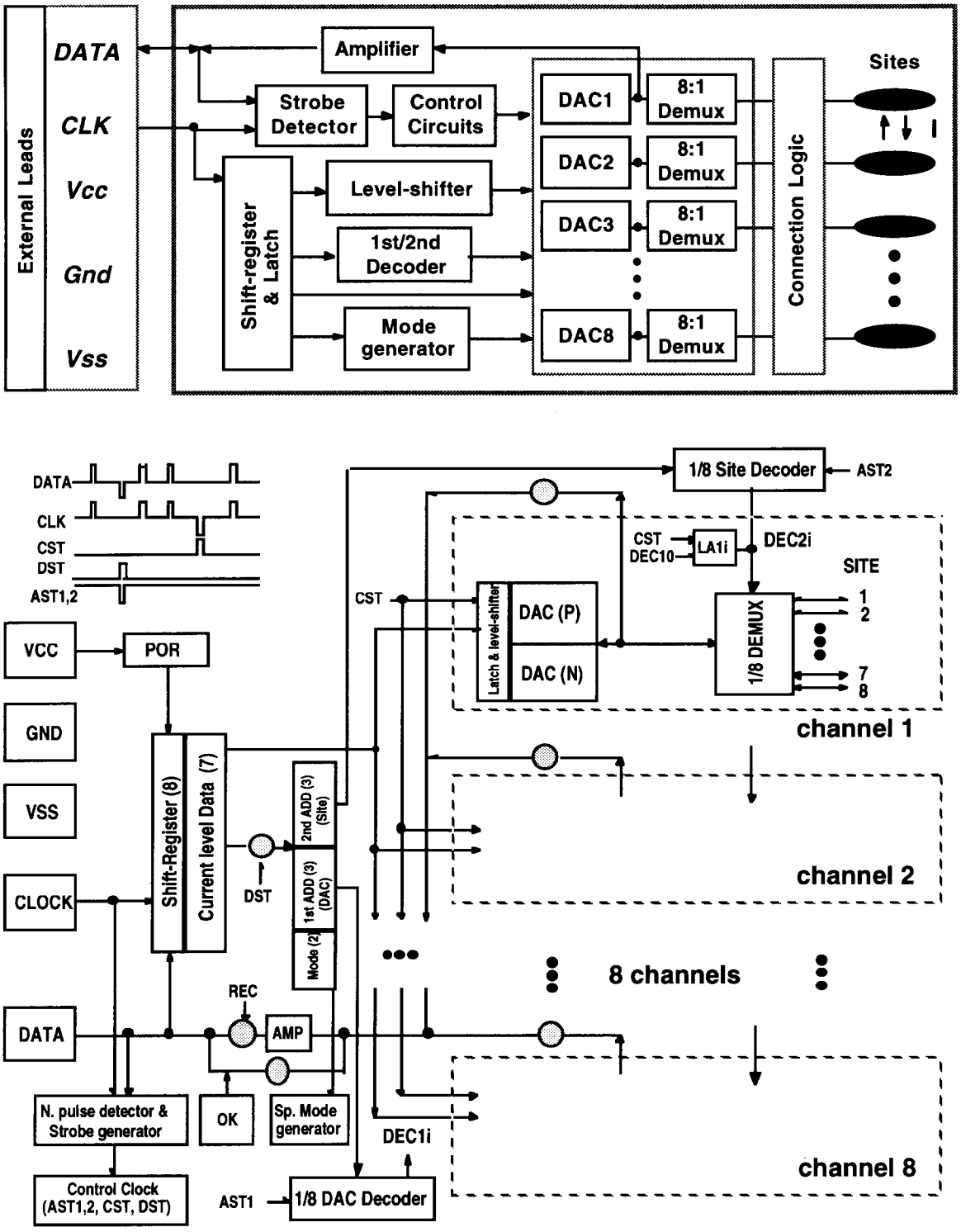

Fig. 33: Overall block diagram of the second-generation stimulating probe, STIM-2.

Table 5: Operating Modes for the Second-Generation Probe, STIM-2

Mode	*Operation*
Normal Stimulation	DAC drives the selected site through the site-selection transfer gate
Site Activation	Occurs on power up; all sites are connected to the data line to be activated by cyclic voltammetry
Impedance Test	The voltage of the selected site is transmitted off-chip on the data lead so that it can be monitored during current stimulation, permitting the site impedance to be assessed.
Recording	The selected site is monitored through a recording amplifier so that neural activity can be observed.
Low-Impedance Shunt	Outputs of inactive channels are connected to ground to remove any potential that might build up on the site due to charge imbalances.
Anodic Bias	The sites are connected to a bias of about 0.6V instead of to ground to equalize the charge that can be delivered from the probe in cathodic first operation.
Trouble Flag	Causes the probe to pull down the data line if a series of monitoring points on the chip are operating normally.
Current Calibrate	Allows current stimulation but shunts that current to the ground return line so that the current at a particular setting can be externally monitored and calibrated.
Platform Address	The incoming address is treated as a probe address, allowing subsequent data entry to be steered to a different probe by circuitry on the supradural platform. This address causes no operation on the present probe itself but only causes action in the platform circuitry. This will be mentioned again in section 3.5.

Thus, STIM-2 has a variety of modes to allow its performance and operating characteristics to be fitted to a given application. In spite of this, however, we would already change these modes somewhat as the result of experience with these probes and their passive cousins. For example, we will probably make anodic bias the normal situation, for example, and would make the option turn it off rather than to turn it on. This would guard against voltage buildup on the site as the result of small charge imbalances over time. On the other hand, since this option is global for all sites, it is a simple matter to issue a command to turn this option on. It does not have to be done on a per-pulse basis. We would also add the auto-time-out feature, present on STIM-1, to STIM-2, where it is absent (handled via external software). It should be noted that the self-test (trouble-flag) mode is still built into every frame (as in STIM-1) and it is at the discretion of the external electronics whether to wait for the data line to fall ("I'm OK!") and look at this signal.

Data Designations

A detailed view of the timing and bit designations in STIM-2 is given in Figs. 45 and 46. The upper diagram illustrates the situation when normal data are transmitted to the probe as a 16-bit word instruction. A 16-bit word is serially clocked into the 8-bit serial shift register from the data line. The first two bits represent the desired mode, followed by six address bits. The first three address bits are decoded to select one of the eight DACs, and the second three bits are decoded to select one of eight sites associated with that DAC for stimulation. During half of the ninth time slot, the data line goes low to negative voltage, causing the mode and address latches to latch those bits. Eight bits of current data are then clocked in. These eight bits, representing the amplitude and sign of the sinking or sourcing currents, are directed into the selected level shifters. A strobe then occurs on the clock line, latching these data, followed by a high impedance state that occurs during the last bit time, allowing the probe to transmit the "I'm OK" signal back to the external electronics by pulling down the data line. The remaining three possible combinations of modes are for recording (M01), low impedance shunt (M10), and extended data word (special mode) (M11) operation.

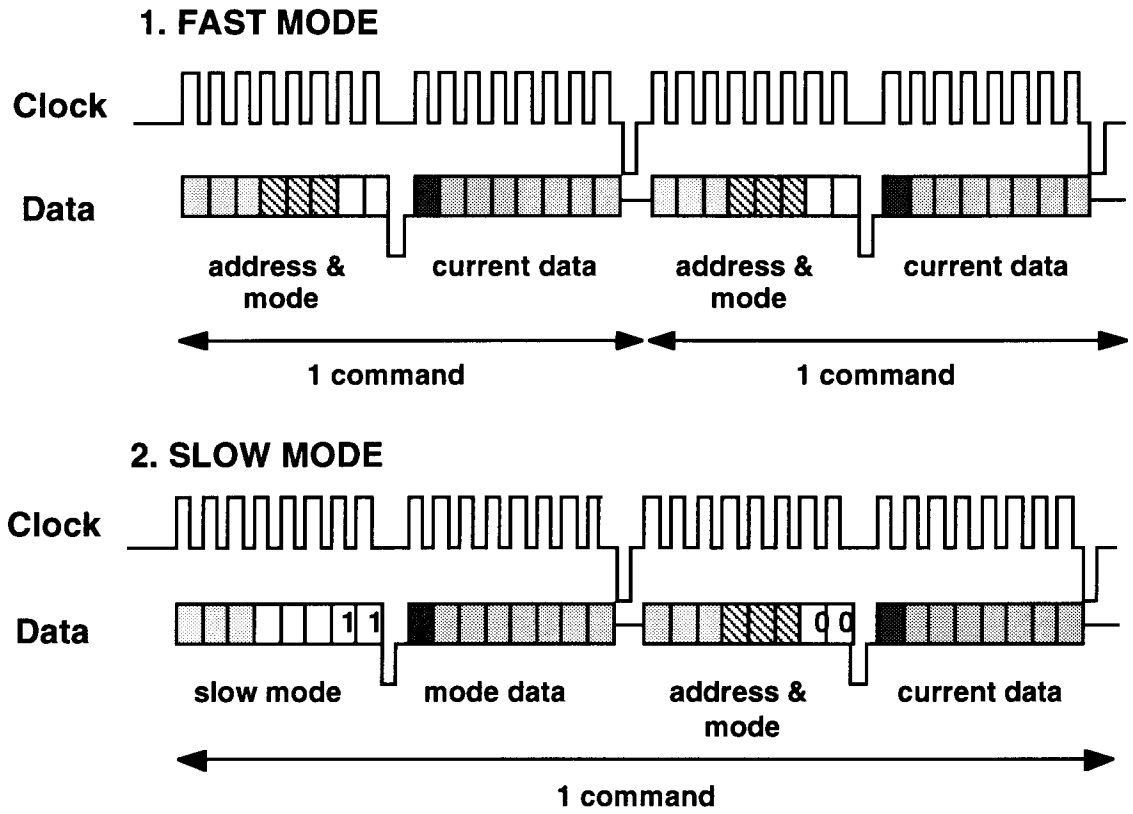

Fig. 45: Overall timing diagram for STIM-2 operation.

The lower portion of Fig. 46 illustrates the operation for a 32-bit instruction for cases which do not require high-speed operation. Once again, the first and second parts of the address and the mode bits are clocked in and latched on the data strobe. At this time, the mode bits are "11", indicating an extended instruction for special modes. In this case, the first three address bits in this first word are interpreted as special mode information and are latched to allow up to eight special modes. For example, at present the first four special

modes are designated for anodic bias, impedance test, current calibration, and platform address as noted in Fig. 44. These could be used to address as many as 256 (=2^8) different probes in a distributed system, each probe having 64 sites. One special mode could be defined to allow a third data word as well, allowing the address space to be expanded further. The second 16-bit data frame is a standard probe command as used in a single instruction.

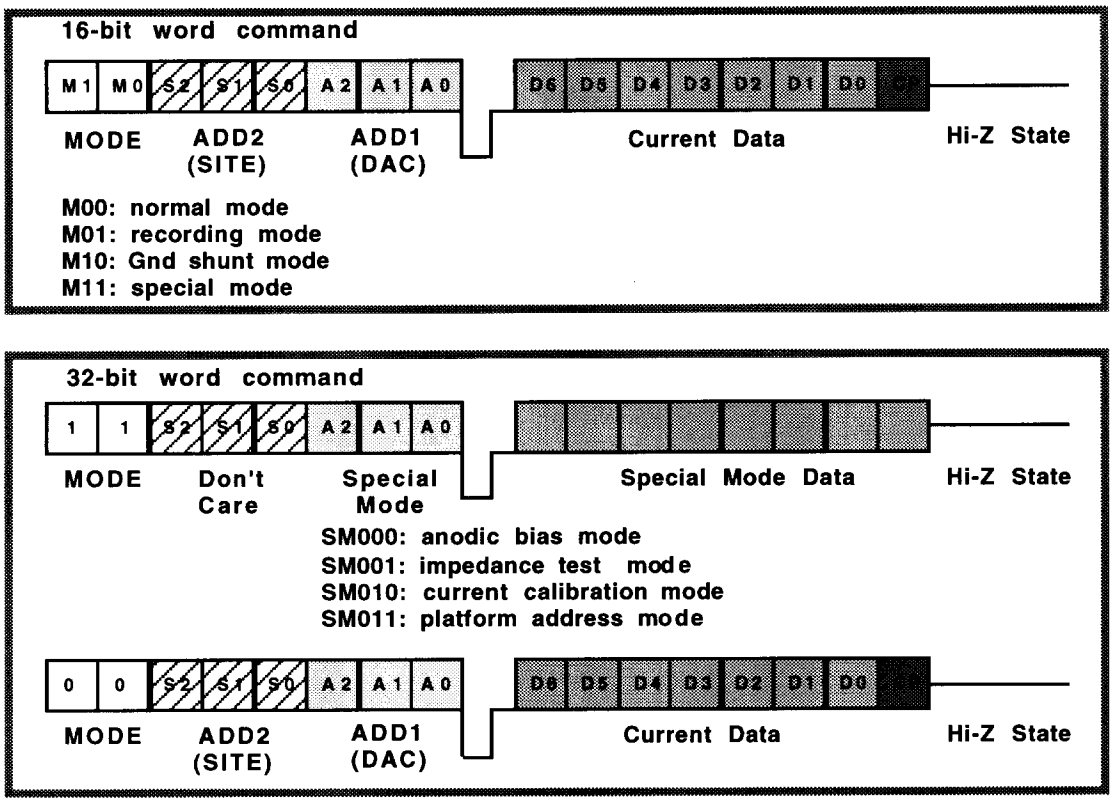

Fig. 46: Data designations for the second-generation stimulating probe.

Channel Selection and Stimulation Patterns

There are many useful combinations of stimulation patterns that could be used with 64 sites. In order to allow a wide selection of these and yet maintain a reasonable level of complexity in the selection circuitry, a simple two-shank combination scheme has been chosen for STIM-2. Figure 47 shows a few of the possible stimulation patterns that can be implemented using this simple two-shank combination option. Each DAC can be switched to any one of eight sites, distributed over two adjacent shanks. In this example, DAC1 controls sites 1-8, while DAC2 controls sites 9-16. This allows any two adjacent sites to be selected, for example, either laterally or in depth. A wide variety of patterns are possible. Figure 48 shows the physical probe shapes and site address maps for the 8-shank and 16-shank versions of STIM-2, respectively. Using this scheme, any two adjacent sites can be addressed and used for bipolar stimulation.

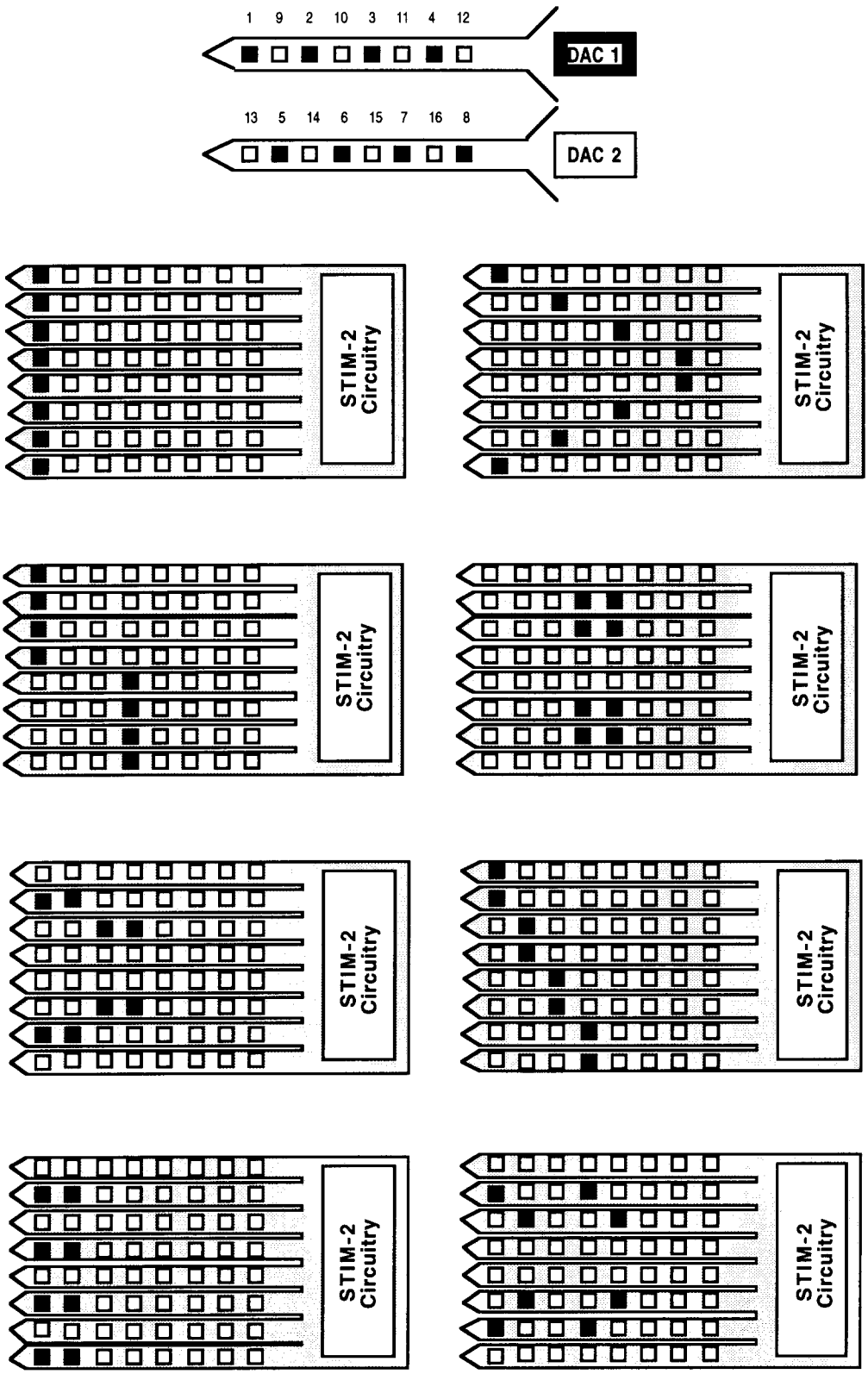

Fig. 47: Examples of possible stimulation patterns using a simple two-shank combination option for the organization of the DACs and the site selection matrix.

Probe Height Optimization

For in-vivo applications of these stimulating probes, their height above the cortex, which is determined by the circuit dimensions implemented in the probe, must be low enough to allow the dura to be folded back over the implant so that tissue overgrowth does not anchor the implant area to the skull. While the maximum allowable probe profile above cortex is not known at this time, it is assumed that this rise should be less than 1mm. However, as additional useful features are implemented on the probes, the chip size naturally increases, making a low profile increasingly difficult. On the other hand, as the number of shanks increases and the width of the probe structure expands, more room is available to expand the circuitry in width while shortening it in height. Thus, there are two approaches to limiting the probe height: 1) taking advantage of the larger width available on wider probes, and 2) bending the probe using ribbon cables between the shanks and the circuitry so that the circuitry lies flat against the cortex. One of the versions of STIM-2 has been designed with the second approach implemented as shown in the upper part of Fig. 48 and Fig. 49. As of this writing, however, it appears that for larger 2D and 3D probes, the expanded width option is the more promsing, and this will be initially pursued under the new contract.

4.3 Active Probe Performance

All four of the probes outlined above have been fabricated successfully. They are shown in Figs. 50, 51, and 52. The most recent mask set for active stimulating probes contains STIM-1b, -1a, and -2, along with several test circuit blocks. The procedure used in developing these chips was to first design and layout the various circuits, followed by extensive simulations using our in-house Computer-Aided Engineering Network. The circuits were then fabricated at the MOSIS foundry to confirm operation in hardware. The circuitry was then merged with the complete probe process as explained above, and the active probes were fabricated in our Solid-State Fabrication Facility. In-vitro and then in-vivo testing followed. The probes are all fully functional and meet all of the target performance specifications, although we have noticed a weakness in the negative pull-down characteristics of some of the STIM-2 probes (failure to adequately sink current) which is being explored. In the sections below, we provide a summary of the in-vitro and in-vivo test results for the active stimulation probes developed to date at Michigan. Table 6 compares some the probe characteristics.

STIM-1b

STIM-1b is a monopolar stimulating probe. Site address information is entered serially using the clock to increment an on-chip counter. The counter state is decoded to select the desired site, which receives the externally-generated current via an on-chip analog multiplexer. Figure 53 shows the operation of the monopolar probe. The upper trace is the input clock signal, which is used to set the site address. The address here is set first at site #1 and is then switched to site #4. The middle trace shows the site-drive signal, which in this case is an arbitrary waveform used for illustration only. The bottom trace shows the measured voltage output waveform at site #1 across a 10kΩ resistor. Site #1 receives input only when addressed as it should. This probe has been tested extensively and is fully functional. It was the first of the active probes to be tested in-vivo because of its relatively simple drive requirements and operation.

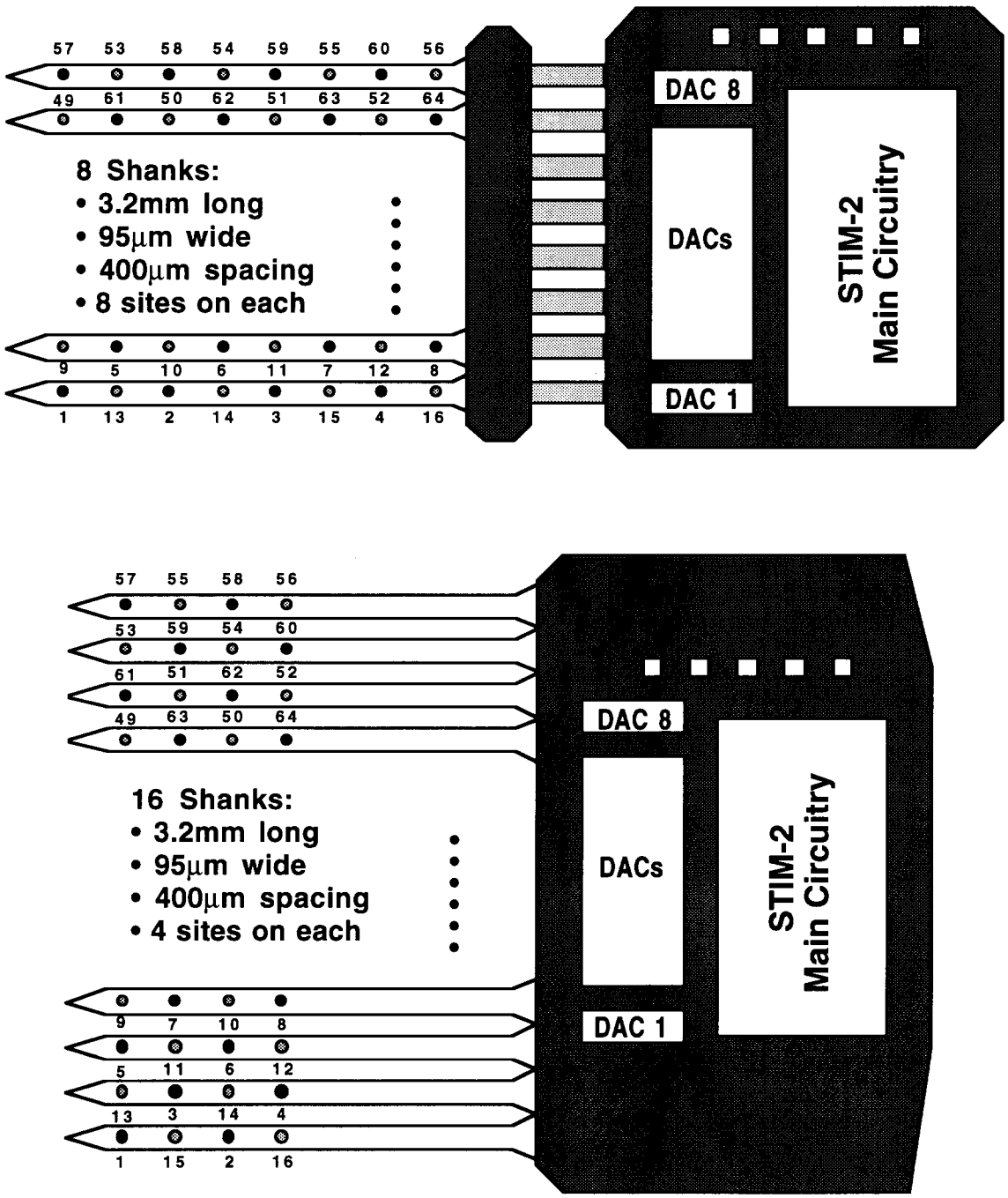

Fig. 48: Physical shapes and site maps of STIM-2. (a) 8-shank version (above) and (b) 16-shank version (below).

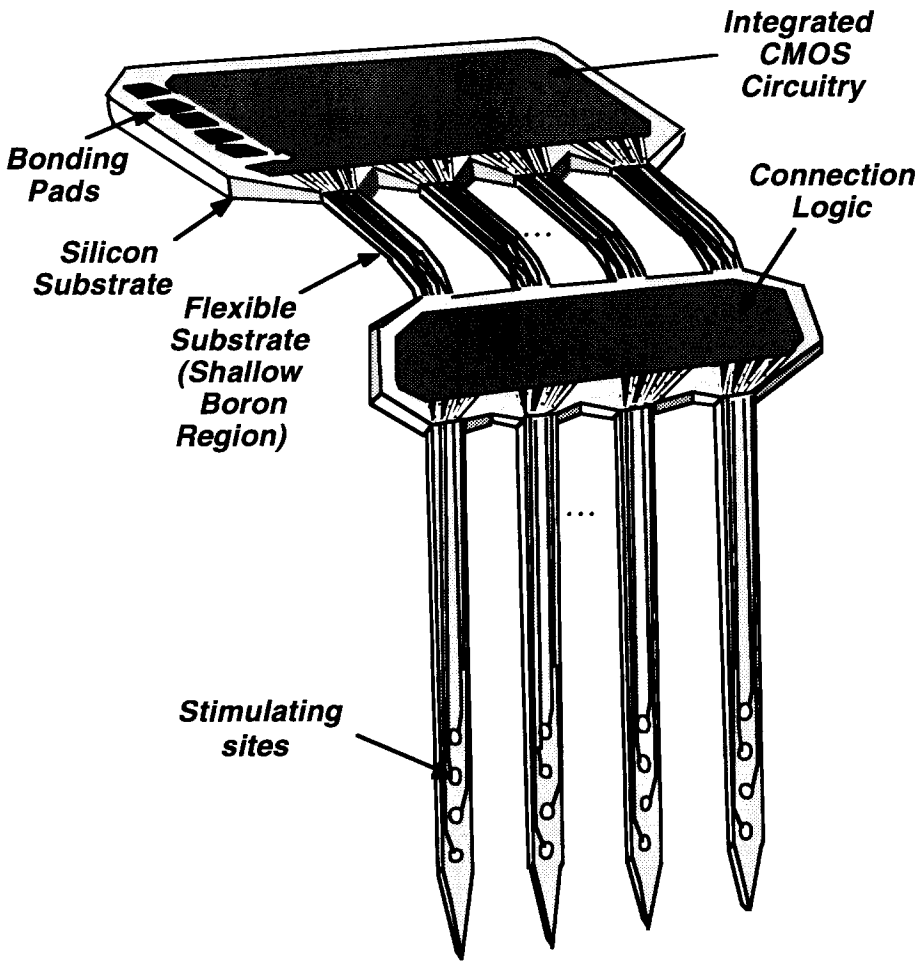

Fig. 49: Perspective view of one version of STIM-2 in which flexible ribbon cables are between the probe body and the circuitry, allowing a low-profile above the cortex for the chronically-implanted structure.

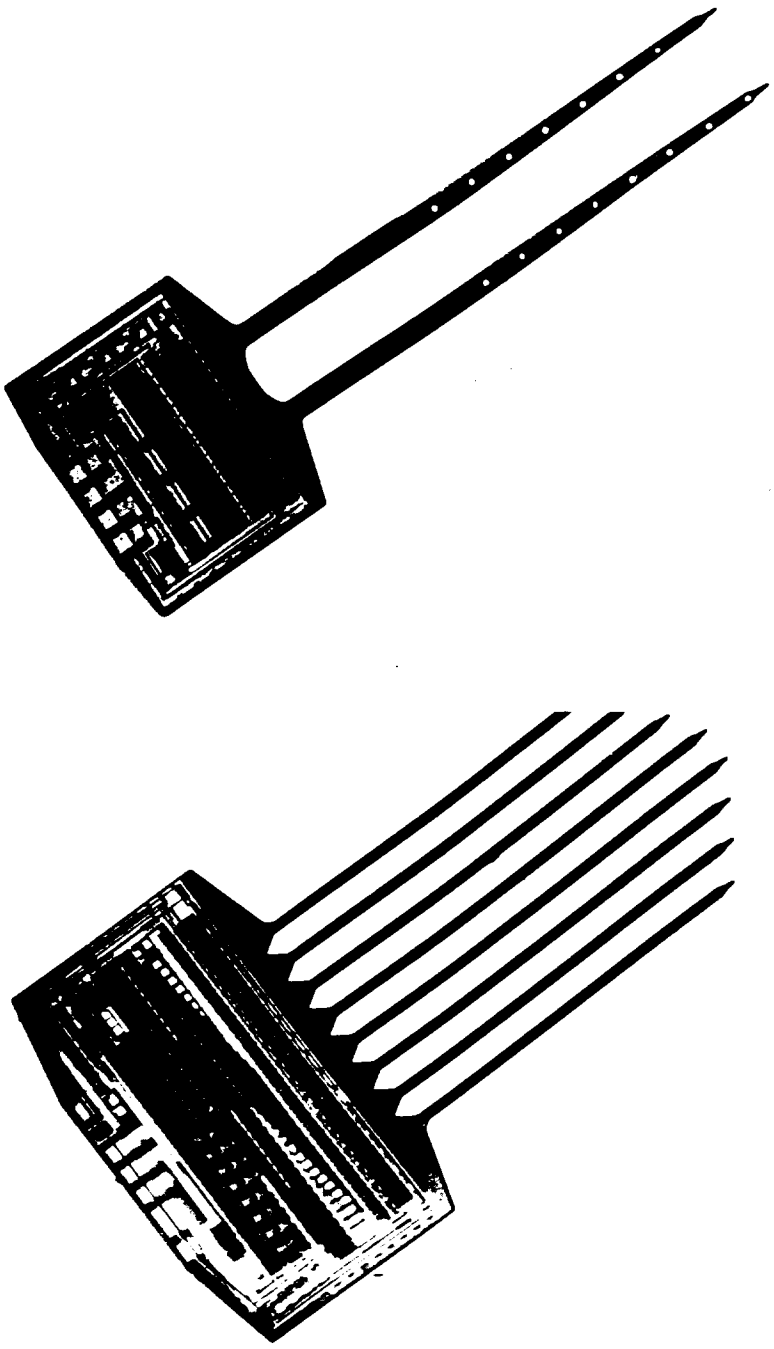

Fig. 50: Photographs of the monopolar STIM-1b probe (above) and the bipolar STIM-1a probe (below).

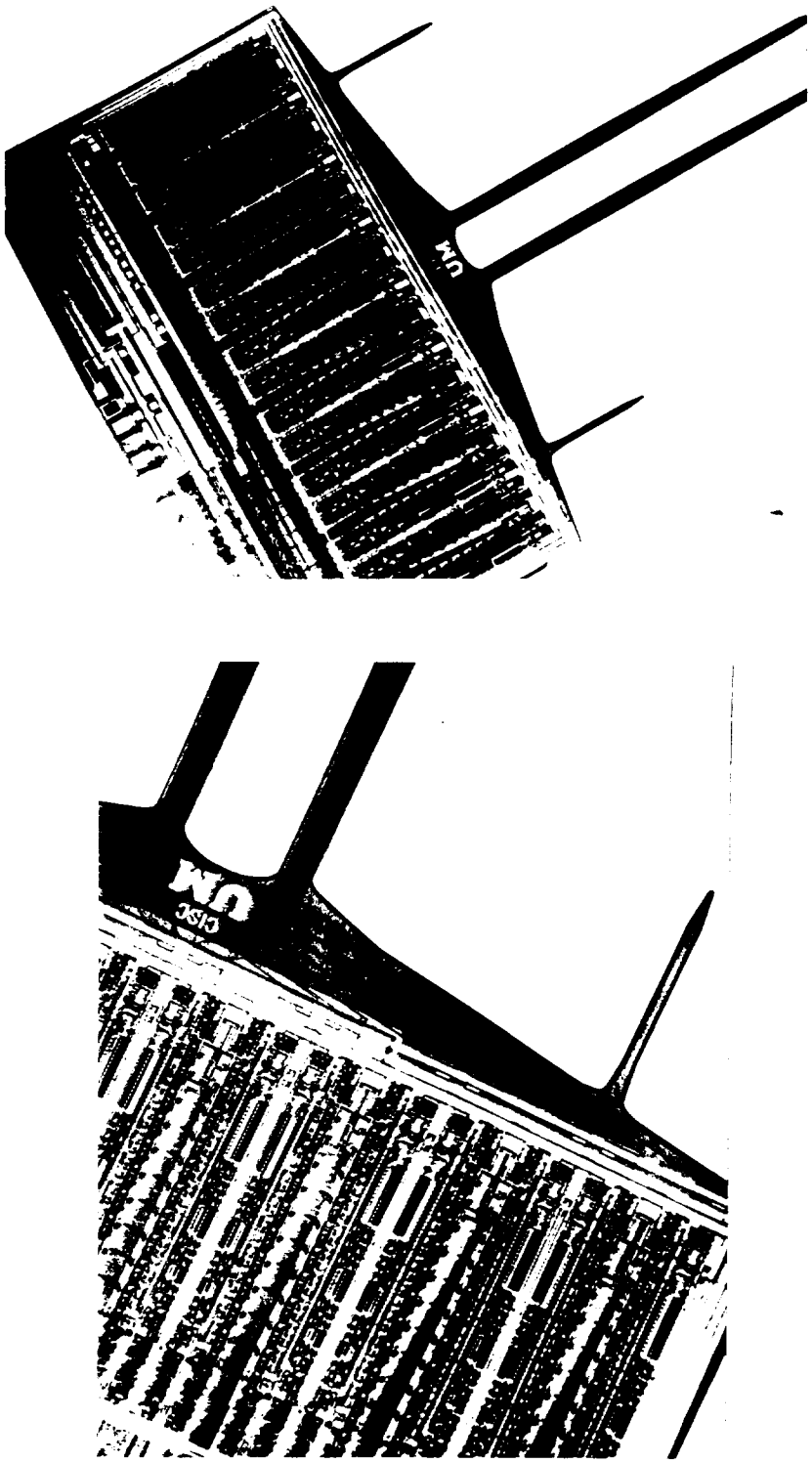

Fig. 51: Photographs of STIM-1, a 16-site 16-channel active stimulating array.

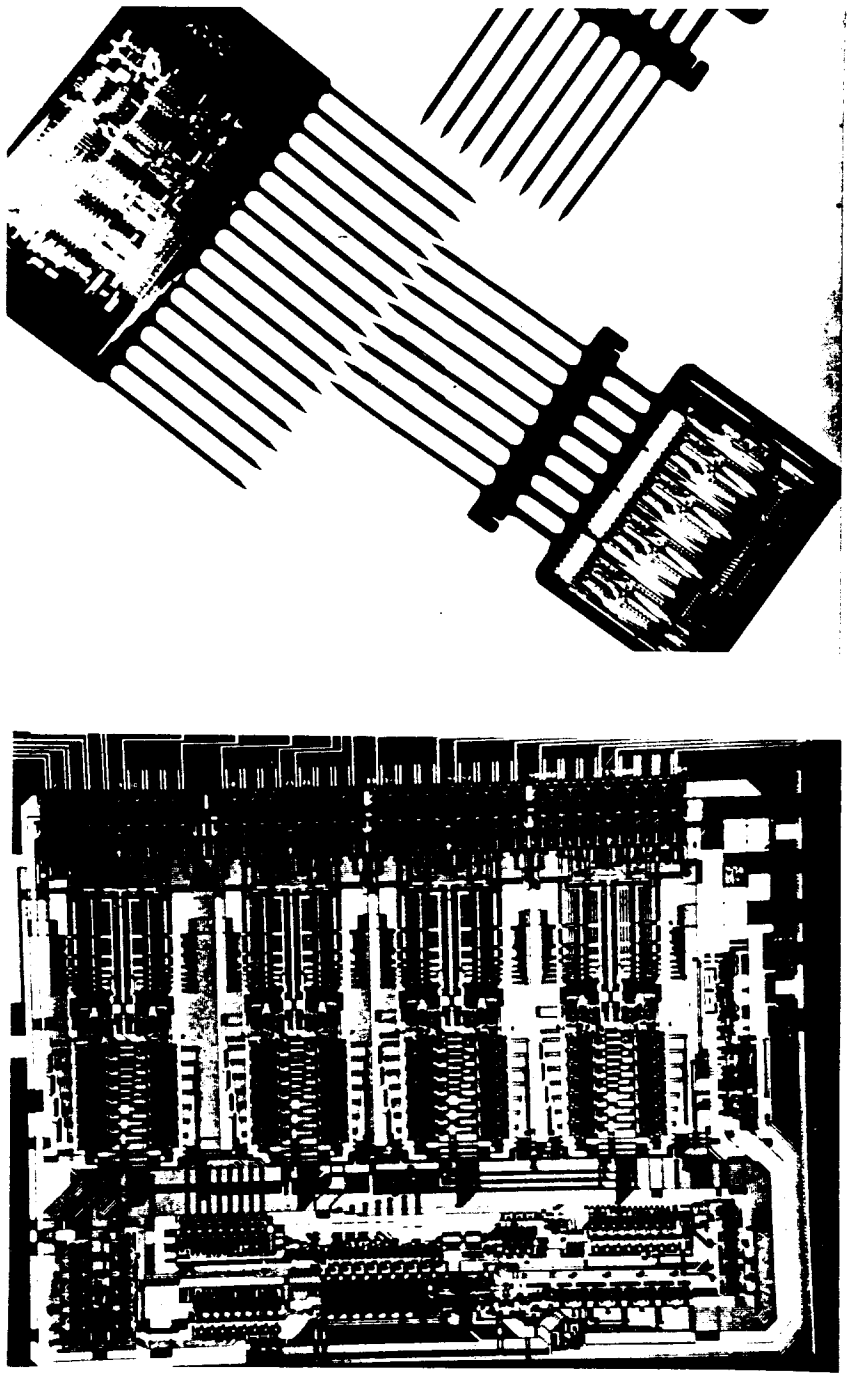

Fig. 52: Photographs of STIM-2, a 64-site 16-channel active stimulating array.

Feature	Monopolar STIM-1b	Bipolar STIM-1a	Full Parallel STIM-1	Full Paralle STIM-2
# Simultaneously Active Channels	1	2	16	8
Voltage Supplies	±2.5 to ±5V	±5V	±5V	±5V
Current Source	Off-Chip	On-Chip	On-Chip	On-Chip
Current Range (μA)	Off-Chip	±254	±254	±127
Resolution (μA)	Off-Chip	2	2	1
Transistor Count	400	1400	7100	5000
# Shanks	2	8	2	8/16
# Sites	16	16	16	64
Circuit Area (mm^2)	0.8	2.6	11	11.2

Table 6: Comparison of the various active stimulating probes developed at Michigan.

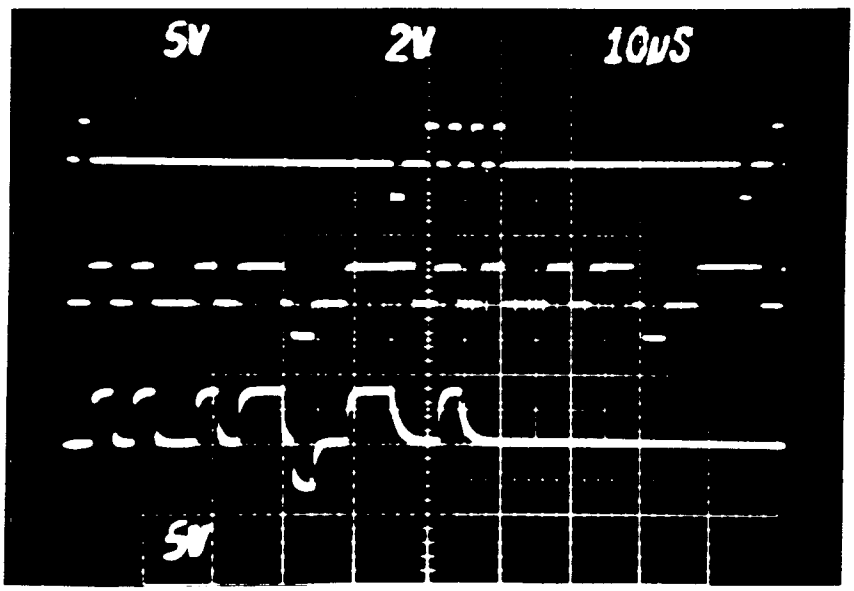

Fig. 53: Operation of the monopolar probe. Upper trace: input clock signal; middle trace: site-drive signal; bottom trace: measured voltage output waveform across a 10kΩ resistor. Site #1 receives input only when addressed.

The STIM-1b probes have also been used for limited in-vivo experimentation using the setup shown in Fig. 54. This testing involved first placing a multi-site silicon recording probe in the inferior colliculus (IC) of a guinea pig and verifying its ability to record the response to an auditory stimulus. The recording electrode was then cemented to the skull with dental acrylic in order to fix its position. The cochlear nucleus (CN) was next exposed and a STIM-1b probe was inserted for stimulation. The CN was presented with a 100Hz sine wave stimulus for 100mSec (10 sinusoidal cycles). This stimulus was

presented 100 times, and the number of spikes above a set threshold were recorded from the IC and summed into 100μSec bins referenced to the onset of each stimulus in order to observe the response versus time. The threshold was set for a given recording site by first cycling through all of the STIM-1b sites while raising the threshold as necessary to eliminate noise from the spike count. This threshold was then maintained constant while recording the responses from the different stimulation sites. This allowed for easy comparison due to the constant reference level for all stimulation sites with respect to a given recording site. The threshold was reset accordingly for each recording site due to the fact that the different sites would be measuring different neural activity.

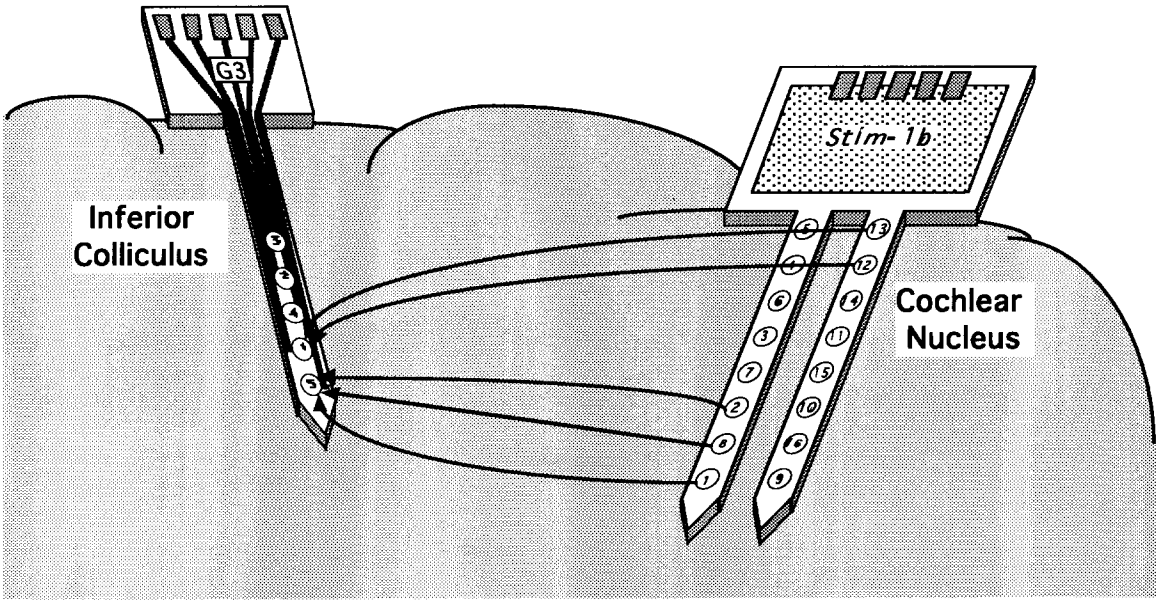

Fig. 54: Experimental setup for the in-vivo testing of STIM-1b. The neural coupling paths, as indicated by the experimental results, are also shown between the appropriate sites on STIM-1b and the sites on the G3 recording probe.

The intent of this experiment was to show that stimulation of certain sites in the CN would produce a response (change in the spike count) at a recording site in the IC, while stimulation at other sites would change or eliminate the response as different neurons were activated. Figures 55-57 demonstrate how the location of STIM-1b sites #1, 2, and 8 map to site #5 of the G3 recording probe. The center site of the three, #8, shows the largest response while the two neighboring sites show a lower response with about half the total number of spike events. The remaining STIM-1b sites elicited no response from site #5 of the recording probe. Figures 58 and 59 show the responses recorded at site #1 of the G3 recording electrode due to stimulation from sites #12 and 13 of STIM-1b. It would appear that the neural path being excited is closer to site #13 than to #12 due to the difference in the responses. In fact, it is interesting to note that even the negative half cycle shows some ability to generate a response though it is greatly reduced compared to the positive half cycle. A previous, similar, experiment did show a response which was preferentially larger during the negative half cycle of the stimulus (Fig. 60) as opposed to the positive half cycle as shown in Figs. 55-59.

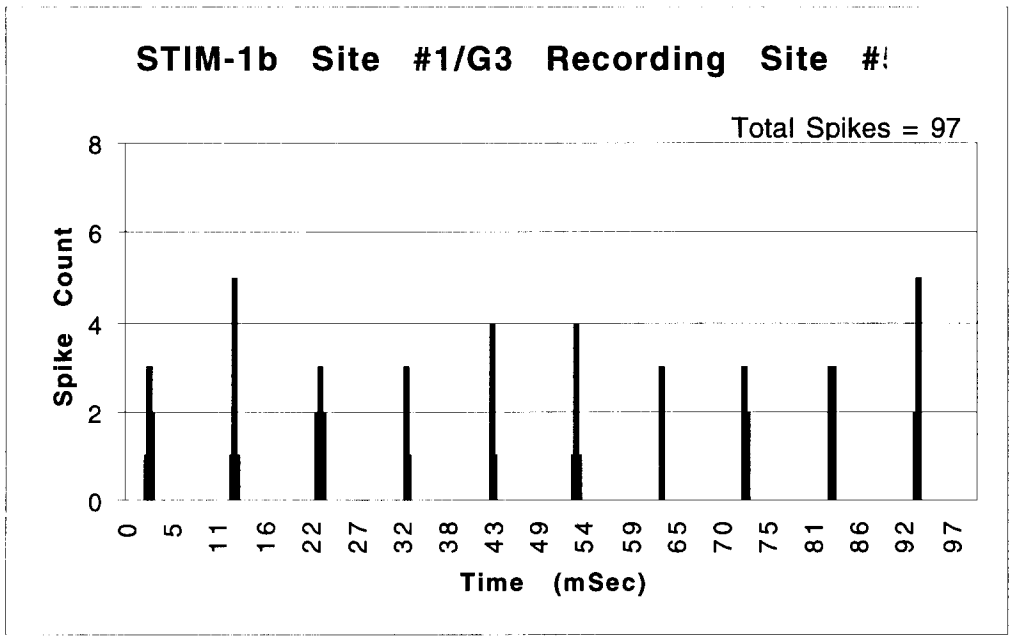

Fig. 55: PST histogram of the response recorded from site #5 of a G3 passive recording electrode in guinea pig IC evoked by a 100Hz 1μA sinusoidal stimulus from site #1 of STIM-1b in the CN (see Fig. 54 for site maps).

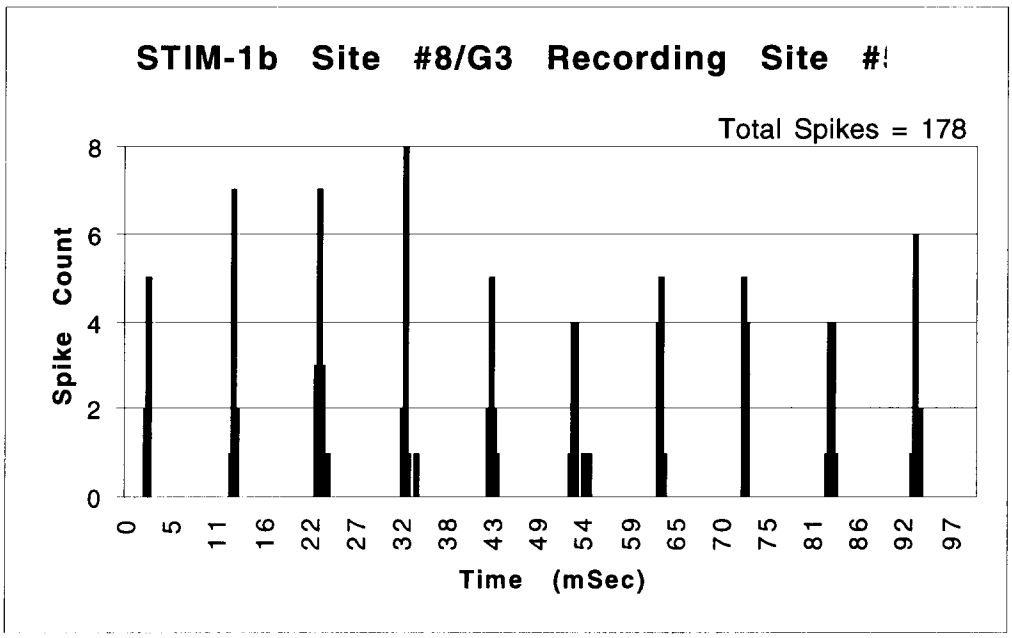

Fig. 56: PST histogram of the response recorded from site #5 of a G3 passive recording electrode in IC evoked by a 100Hz 1μA sinusoidal stimulus from site #8 of STIM-1b in the CN (see Fig. 54 for site maps).

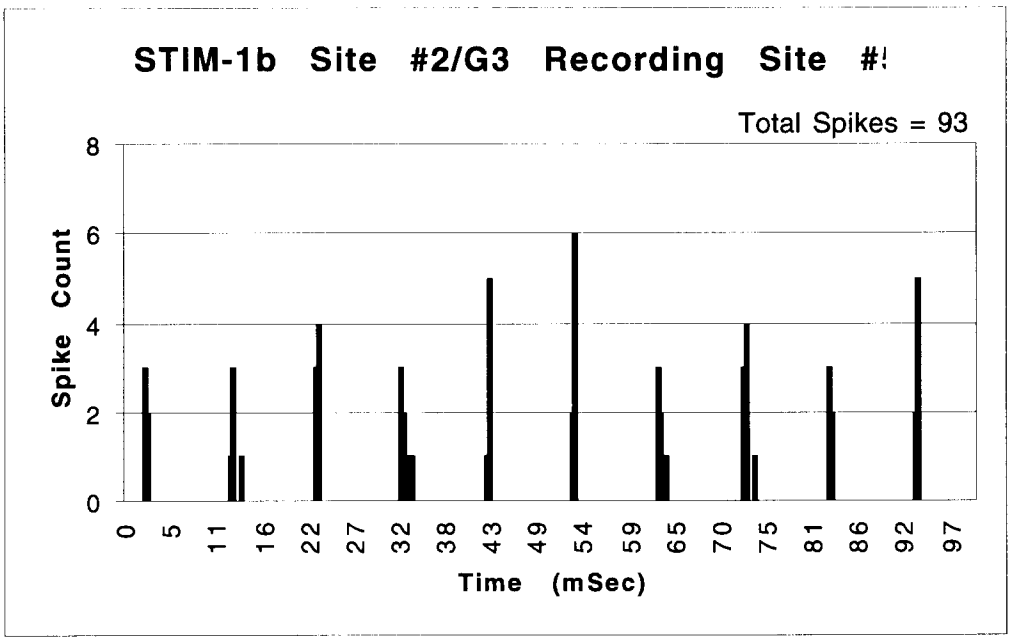

Fig. 57: PST histogram of the response recorded from site #5 of a G3 passive recording electrode in IC evoked by a 100Hz 1μA sinusoidal stimulus from site #2 of STIM-1b in the CN (see Fig. 54 for site maps).

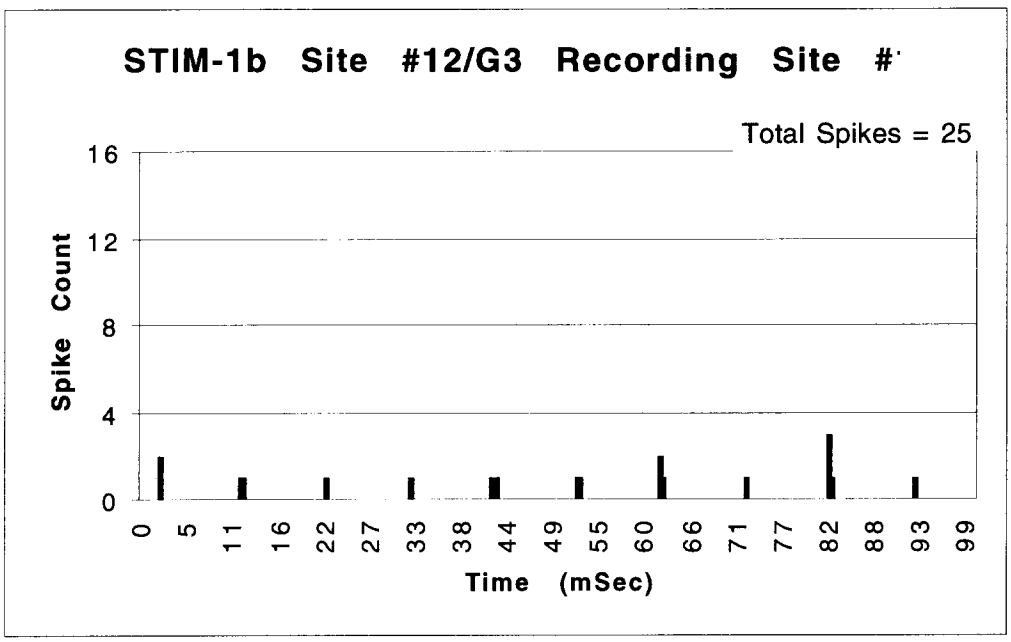

Fig. 58: PST histogram of the response recorded from site #1 of a G3 passive recording electrode in IC evoked by a 100Hz 1μA sinusoidal stimulus from site #12 of STIM-1b in the CN (see Fig. 54 for site maps).

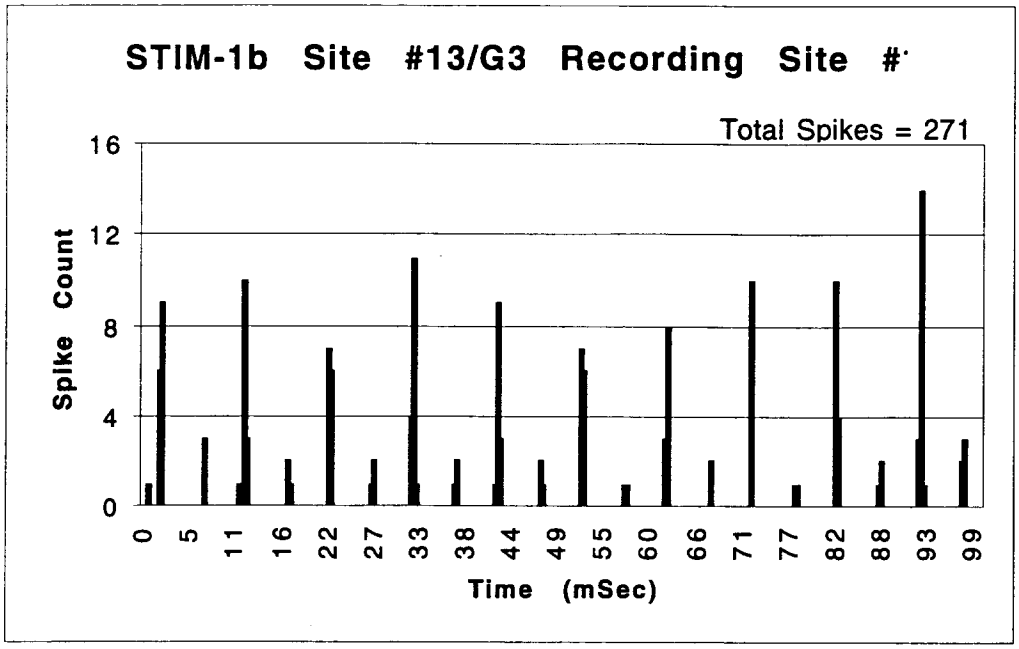

Fig. 59: PST histogram of the response recorded from site #1 of a G3 passive recording electrode in IC evoked by a 100Hz 1μA sinusoidal stimulus from site #13 of STIM-1b in the CN (see Fig. 54 for site maps).

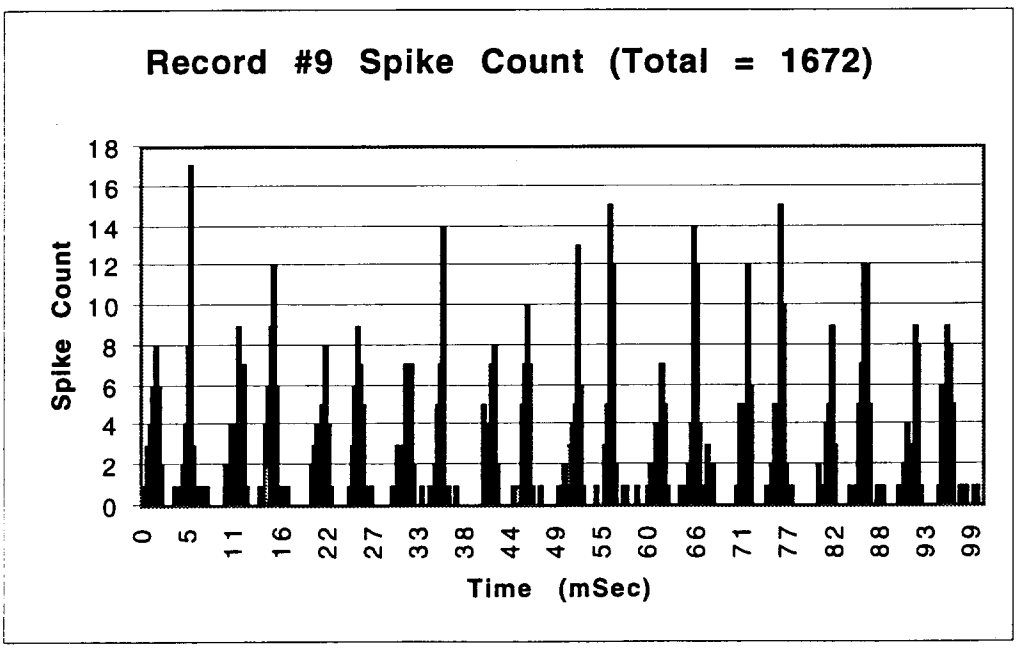

Fig. 60: PST histogram of the response recorded from a G3 passive recording electrode in guinea pig IC evoked by a 100Hz 1μA sinusoidal stimulus from STIM-1b in the CN.

STIM-1a

STIM-1a is a medium-complexity active probe which is used for bipolar stimulation. To effectively stimulate tissue, a bipolar current drive scheme is adopted; both current sourcing and sinking operations are simultaneously possible on two selected sites during the stimulating active cycle. This approach, which is based on charge balance, effectively stimulates tissue while reducing tissue damage and improving probe reliability. In the bipolar case, eight bits of serial data are used to select two sites. The subsequent 8 bits of current amplitude data are then used on-chip to generate the stimulus current for the first site using a current-output digital-to-analog converter (DAC). This current is mirrored to the second site to form a bipolar pair. Figure 61 shows the operation of the bipolar probe. The upper two traces show the 16-state serial input clock signal which controls the shift register in accepting external data information. The center trace shows the site-drive data signal (address and current level). The address here alternates between site #4 and another site in four combination patterns (1111111, 0111111, 0011111, and 0001111) to generate both sinking current and sourcing current. The bottom trace shows the measured voltage output waveform at site #4 across a 10kΩ resistor. Site #4 properly provides both sourcing current and sinking current alternately when addressed. Figure 62 shows STIM-1a delivering full-scale currents into a 5KΩ load at a clock rate of 500kHz.

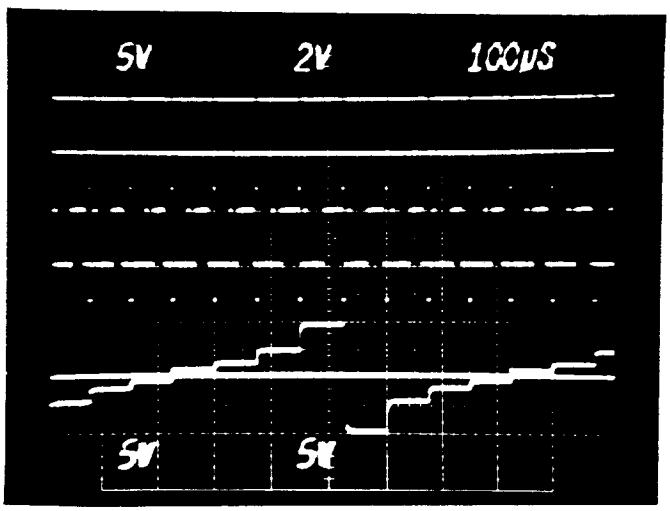

Fig. 61: Operation of the bipolar probe, STIM-1a. The top trace is the 16-cycle input clock and the middle trace is the input address and current level data. In this case, site #4 is selected and several different current levels are provided, both sourcing and sinking, alternating four combinations (1111111, 0111111, 0011111, and 0001111). The bottom trace shows the measured voltage output waveform at site #4 across a 10kΩ resistor.

While the basic STIM-1a probe functions with performance very close to design targets, some of the devices from the most recent fabrication run have exhibited poor contacts to the n+ diffusion and n+ poly areas. This has resulted in nonlinearity in the current sinking abilities of these probes as demonstrated in Fig. 63. The plots show that the output of the positive DAC is linear while the output of the negative DAC is nonlinear. An improved contact technology is being developed that will ensure that such problems do not occur in the future.

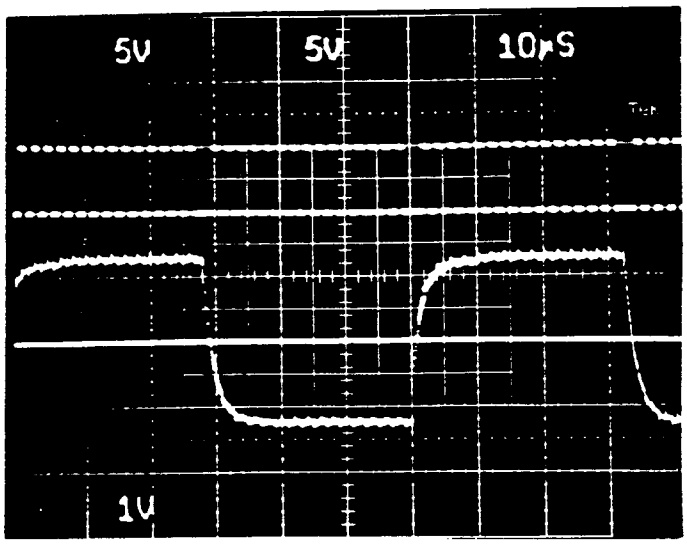

Fig. 62: Operation of STIM-1a at a clock rate of 500kHz. The upper trace shows the input clock, while the lower trace shows the output current being switched between full scale values of ±254µA across a 5KΩ load. The time constant here is due to test-setup capacitance.

Some of the STIM-1a probes also underwent *in-vivo* testing in a guinea pig. The probe was inserted into the dorsal cochlear nucleus and responses to stimulation were recorded from a head screw mounted on the cranium as in Fig. 64. Although not the expected middle latency response (MLR), a neural response was recorded. The stimulation protocol used was a bipolar biphasic (100µsec/phase) current. The response was observed to increase with increasing current intensities once a certain threshold level was reached. There was no response to the opposite stimulus polarity. Figure 65 displays the responses due to bipolar stimulation from sites #1 and 15, which span the array and are 1700µm apart (see Fig. 64 for site mapping). The recorded response was also shown to have a higher threshold when on directly adjacent shanks as illustrated by the threshold level of Fig. 66 compared to that in Fig. 65. In order to show that what was observed was actually a response and not just stimulus artifact, the animal was sacrificed without the disturbing the brain or probe, and the response was again recorded. Although the stimulus artifact in the two cases were similar, the "neural" response was no longer present after sacrifice, indicating that it was indeed neural in origin. These experiments have been very helpful in giving us experience using the probes in-vivo. As with STIM-1b, STIM-1a has been found to perform well. Its development is considered complete with the exception of eliminating the contact problems, improving our yield, and fabricating more of the structures.

STIM-1

STIM-1 is a high-end 16-channel 16-site probe in which site address data is entered first followed by 8 bits of current amplitude information. This probe is fully functional up to 10MHz. Sourcing and sinking currents are matched well within the 2µA design target over the entire operating range of ±254µA. When not sourcing or sinking current, the measured power dissipation is 81µW from ±5V. Fig. 67 shows the STIM-1 DAC output as the input code is stepped through the entire range (±254µA) across a 6.8KΩ load. The outputs are linear both sourcing and sinking as expected. Figure 68 shows the output

current delivered to the same load as the input data switches the output current between full scale sourcing and sinking levels with a 1MHz clock. Again, operation is as expected.

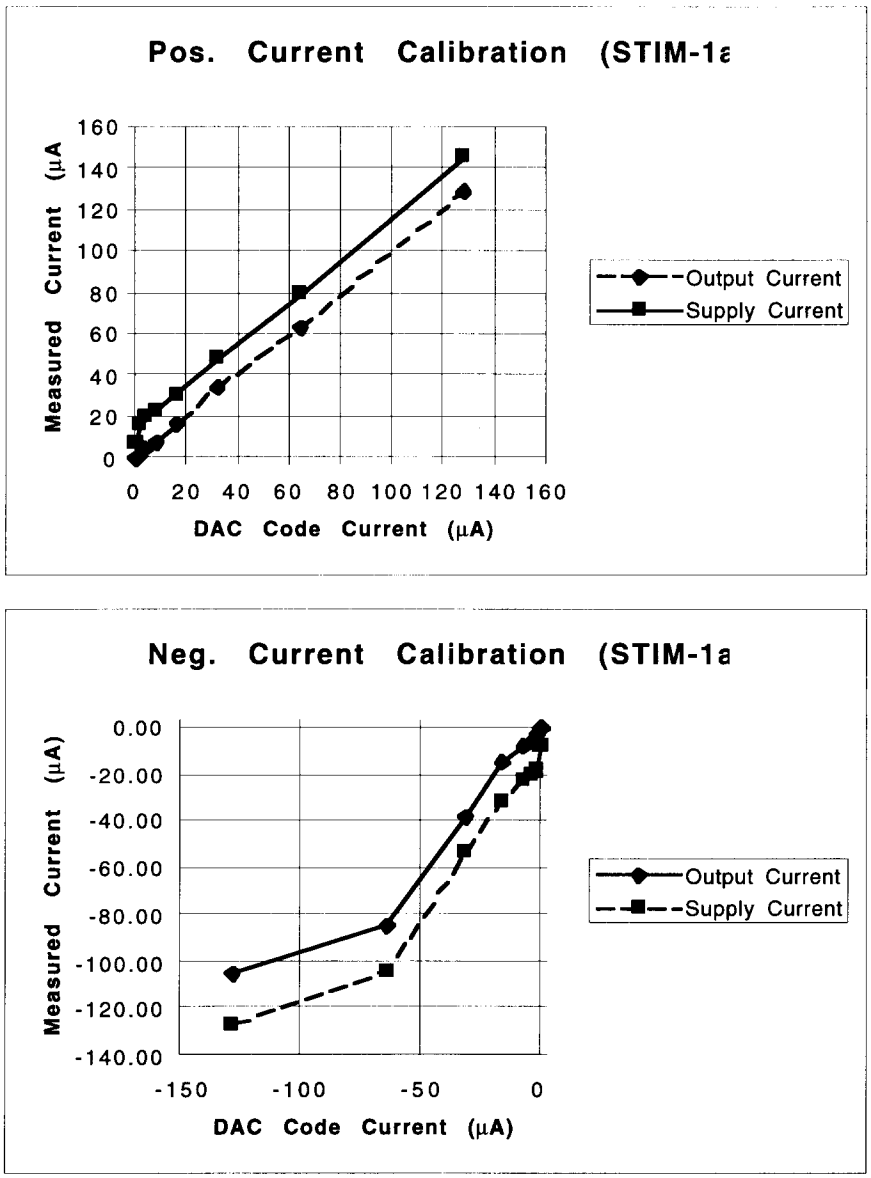

Fig. 63: Comparison of the sourcing (above) and sinking (below) output stimulation current and the supply current versus the specified current delivery levels for a STIM-1a probe having contact problems. The current sinking capability is degraded by the poor contacts.

STIM-2

STIM-2 is a second-generation probe that significantly extends the first-generation STIM-1 design in a number of areas: 1) flexible interconnects, fabricated as part of the chip, allow the rear portion of the circuit area to be folded flat against the cortical surface to reduce the probe height above the cortex to <1mm, which results in a low-profile probe; 2)

the probe offers a variety of new circuit designs to reduce power and circuit area while increasing functionality; 3) a front-end channel selector allows any 8 of 64 sites to be driven simultaneously, effectively implementing electronic site positioning; and 4) the probe is directly compatible with use in multi-probe three-dimensional arrays, initially targeted at 128 shanks and 512 sites. The addressed per-channel data latches lock onto the data when the clock line is strobed negatively and the DAC generates the appropriate currents. Figure 69 shows output voltage waveforms across a 20kΩ resistor load when the current level data alternate from (1111111) to (0000111) (16 combinations) for a sourcing case (CP=1). Figure 70 shows the output of one channel as the DAC is stepped through its entire range ±127μA into a 7KΩ load.

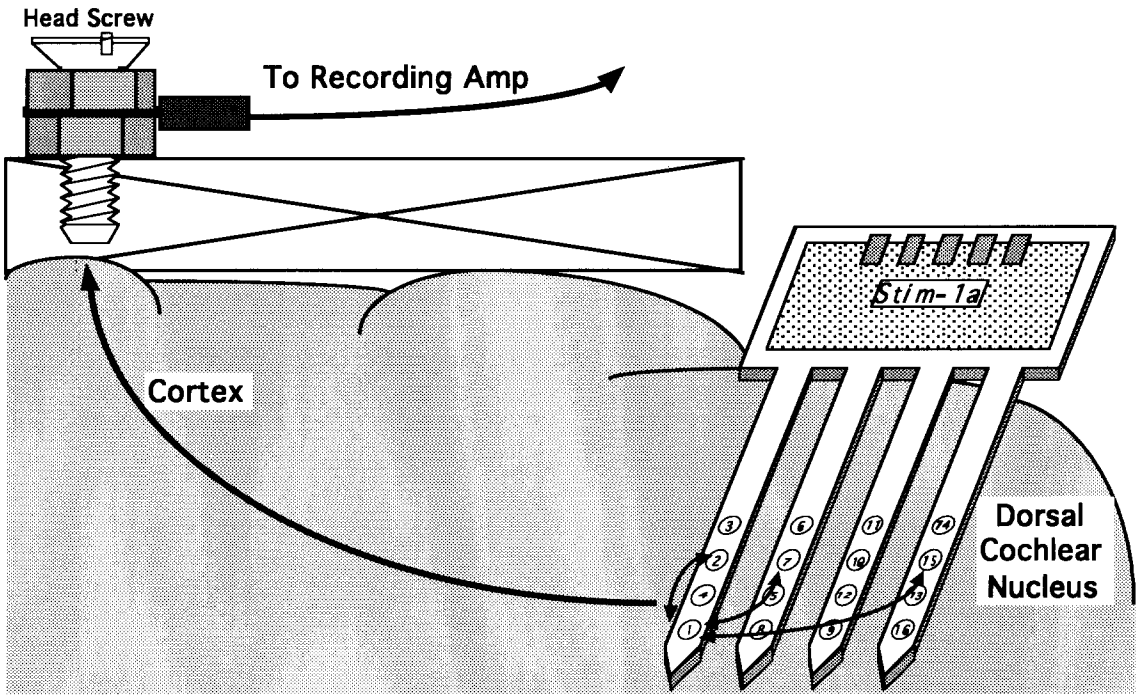

Fig. 64: Experimental setup for in-vivo testing of STIM-1a.

Again, the most recent fabrication run had a problem with poor ohmic contacts to the n+ diffusion and to n+ polysilicon. This was also reflected in weak sinking performance in the output DACs. By increasing the negative supply to -5.8V, the maximum sink current (1111111) was increased to -66μA, which is enough to do a number of in-vivo experiments. By adjusting both supply voltages (V_{DD} = 5.80V, V_{SS} = -5.95V), the probe was able to run with a clock frequency of 400kHz and still sink up to 66μA of current. We are considering a number of changes to this probe on the next iteration. In addition to fixing the contact problems using process modifications, we plan to increase the DAC setup currents to make them less sensitive to process variations and plan to connect the recording amplifier to a dedicated output line. This on-chip amplifier has a measured gain of 29.5dB with a 3dB bandwidth from 50Hz to 9kHz. In the present setup, the recording mode option permits this amplifier to be connected to any selected site. Its output is then placed on the data line and remains there until disconnected by the next clock signal. This means that no changes can be made in the stimulus current pattern from the probe while monitoring any of its sites. With ribbon cable interconnects, the addition of one more output lead is not significant; therefore, it is attractive to give the recording

amplifier a dedicated output line so that monitoring can continue as changes are made to the stimulus patterns launched by the probe. We also plan to modify this amplifier from an open-loop to a closed-loop design to make the gain characteristic independent of process variations.

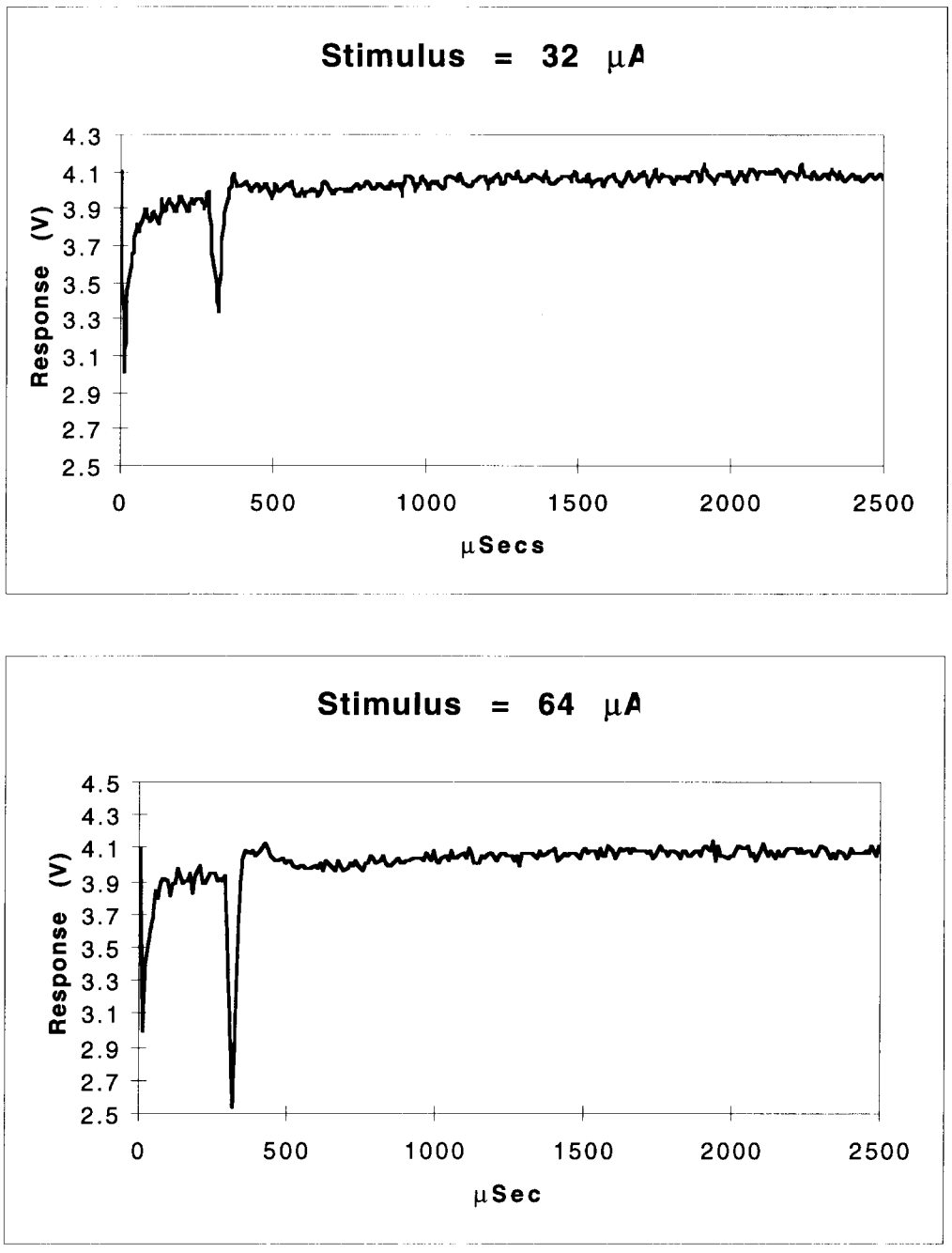

Fig. 65: Recorded responses due to 32μA and 64 μA bipolar biphasic 100 μsec/phase current pulses delivered from sites (#15/#1) on separate shanks of STIM-1a according to the experimental setup of Fig. 64.

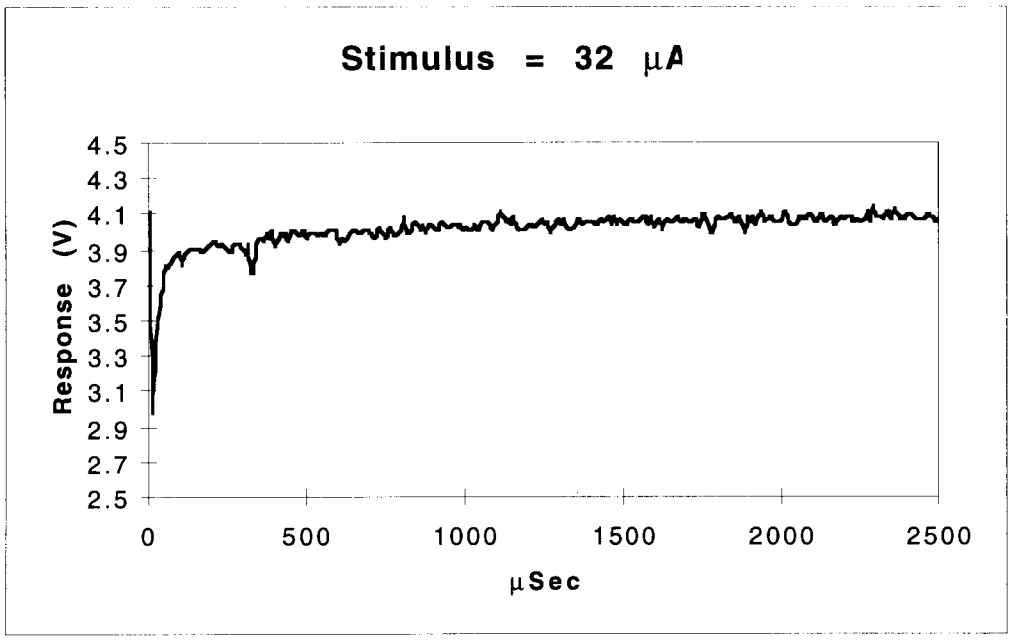

Fig. 66: Recorded response to a 32μA bipolar biphasic 100μsec/phase current pulse delivered from sites (#7/#1) (900μm apart) on adjacent shanks of STIM-1a as shown in Fig. 64.

The use of ribbon cables on STIM-2 has also pointed out that when active circuitry is present it is imperative that the ribbon cables be undercut from the front in order that their formation can take place while adequate silicon is retained under the circuitry at the back of the probe. It is not feasible to wait until a full etch-stop is achieved everywhere since in the current process there is no etch stop over the circuit area. This can be achieved only if the ribbon cables are oriented at ≥10° with respect to the <110> crystallographic axes of the silicon. This can be done by angling the cable slightly (off the usual 90° or 0° alignment with the probe/shank axis) or by rotating the entire probe/cable structure with respect to the silicon orientation flat. Aside from these minor iterations, STIM-2 appears ready for in-vivo applications and these will be pursued under the new contract.

The above results are an outline of extensive testing that has occurred on both the first- and the second-generation probes. Details of some of these test results can be found in cited papers in the literature and in the doctoral dissertations of Steven J. Tanghe [Tanghe 92-2] and Changhyun Kim [Kim 94-2].

4.4 External Electronics for Active Stimulating Probes

The external electronics developed to support the various versions of active stimulating probes must accomplish several functions. This system must first provide a friendly interface for the user, allowing the easy selection of desired stimulation waveforms and the sites to which they are to be directed. The external system will soon be used in experiments to evaluate the probes and to study cellular physiology using multipoint stimulation. These applications allow the user-selected stimuli to be represented by the appropriate commands in memory (loaded "off line") to be sent to the probe at high speed

when the stimulation is triggered. In the longer term, however, the system will have to allow electronically-generated signals (derived from a video camera or a microphone) to be routed to the probe in real time. This will require much higher-speed data processing than could be obtained with a microprocessor-driven system, demanding the use of high-speed digital signal processing (DSP) chips. In addition to encoding the appropriate data for use by the probes, the system must provide clock and power as well.

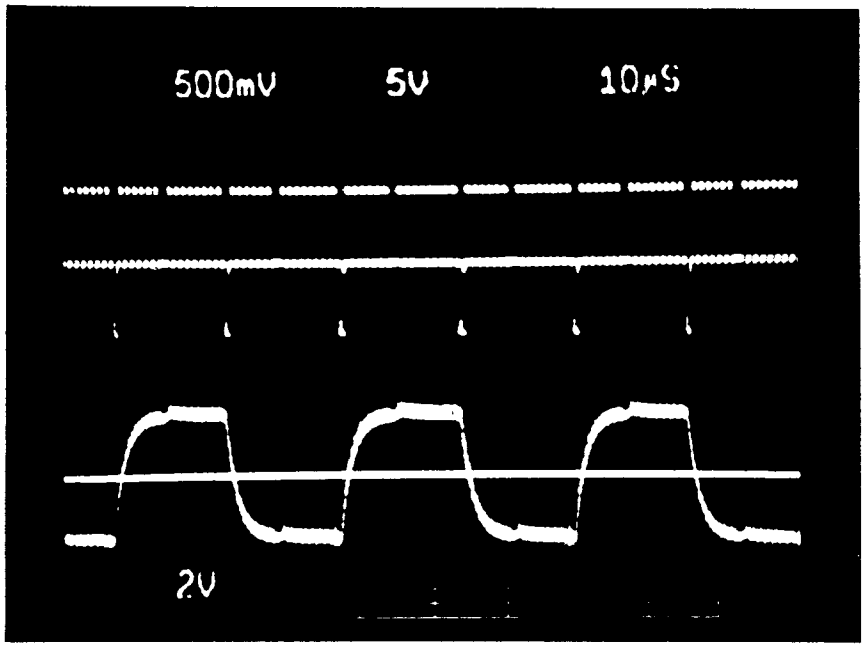

Fig. 67: Performance of STIM-1 at an input clock frequency (top trace) of 1MHz. The output current (lower trace) is being driven between the full-scale limits of ±254µA into an 6.8KΩ load.

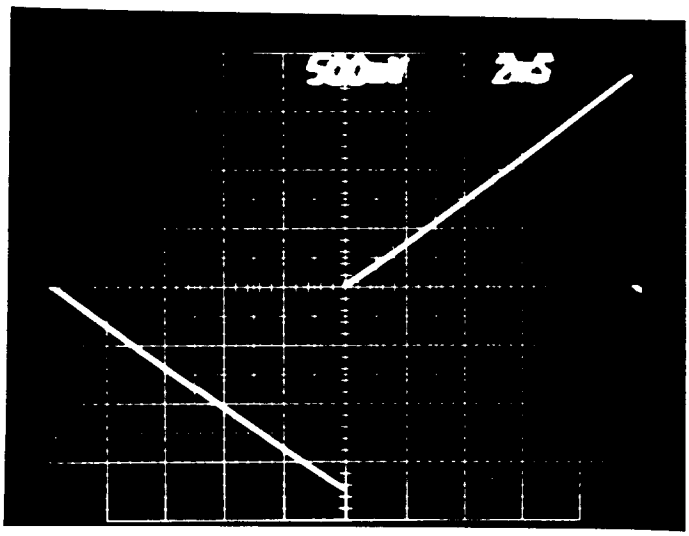

Fig. 68: DAC output on STIM-1 as the input is stepped through its entire range of values (-254µA to +254µA) into a 6.8KΩ load.

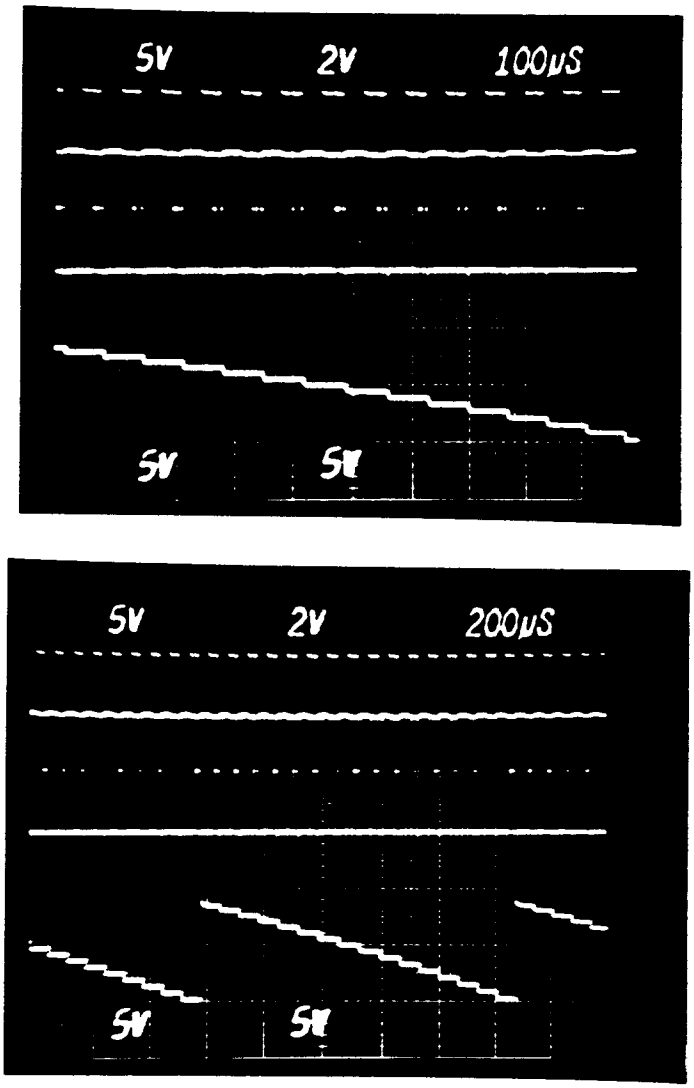

Fig. 69: Output voltage waveforms across a 20kΩ resistor load generated by STIM-2 when the current level data alternate from (1111111) to (0000111) for the sourcing case (CP=1).

Two serial lines supply the data and clocking signals to these probes. The binary bit rate on these lines is specified at about 4Mbits/sec. The signals employ ternary logic, utilizing signal levels of +5, 0, and -5 volts. These must be variable to match the supply voltages. There are three additional interface lines to these probes. One is a ground reference, and the other two are +5 and -5 supplies (VDD and VSS). These must also be variable, both to calibrate the DAC currents and for use with low-voltage probe designs. Some probes may have an additional line that measures the on-probe positive supply voltage to allow on-chip supply regulation utilizing off-chip electronics.

Figure 71 shows the overall external electronic system developed for these probes. The system consists of an IBM PC/AT-compatible computer equipped with a high-speed DSP board (Atlanta Signal Processors Chimera DSP Board). A customized circuit board, a

implementations of the STIM-1 probe, the prototype hardware was tested and verified. Some slight problems were found and corrected, but the overall design was judged to be sound enough to implement on printed circuit boards. As the first prototypes of STIM-2 dies became available, the hardware was also tested successfully with these new probes.

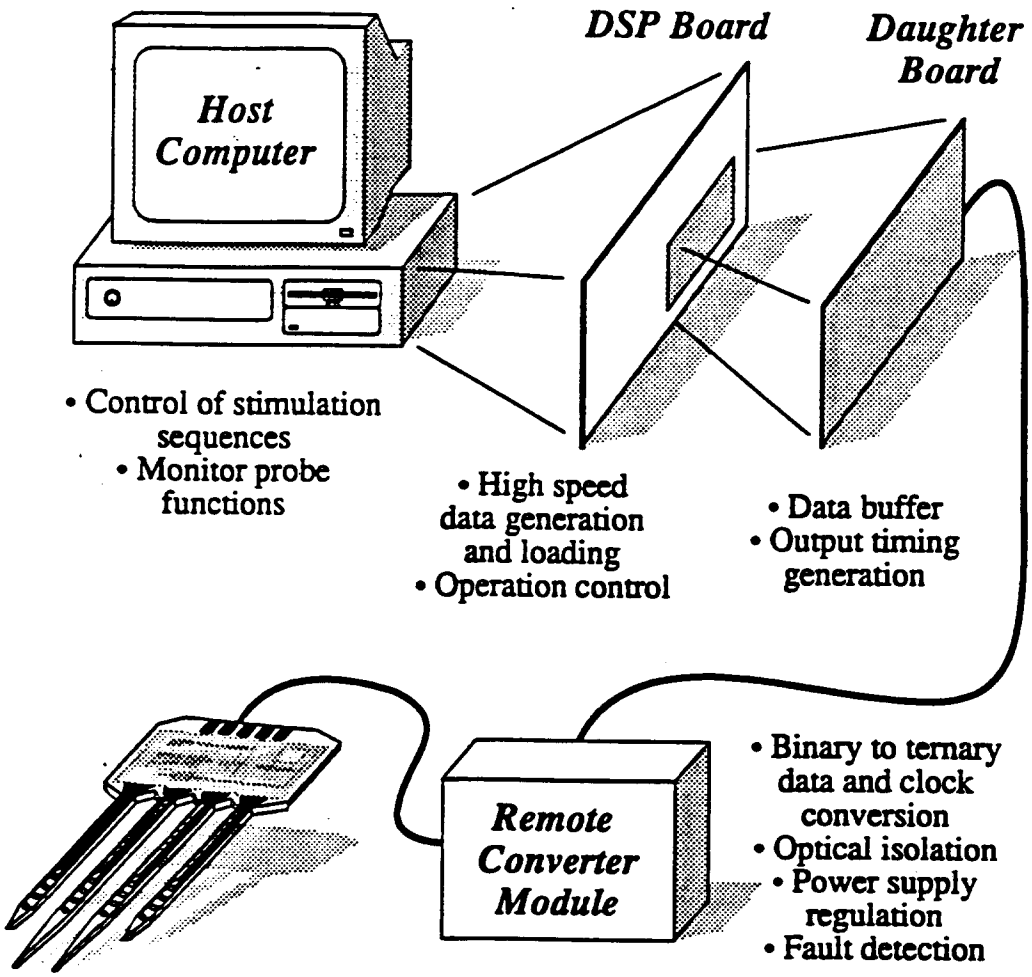

Fig. 71: An overview of the external electronic system used to control the active stimulating probes.

The manufacture of the printed circuit boards for system implementation was a process that required much more effort than the simple wire-wrap prototypes. To aid in this process, a computer-assisted schematic capture and board layout software package (named PADS) was purchased. Using PADS, the entire designs of the daughterboard and remote converter were captured in electronic form, using a hierarchical block diagram model of the circuit design. These schematics were then transferred to the board layout module of PADS. The board design process was one of the most tedious and painstaking aspects of the work due to the large number of real-world considerations, such as the spacing of components, the hole sizes of various discrete components, the spacing of routed traces, and most importantly the need to ensure that there were no errors in the layout, given the high cost of re-manufacturing the boards. All traces and holes were manually checked before submission for manufacturing in order to ensure a high probability that no such re-manufacture would be required.

The final board layouts were submitted for manufacture to a service bureau. The first half of the manufacturing lot has been completed and received, consisting of five units of the Chimera daughterboard. The remainder of the order, five units of the remote converter, are currently being manufactured with delivery expected within a few weeks. Once this shipment is received, a brief testing phase will be required to isolate and correct any errors in the design or the boards themselves.

The software interface to all of the hardware described above has progressed to keep up with the development of the hardware. At first, simple stand-alone programs were written to perform rudimentary tasks such as sending out single data bytes to the daughterboard. These programs were sufficient to support the initial design and prototype of the circuits. Once a workable, complete hardware system was in place, a more powerful second-generation software system was developed. This system was designed with the goal of being flexible and programmable, while still allowing the most common tasks to be performed without requiring a knowledge of programming.

This software system was designed around a procedure-oriented interpreted language known as TCL. The TCL language seemed perfectly suited to the needs of testing and debugging. It allowed for simple one-word commands to be issued for performing tasks such as resetting the hardware and sending out data to the probe, while at the same time it allowed for those commands to be grouped with programming constructs such as loops and conditionals to create small programs that performed higher-level tasks, such as sending out pulses. Since TCL is an interpreted language, development of these small programs could be done on-the-fly, without the need for the write-compile-link process of non-interpreted languages.

While TCL may be well-suited for testing and debugging, it is clear that a more user-friendly system will be required for the general user. To this end, a Windows-based program is in development that provides a more convenient and intuitive interface than the current text-only command-line based interface. Currently, a prototype version of this software has been developed which attempts to explore the issues of specifying a user interface to the stimulating probe.

The challenges in this development effort are the same as for most Windows-based programs: trying to develop an interface that is clean, simple, usable, and yet powerful enough to allow the generation of any waveform that the user may want to employ in stimulation. As the industry-standard windowing environment shifts from Windows 3.1 to Windows 95, some effort will be required to port the existing code base to the new platform since it is expected that most customers of the external electronics system will also take part in this migration.

5. *Future Research*

The past contract has moved us significantly closer to the goal of practical engineering structures that can support the key experiments needed to shown the feasibility of neural prostheses. However, work remains in a number of areas that will be addressed in a new contract from the Neural Prosthesis Program. Comments on these planned activities are given in this section.

One of the first areas to be addressed will be the development of a low-resistance interconnect material. This will be tackled in conjunction with efforts on an improved contact structure for probe circuitry. In order to ensure low-resistance contacts to both n- and p-type silicon, we will explore several options presently used by the semiconductor industry. These include the use of Ti:W or TiN plugs, the use of Ti sacrificial layers, and the use of PtSi at the silicon surface. Both aluminum and refractory metals and silicides will be explored for the interconnect material itself as mentioned in section 2.2. As part of this effort, we will also seek to develop a two-layer interconnect scheme that will allow the stacking of leads and hence will permit narrower shanks on our stimulating electrodes. For 16-shank structures having 4 contacts per shank this is not critical using the new overlapping site structure, and shank widths below 40μm appear feasible. For 8-shank probes, a two-layer interconnect would allow us to maintain these narrow widths while packing 8 sites per shank.

As part of the interconnect development process, we will also explore the behavior of LTO and other dielectrics for chronic encapsulation of the probes. Two new films deserve special mention as possible long-term aids for probe encapsulation: silicon carbide and diamond. Both of these films are highly inert and appear potentially attractive for probe use. We are currently working with EIC Laboratories to evaluate silicon carbide films they have been depositing. The films have been deposited on "probe" wafers to study stress and step coverage properties and the use of RIE for film patterning. During the new contract, we plan to continue to work with EIC in this area with the hope that the carbide films can be added as an outer layer over the oxide/nitride dielectrics to provide an additional barrier against the biological environment. In addition, diamond films are being deposited by CVD at temperatures as low as 450°C by other groups, and we plan to track progress in these films during the coming contract as well. The films have a very fine grain, and growth can be catalyzed in selective areas. However, the technology for both types of films is still relatively early in its development. The primary thrust of our efforts under the new contract will therefore continue to be directed at nitride/oxide dielectrics, with silicon carbide and diamond studied as alternatives (or more likely supplements) for possible use in longer-term implant situations.

We will continue to support other investigators in the NPP with the development of passive probe structures and hope to supply limited numbers of the active probes to other investigators by contract end. In addition, a new active stimulating probe will be designed and fabricated having an on-chip multiplexer but with off-chip current generation. The probe will have 64 400μm^2 sites distributed over 16 shanks. This probe will be similar in current range to STIM-2 and should permit monitoring of the selected site voltage when not stimulating as on STIM-2. We tentatively call this probe STIM-2b. In fact, it amounts to four STIM-1b probes with the addition of the recording option from STIM-2. All circuitry will share the three power supply inputs as well as a clock and data (address) line. Unlike STIM-1b, which uses a clock to serially count up the address, we tentatively plan to provide a serial address as in STIM-2. The clock line will serially enter a 16b data word which will be interpreted by STIM-2b as four 4b (1 of 16) addresses. These will be used to set up four paths linking the four input channels to the four selected sites. The negative

clock strobe will cause these to be latched. The corresponding input stimulating currents will thus be steered to the selected sites. Again, the probe will use the standard five-lines from the external system, plus in this case four additional stimulus lines corresponding to the externally-generated stimulus currents.

There are many possible configurations in which the sites from STIM-2b can be grouped. One possibility is shown below in Fig. 72 for four shanks of a 16-shank 64-site probe. Each shank here has four sites, one from each of the four channels. Thus, any four sites on a given shank can be driven simultaneously. By staggering the sites on neighboring shanks, it is also possible to stimulate any lateral site pairs or any four lateral sites (at the same depth). This and other possible configurations will be reviewed prior to a final selection of the grouping to be used. This probe should be quite useful, representing a relatively simple electronics package but a capability nearly equal to that of the larger devices.

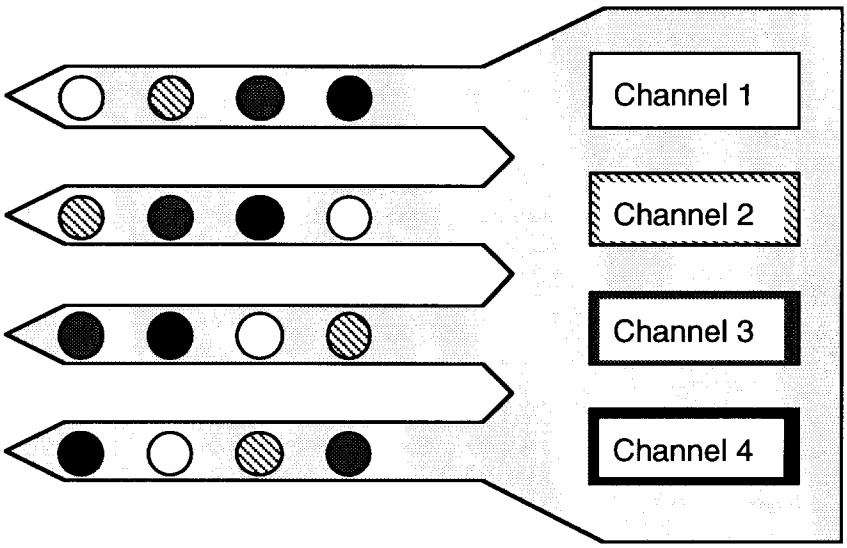

Fig. 72: One possible grouping of 16 sites from a 64 site 16-shank probe, partitioning the sites among four channels which provide externally-generated stimulus currents. The four shanks shown would be repeated four times to make the total 16-shank probe.

In addition to STIM-2b, a multi-probe stimulating array (STIM-3) consisting of 16 16-shank probes, each probe having four sites per shank, will be developed. We plan to base our approach to this array on our past work with STIM-2 and the 3D microassemblies described in section 2. A micromachined silicon platform will be used as a base for probe assembly. Individual active probes will be inserted through the platform, with bent-beam lead transfers to the platform. It is expected that five leads will be required per probe as noted above. With the probes in place, the array will span an area of 6.4mm x 6.4mm with shanks on 0.4mm centers. With four sites per shank, a vertical tissue depth of 1.6mm will be instrumented. This array will bring together state-of-the-art technology for the active probes and for three-dimensional multi-chip assemblies. We are confident that the active probe technology will permit yields consistent with the realization of 3D arrays of the type required. The 3D assembly technology is especially important because it involves some hand assembly in the placement and interconnection of the probes; however, on the basis of

the results already achieved with passive assemblies and with STIM-2 (which in the 8-shank version includes slots for 3D assembly spacers), we believe this assembly process can also be accomplished with high yield.

As these probes move from research into application, where special-purpose user needs begin to dominate, the need for a flexible, programmable, user-friendly external electronic system becomes increasingly important. In addition, the proposed growth in complexity of the basic designs, including the 3D stimulating array, increases the challenges in fully testing each probe to ensure that it is completely operational. The primary goal in further developing the external electronics will be to develop the software capability on the host computer side needed to achieve a user interface that meets the needs of the research community and a second interface that meets the needs of device quality assurance. Our efforts will be directed primarily at software development, with little additional work on the DSP or interface electronics anticipated. This software development will include:

- Development of a fully functioning testbed system for quality assurance and diagnostic evaluation of our present stimulating probes. This system will be DOS/Windows-based and will not involve any changes to the current firmware and hardware design. Along with this software system, we will have PC board implementations of the two components of the interface electronic subsystem.

- Development of a graphical user interface that can serve the user community. This interface will be developed and run under DOS/Windows to implement a suite of neurophysiological measurement blocks, including several prototype interfaces for sequencing stimulation across multiple electrode sites.

- Designing control protocols for new probes that will be developed during the coming contract (primarily STIM-2b).

- Moving the completed software and hardware system from a DOS environment to Windows 95, which will be more likely to be used by the research community.

6. *Summary and Conclusions*

The goal of the contract reported here was to develop stimulating electrode arrays capable of delivering precisely controlled stimulation at multiple points in the central nervous system on a chronic basis. Building on a technology base established during a previous contract, the results obtained during the past three year period have moved us significantly closer to that goal. The basic probe technology has been improved in a number of important ways. Continuing problems with the adhesion of iridium oxide sites to their underlying conductors were solved by modifying the site structure and introducing improved cleaning procedures for removing fluorocarbon residues left as the result of dry etching processes. The new site structures also allow the site to overlap adjacent conductors, decoupling the shank width from the size of the site. The use of a shallow boron diffusion was introduced to allow the formation of sharper tips on the probes than can be obtained using a deep diffusion; this process requires no additional process steps when used on chronic probes since the same diffusion is employed for ribbon cables. Preliminary work on the development of a low-resistance interconnect structure has shown that titanium silicide can be used to reduce lead resistances by a factor of from five to ten below those provided by polysilicon conductors. Such leads remain viable at temperatures up to 820°C, making them compatible for use with low-temperature oxide (LTO), PECVD silicon nitride, and LPCVD silicon nitride encapsulating dielectrics. During the past contract period, we have continued to develop both acute and chronic stimulating and recording probes for other investigators in the Neural Prosthesis Program. More than 1500 fully-tested probes of over 100 different designs have now been provided to investigators nationwide.

Work to characterize the probes in-vivo is underway both in-house and in the laboratories of our collaborating investigators. The feedback obtained is essential in continuing the optimization process and in understanding the limitations of the technology. During the past contract we have established automated facilities for iridium activation using cyclic voltammetry and for making in-vitro impedance measurements. In addition, we have established facilities for doing in-vivo measurements of site impedance and charge capacity for probes implanted chronically. Measurements on probes implanted for two weeks and then stimulated for four hours per day over five days with charge-balanced bipolar 50μA 100μsec/phase current pulses have shown the back voltages and site impedances for 1600μm^2 sites to be stable over time. The charge capacity measured for 400μm^2 sites gradually declined in-vivo, and this decline is not yet understood. No significant changes in current flow paths along probe shanks (between sites on the same shanks) or between shanks (sites on different shanks) have been observed during these measurements. In addition, sites produced using the new fabrication procedures have been pulsed in PBS solution using similar protocols (50μA, 100μsec/phase, 1000μm^2) for over 200 million pulses with no change in their impedance characteristics. We have also explored the ability of single- and multi-shank probes to penetrate pia arachnoid in guinea pig using probes fabricated with strain gauges on their shanks. Probes having tip angles that varied from 10° to 45° were used with both shallow- and deep-diffused tips. Pia dimpling is over 700μm for the larger tips and less than 300μm for the sharper ones. A significant observation in using the sharper tips is that penetrated blood vessels appear to self-seal around them so that no detectable bleeding is observed, whereas the larger tips cause bleeding upon penetration. Preliminary experiments with 8x8-shank three-dimensional probe arrays have shown that these structures, which have shallow-diffused sharp tips, penetrate guinea pig pia quite readily. The 3D array technology was developed under a companion recording contract but is ready to apply to stimulating arrays.

During the past contract, considerable progress has been made in the development of active probes containing on-chip signal processing. At the beginning of the contract, a set of first-generation active stimulating probes had been realized and were undergoing test. Since that time, these tests were completed, the designs were iterated, and a set of second-generation probes were fabricated and tested. In order to complete these probes, a successful encapsulation/interconnect process was developed in which LPCVD silicon dioxide and silicon nitride are used over polysilicon conductors on the probe shanks and aluminum interconnects are used in circuit areas under an overcoat of LTO. Additional layers of PECVD silicon nitride, metal barriers, and polymers can be used for chronic structures. The three active probes implement monopolar, bipolar, and multipolar (8-channel) designs. The monopolar and bipolar probes offer one and two simultaneously active channels, respectively, selected from among 16 sites. The monopolar design routes an externally-generated current to the selected site, while on the bipolar probe the current and sites are both selected digitally and the current is generated on-chip over a biphasic range from -254μA to +254μA ±2μA. Both of these active probes have now been used in preliminary in-vivo tests and both developments are considered complete. The high-end second-generation probe, STIM-2, contains 64 sites on 8 or 16 shanks. A front-end selector allows the user to select 8 of these sites for simultaneous stimulation using currents generated on-chip over a biphasic range from -127μA to +127μA ±1μA. This probe offers seven different operating modes including the ability to test site impedances, externally measure stimulus currents, record from any selected site, ground unused sites, or anodically bias the sites between pulses. While this probe is also fully functional, several changes are planned for a coming iteration to improve electrical contacts, reduce sensitivity to process variations, and allow recording while the current flow patterns from the probe are changed. The development of a high-performance external circuit interface for the active probes has also been completed. This circuit interface will soon facilitate the testing of STIM-2 in-vivo in both acute and chronic situations.

These results will be extended under a new contract through work in several areas. An improved contact technology for active probe circuitry will be developed along with a low-resistance interconnect material for use on probe shanks and ribbon cables. In addition, studies of probe encapsulation and probe performance in chronic situations will be continued. The design of STIM-2 will be iterated and a new probe capable of steering externally-generated currents to four sites selected from among 64 available on the probe will be developed. One version of STIM-2 will be fabricated to be compatible with a 3D 16x16-shank array, and such arrays, consisting of 128 channels and 1024 sites, will be developed. It is our hope that this technology will be applied in prosthetic applications before the year 2000 and that 3D active probe arrays will set the stage for a new generation of neural prostheses by the beginning of the new millennium.

7. *References*

[Anderson 89] D. J. Anderson, K. Najafi, S. J. Tanghe, D. A. Evans, K. L. Levy, J. F. Hetke, X. Xue, J. J. Zappia, K. D. Wise. Batch-Fabricated Thin-Film Electrodes for Stimulation of the Central Auditory System. *IEEE Trans. Biomed. Eng.* 36:693-704, 1989.

[Beebe 88] X. Beebe, T. L. Rose. Charge injection limits of activated iridium oxide electrodes with 0.2 ms pulses in bicarbonate buffered saline. *IEEE Trans. Biomed. Eng.* 35:494-495, 1988.

[BeMent 86] S.L. Bement, K. D. Wise, D. J. Anderson, K. Najafi, and K. L. Drake, "Solid-state electrodes for multichannel multiplexed intracortical neuronal recording," *IEEE Trans. Biomed. Eng.* 33:230-241, 1986.

[Bohg 71] A. Bohg, "Ethylene-diamine-pyrocatechol-water mixture shows etching anomaly in boron-doped silicon," *J. Electrochem. Soc.*, 118:401, 1971.

[Chen 94] J. K. Chen and K. D. Wise, "A Multichannel Neural Probe for Selective Chemical Delivery at the Cellular Level," *Digest Solid-State Sensor and Actuator Workshop*, Hilton Head, S.C., pp. 256-259, June 1994.

[Drake 88] K. L. Drake, K. D. Wise, J. Farraye, D. J. Anderson, and S. L. BeMent. Performance of planar multisite microprobes in recording extracellular single-unit intracortical activity. *IEEE Trans. Biomed. Eng.*, 35:719-732, 1988.

[Hetke 94] J. F. Hetke, J. L. Lund, K. Najafi, K. D. Wise, and D. J. Anderson, "Silicon Ribbon Cables for Chronically Implantable Microelectrodes Arrays," *IEEE Trans. Biomed. Eng.*, vol. 41, pp. 314-321, April 1994.

[Hoogerwerf 91] A. C. Hoogerwerf and K. D. Wise, "A Three-Dimensional Neural Recording Array," *Digest IEEE Int. Conf. on Solid-State Sensors and Actuators*, San Francisco, pp. 120-123, June 1991.

[Hoogerwerf 94] A. C. Hoogerwerf and K. D. Wise, "A Three-Dimensional Microelectrode Array for Chronic Neural Recording," *IEEE Trans. Biomed. Engr.*, pp. 1136-1146, December 1994.

[Ji 90] J. Ji and K. D. Wise, "An Implantable CMOS Analog Signal Processor for Multiplexed Microelectrode Recording Arrays," *Digest 1990 IEEE Solid-State Sensor and Actuator Workshop*, Hilton Head, S.C., pp. 107-110, June 1990.

[Ji 92] J. Ji, K. D. Wise. An Implantable CMOS Circuit Interface for Multiplexed Microelectrode Recording Arrays. *IEEE J. of Solid-State Circuits*, Vol. SC-26, no. 3, pp. 433-443, Mar. 1992.

[Kim 93] C. Kim, S. J. Tanghe, and K. D. Wise, "Multichannel Neural Probes with On-Chip CMOS Circuitry and High-Current Stimulating Sites," *Digest IEEE Int. Conf. on Solid-State Sensors and Actuators (Transducers'93)*, Yokohama, pp. 454-457, June 1993.

[Kim 94-1] C. Kim and K. D. Wise, "A 64-Site Multiplexed Low-Profile Neural Probe with On-Chip CMOS Circuitry," *Digest 1994 IEEE Symposium on VLSI Circuits*, Honolulu, pp. June 1994.

[Kim 94-2] Changhyum Kim, A 64-Site Multiplexed Low-Profile Neural Probe for use in Neural Prostheses, Ph.D. Dissertation, The University of Michigan, 1994.

[Lund 94] J. L. Lund and K. D. Wise, "Chip-Level Encapsulation of Implantable CMOS Microelectrode Arrays," *Digest Solid-State Sensor and Actuator Workshop*, Hilton Head, S.C., pp. 29-32, June 1994.

[McCreery 86] D. B. McCreery, L. A. Bullara, and W. F. Agnew, "Neuronal Activity Evoked by Chronically Implanted Intracortical Microelectrodes," *Experimental Neurology, 92*, pp. 147-161, April 1986.

[Najafi 85] K. Najafi, K. D. Wise, and T. Mochizuki, "A high-yield IC-compatible multichannel recording array," *IEEE Trans. Electron Devices,* 32:1206-1211, 1985.

[Najafi 90-1] K. Najafi, J. Ji, and K. D. Wise, "Scaling Limitations of Silicon Multichannel Recording Probes," *IEEE Trans. Biomed. Eng.,* 37:1-10, 1990.

[Najafi 90-2] K. Najafi, and J.F. Hetke, "Strength Characterization of Silicon Microprobes in Neurophysiological Applications," *IEEE Trans. on Biomed. Eng.,* Vol. 37, No. 5, pp. 474-481, May 1990

[Niparko 89a] J.K. Niparko, R.A. Altschuler, D.A. Evans, X. Xue, J. Farraye, and D.J. Anderson, "Auditory Brainstem Prosthesis: Biocompatibility of Stimulation," *Otolaryngol. Head and Neck Surg.,* Vol. 101, np. 3, pp. 344-352, 1989

[Niparko 89b] J.K. Niparko, R.A. Altschuler, X. Xue, J.A. Wiler, and D.J. Anderson, "Surgical Impantation and Biocompatibility of CNS Auditory Prostheses," *Ann. Otolo. Rhinol. Larynol.,* vol. 98, pp. 965-970, 1989

[Roblee 90-1] L. S. Robblee, S. F. Cogan, T. L. Rose, D. V. Hills, A. G. Kimball. Studies of the electrochemistry of stimulating electrodes. Eighth quarterly progress report for the National Institute of Health, Contract no. NO1-NS-8-2313, November, 1990

[Robblee 90-2] L. S. Robblee, T. L. Rose. *Neural Prostheses: Fundamental Studies,* W. Agnew, D. McCreery, Ed., chapter 2, Englewood Cliffs, New Jersey, 1990.

[Starr 73] A. Starr, K. D. Wise, and J. Csongradi, "An Evaluation of Photoengraved Microelectrodes for Extracellular Single-Unit Recording," *IEEE Trans. Biomed. Engr., 20,* pp. 291-293, July 1973.

[Tanghe 92-1] S. J. Tanghe and K. D. Wise, "A 16-Channel CMOS Neural Stimulating Array," *IEEE J. Solid-State Circuits*, vol. 27, pp. 1819-1825, Dec. 1992.

[Tanghe 92-2] Steven J. Tanghe, Micromachined Silicon Stimulating Probes with CMOS Circuitry for use in the Central Nervous System, Ph.D. Dissertation, The University of Michigan, 1992.

[Kim 94-1] C. Kim and K. D. Wise, "A 64-Site Multiplexed Low-Profile Neural Probe with On-Chip CMOS Circuitry," *Digest 1994 IEEE Symposium on VLSI Circuits*, Honolulu, pp. June 1994.

[Kim 94-2] Changhyum Kim, A 64-Site Multiplexed Low-Profile Neural Probe for use in Neural Prostheses, Ph.D. Dissertation, The University of Michigan, 1994.

[Lund 94] J. L. Lund and K. D. Wise, "Chip-Level Encapsulation of Implantable CMOS Microelectrode Arrays," *Digest Solid-State Sensor and Actuator Workshop*, Hilton Head, S.C., pp. 29-32, June 1994.

[McCreery 86] D. B. McCreery, L. A. Bullara, and W. F. Agnew, "Neuronal Activity Evoked by Chronically Implanted Intracortical Microelectrodes," *Experimental Neurology, 92*, pp. 147-161, April 1986.

[Najafi 85] K. Najafi, K. D. Wise, and T. Mochizuki, "A high-yield IC-compatible multichannel recording array," *IEEE Trans. Electron Devices,* 32:1206-1211, 1985.

[Najafi 90-1] K. Najafi, J. Ji, and K. D. Wise, "Scaling Limitations of Silicon Multichannel Recording Probes," *IEEE Trans. Biomed. Eng.,* 37:1-10, 1990.

[Najafi 90-2] K. Najafi, and J.F. Hetke, "Strength Characterization of Silicon Microprobes in Neurophysiological Applications," *IEEE Trans. on Biomed. Eng.,* Vol. 37, No. 5, pp. 474-481, May 1990

[Niparko 89a] J.K. Niparko, R.A. Altschuler, D.A. Evans, X. Xue, J. Farraye, and D.J. Anderson, "Auditory Brainstem Prosthesis: Biocompatibility of Stimulation," *Otolaryngol. Head and Neck Surg.,* Vol. 101, np. 3, pp. 344-352, 1989

[Niparko 89b] J.K. Niparko, R.A. Altschuler, X. Xue, J.A. Wiler, and D.J. Anderson, "Surgical Impantation and Biocompatibility of CNS Auditory Prostheses," *Ann. Otolo. Rhinol. Larynol.,* vol. 98, pp. 965-970, 1989

[Roblee 90-1] L. S. Robblee, S. F. Cogan, T. L. Rose, D. V. Hills, A. G. Kimball. Studies of the electrochemistry of stimulating electrodes. Eighth quarterly progress report for the National Institute of Health, Contract no. NO1-NS-8-2313, November, 1990

[Robblee 90-2] L. S. Robblee, T. L. Rose. *Neural Prostheses: Fundamental Studies,* W. Agnew, D. McCreery, Ed., chapter 2, Englewood Cliffs, New Jersey, 1990.

[Starr 73] A. Starr, K. D. Wise, and J. Csongradi, "An Evaluation of Photoengraved Microelectrodes for Extracellular Single-Unit Recording," *IEEE Trans. Biomed. Engr., 20,* pp. 291-293, July 1973.

[Tanghe 92-1] S. J. Tanghe and K. D. Wise, "A 16-Channel CMOS Neural Stimulating Array," *IEEE J. Solid-State Circuits*, vol. 27, pp. 1819-1825, Dec. 1992.

[Tanghe 92-2] Steven J. Tanghe, Micromachined Silicon Stimulating Probes with CMOS Circuitry for use in the Central Nervous System, Ph.D. Dissertation, The University of Michigan, 1992.

[Wise 70] K. D. Wise, J. B. Angell, and A. Starr, "An Integrated Circuit Approach to Extracellular Microelectrodes," *IEEE Trans. Biomed. Engr., 17*, pp. 238-247, July 1970.

[Wise 75] K. D. Wise and J. B. Angell, "A Low-Capacitance Multielectrode Probe for Neurophysiology," *IEEE Trans. Biomed. Engr., 22*, pp. 212-219, May 1975.

[Wise 90] K. D. Wise, "VLSI Circuit Challenges in Integrated Sensing Systems," (Invited), *IEEE VLSI Circuits Symposium*, Honolulu, pp. 19-22, June 1990.

[Wise 91-1] K. D. Wise and K. Najafi, "Microfabrication Techniques for Integrated Sensors and Microsystems," (Invited), *Science*, November 29, 1991.

[Wise 91-2] K. D. Wise and N. Najafi, "The Coming Opportunities in Microsensor Systems," (Invited), *Digest IEEE Int. Conf. on Solid-State Sensors and Actuators*, San Francisco, pp. 2-7, June 1991.

[Zappia 90] J.J. Zappia, J.F. Hetke, R.A. Altschuler, and J.N. Niparko, "Evaluation of a Silicon-Substrate Madiolar Eighth Nerve Implant in a Guinea Pig," *Otolaryngol. Head and Neck Surg.,* vol. 103, pp. 575-582, 1990

Appendix

*RECENT PUBLICATIONS FROM THE UNIVERSITY OF MICHIGAN AND EXTERNAL USERS ON MICROMACHINED MICROELECTRODE ARRAYS**

Journal Articles

K. L. Drake, K. D. Wise, J. Farraye, D. J. Anderson, and S. L. BeMent, "Performance of Planar Multisite Microprobes in Recording Extracellular Single-Unit Intracortical Activity", *IEEE Trans. Biomed. Engr.*, 35, pp. 719-732, September 1988.

D.A. Evans, J.K. Niparko, J.M. Miller, R. Jyung and D.J. Anderson, "Multiple-channel Stimulation of the Cochlear Nucleus", *Otolaryngol. Head Neck Surg.*, vol. 101, pp. 651-657, 1989.

J. K. Niparko, R. A. Altschuler, X. Xue, J. A. Wiler and D. J. Anderson, "Surgical Implantation and Biocompatibility of Central Nervous System Auditory Prostheses", *Ann. Otol. Rhinol. Laryngol.*, vol. 98, pp. 965-970, 1989.

D. J. Anderson, K. Najafi, S. J. Tanghe, D. A. Evans, K. L. Levy, J. F. Hetke, X. Xue, J. J. Zappia, and K. D. Wise, "Batch-Fabricated Thin-Film Electrodes for Stimulation of the Central Auditory System", *IEEE Trans. Biomed. Engr.*, pp. 693-704, July 1989.

S. J. Tanghe, K. Najafi, and K. D. Wise, "A Planar IrO Multichannel Stimulating Electrode for Use in Neural Prostheses", *Sensors and Actuators*, B1, pp. 464-467, January 1990.

K. Najafi, J. Ji, and K. D. Wise, "Scaling Limitations of Silicon Multichannel Recording Probes", *IEEE Trans. Biomed. Engr.*, 37, pp. 1-11, January 1990.

J. Ji, K. Najafi, and K. D. Wise, "A Scaled Electronically-Configurable Multichannel Recording Array", *Sensors and Actuators*, A22, pp. 589-591, March 1990.

J. F. Hetke, K. Najafi, and K. D. Wise, "Flexible Miniature Ribbon Cables for Long-Term Connection to Implantable Sensors", *Sensors and Actuators*, A23, pp. 999-1002, April 1990.

K. Najafi and J. F. Hetke, "Strength Characterization of Silicon Microprobes in Neurophysiological Tissues", *IEEE Trans. Biomed. Engr.*, 37, pp. 474-481, May 1990.

J. J. Zappia, J. F. Hetke, R. A. Altschuler and J. K. Niparko, "Evaluation of a Silicon-substrate Modiolar Eighth Nerve Implant in a Guinea Pig", *Otolaryngol. Head Neck. Surg.*, vol. 103, pp. 575-582, October 1990.

J. Ji, K. Najafi, and K. D. Wise, "A Low-Noise Demultiplexing System for Active Multichannel Microelectrode Arrays", *IEEE Trans. Biomed. Engr.*, 38, pp. 75-81, January 1991.

---

* *Includes some papers co-authored with external investigators.*

J. F. Hetke, K. Najafi, and K. D. Wise, "Flexible Silicon Interconnects for Microelectro-mechanical Systems," *Digest IEEE Int. Conf. on Solid-State Sensors and Actuators*, San Francisco, pp. 764-767, June 1991.

A. C. Hoogerwerf and K. D. Wise, "A Three-Dimensional Neural Recording Array," *Digest IEEE Int. Conf. on Solid-State Sensors and Actuators*, San Francisco, pp. 120-123, June 1991.

S. J. Tanghe and K. D. Wise, "A 16-Channel CMOS Neural Stimulating Array," *Digest IEEE Int. Solid-State Circuits Conf.*, San Francisco, pp. 128-129, February 1992.

D. R. Kipke, B. M. Clopton and D. J. Anderson, "Shared-stimulus Driving and Connectivity in Groups of Neurons in the Dorsal Cochlear Nucleus", *Hear. Res.*, vol. 55, pp. 24-38, 1991.

J. Ji and K. D. Wise, "An Implantable CMOS Circuit Interface for Multiplexed Microelectrode Recording Arrays", *IEEE J. Solid-State Circuits*, vol. 26, pp. 433-443, March 1992.

G. Buzsaki, Z. Horvath, R. Urioste, J. Hetke, and K. Wise, "High-Frequency Network Oscillation in the Hippocampus," *Science, 256*, pp. 1025-1027, 15 May 1992.

S. J. Tanghe and K. D. Wise, "A 16-Channel CMOS Neural Stimulating Array," *IEEE J. Solid-State Circuits*, vol. 27, pp. 1819-1825, Dec. 1992.

C. Kim, S. J. Tanghe, and K. D. Wise, "Multichannel Neural Probes with On-Chip CMOS Circuitry and High-Current Stimulating Sites," *Digest IEEE Int. Conf. on Solid-State Sensors and Actuators (Transducers'93)*, Yokohama, pp. 454-457, June 1993.

J. F. Hetke, J. L. Lund, K. Najafi, K. D. Wise, and D. J. Anderson, "Silicon Ribbon Cables for Chronically Implantable Microelectrodes Arrays," *IEEE Trans. Biomed. Eng.*, vol. 41, pp. 314-321, April 1994.

J. L. Lund and K. D. Wise, "Chip-Level Encapsulation of Implantable CMOS Microelectrode Arrays," *Digest Solid-State Sensor and Actuator Workshop*, Hilton Head, S.C., pp. 29-32, June 1994.

J. K. Chen and K. D. Wise, "A Multichannel Neural Probe for Selective Chemical Delivery at the Cellular Level," *Digest Solid-State Sensor and Actuator Workshop*, Hilton Head, S.C., pp. 256-259, June 1994.

C. Kim and K. D. Wise, "A 64-Site Multiplexed Low-Profile Neural Probe with On-Chip CMOS Circuitry," *Digest 1994 IEEE Symposium on VLSI Circuits*, Honolulu, pp. June 1994.

A. C. Hoogerwerf and K. D. Wise, "A Three-Dimensional Microelectrode Array for Chronic Neural Recording," *IEEE Trans. Biomed. Engr.*, pp. 1136-1146, December 1994.

A. Bragin, G. Jando, Z. Nadasdy, J. Hetke, K. Wise, and G. Buzsaki, , "Gamma (40Hz - 100Hz) Oscillation in the Hippocampus of the Behaving Rat," *J. Neuroscience, 15*, pp. 47-60, January 1995.

C. Kim and K. D. Wise, "A 64-Site Multishank CMOS Low-Profile Neural Stimulating Probe," submitted to the *IEEE J. Solid-State Circuits*, September 1995.

M. N. Ghazzi, K. D. Wise, D. J. Anderson, and A. Rees Midgley, Jr., "Computer-Assisted Analysis of Single-Unit Neuronal Activity Obtained using Multichannel Microprobes," *Journal of Neuroscience Methods,* in review.

M. N. Ghazzi, K. D. Wise, D. J. Anderson, and A. R. Midgley, "Performance of Silicon-Based Multichannel Microprobes for Monitoring the Activity of Neurons in Deep Brain Structures: Characterizing the Activity of Neurons in the Anterior Hypothalamus," submitted to *IEEE Trans. Biomedical Engineering*, in review.

Conference Papers

K. D. Wise, "Microfabrication of Solid-State Sensors and Actuators for Cellular Studies", *Symposium on Cellular Bioengineering*, University of Michigan, May 1987.

S. L. BeMent, K. L. Drake, and K. D. Wise, "Spatial and Geometrical Factors in Multisite Neuronal Recording", *Digest 40th Annual Conf. on Engr. in Med. and Biol.*, Niagara Falls, N. Y., pg. 106, September 1987.

K. L. Drake, S. L. BeMent, K. D. Wise, and J. Farraye, "Silicon Multichannel Microprobes for Recording Intracortical Single-Unit Activity", *IEEE EMBS 9th Annual Conference Digest*, Boston, November 1987.

J. K. Niparko, J. J. Zappia, X. Xue, D. J. Anderson and R. A. Altschuler, "Surgical Implantation and Biocompatibility of CNS Auditory Prostheses", *Society for Neuroscience Abstracts*, vol. 13, p. 543, 1987.

D. J. Anderson, B. M. Clopton and D. R. Kipke, "Signal Processing of Thin-film Recording Array Data to Separate Channels of Point Process Information", in *9th IEEE Engineering in Medicine and Biology Conference Abstracts*, pp. 743-744, 1987.

J. F. Hetke, D. J. Anderson, D. A. Evans, J. A. Wiler, K. Najafi and R. A. Altschuler, "Tissue Volume Selectivity in the Cochlear Nucleus to Electrical Stimulation with Multichannel Silicon-substrate Arrays", in *Abstracts, Association for Research in Otolaryngology*, St. Petersburg, p. 146, February 1989.

S. J. Tanghe, K. Najafi, and K. D. Wise, "A Planar IrO Multichannel Stimulating Electrode for Use in Neural Prostheses", *Digest 5th Int. Conf. on Solid-State Sensors and Actuators (Transducers'89)*, Montreux, pp. 297-298, June 1989.

J. F. Hetke, K. Najafi, and K. D. Wise, "Flexible Miniature Ribbon Cables for Long-Term Connection to Implantable Sensors", *Digest 5th Int. Conf. on Solid-State Sensors and Actuators (Transducers'89)*, Montreux, pp. 277-278, June 1989.

J. Ji, K. Najafi, and K. D. Wise, "A Scaled Electronically-Configurable Multichannel Recording Array", *Digest 5th Int. Conf. on Solid-State Sensors and Actuators (Transducers'89)*, Montreux, pp. 195-196, June 1989.

K. D. Wise, "Fabrication and Characterization of Thin-Film Microelectrodes", *4th Biennial Conference on Implantable Auditory Prostheses*, Potosi, Mo., July 1989.

J. Ji and K. D. Wise, "An Implantable CMOS Analog Signal Processor for Multiplexed Microelectrode Recording Arrays", *Digest 1990 IEEE Solid-State Sensor and Actuator Workshop*, Hilton Head, S.C., pp. 107-110, June 1990.

K. D. Wise, "VLSI Circuit Challenges in Integrated Sensing Systems", (Invited), *IEEE VLSI Circuits Symposium*, Honolulu, pp. 19-22, June 1990.

K. D. Wise, K. Najafi, J. Ji, J. F. Hetke, S. Tanghe, A. Hoogerwerf, D. J. Anderson, S. L. BeMent, M. Ghazzi, W. Baer, T. Hull, and Y. Yang, "Micromachined Silicon Microprobes for CNS Recording and Stimulation", (Invited), *Digest IEEE EMBS Conference*, Philadelphia, November 1990.

J. F. Hetke, D. J. Anderson, J. A. Wiler, K. Najafi and K. D. Wise, "An Implantable, Multichannel Silicon-substrate Array for Chronic Stimulation of the Central Nervous System", in *Abstracts, Association for Research in Otolaryngology*, St. Petersburg, p. 20, February 1991.

D. R. Kipke, B. M. Clopton and D. J. Anderson, "Shared-stimulus Driving and Connectivity in Groups of Neurons in the Dorsal Cochlear Nucleus", in *Abstracts, Association for Research in Otolaryngology*, St. Petersburg, p. 141, February 1991.

X. Xue and D. J. Anderson, "Finite Element Analysis of Electrical Current Fields Induced by Stimulating Electrodes", in *Abstracts, Association for Research in Otolaryngology*, St. Petersburg, p. 134, February 1991.

J. F. Hetke, K. Najafi, and K. D. Wise, "Flexible Silicon Interconnects for Microelectro-mechanical Systems", *Digest IEEE Int. Conf. on Solid-State Sensors and Actuators*, San Francisco, pp. 764-767, June 1991.

A. C. Hoogerwerf and K. D. Wise, "A Three-Dimensional Neural Recording Array", *Digest IEEE Int. Conf. on Solid-State Sensors and Actuators*, San Francisco, pp. 120-123, June 1991.

M. N. Ghazzi, K. D. Wise, D. J. Anderson, S. W. Newman, and A. R. Midgley, "Use of Silicon-Based Multichannel Microelectrodes to Characterize Single-Unit Activity of Neurons in the Rat Suprachiasmatic Nucleus", *1991 Neuroscience Meeting*, New Orleans, November 1991.

Z. Horvath, R. Urioste, J. Hetke, K. D. Wise, and G. Buzsaki, "Fine Structure and Cellular Correlates of Hippocampal Sharp-Wave Bursts", *1991 Neuroscience Meeting*, New Orleans, November 1991.

J. F. Hetke, D. J. Anderson, J. A. Wiler and B. M. Clopton, "Chronic Multichannel Recording from Guinea Pig Inferior Colliculus", in *Abstracts, Association for Research in Otolaryngology*, St. Petersburg, p. 62, February 1992.

S. J. Tanghe and K. D. Wise, "A 16-Channel CMOS Neural Stimulating Array", *Digest IEEE Int. Solid-State Circuits Conf.*, San Francisco, February 1992.

D. J. Anderson, K. D. Wise and K. Najafi, "Micromachined Silicon Substrate Electrodes for Extracellular Recording," *Proceedings of the 14th Annual International Conference of the IEEE EMBS*, Paris, October 1992.

C. Kim, S. J. Tanghe and K. D. Wise, "Multichannel Neural Probes with On-Chip CMOS Circuitry and High-Current Stimulating Sites," *Int. Conf. on Solid-State Sensors and Actuators (Transducers '93),* Yokohama, pp. 454-457, June 1993.

K. D. Wise, "The Development and Application of Micromechanical Devices in Biosystems," (Invited), *Engineering Foundation Conf. on Nanofabrication and Biosystems: Frontiers and Challenges,* Kona, Hawaii, May 1994.

J. L. Lund and K. D. Wise, "Chip-Level Encapsulation of Implantable CMOS Microelectrode Arrays," *Digest Solid-State Sensor and Actuator Workshop*, Hilton Head, S.C., pp. 29-32, June 1994.

J. K. Chen and K. D. Wise, "A Multichannel Neural Probe for Selective Chemical Delivery at the Cellular Level," *Digest Solid-State Sensor and Actuator Workshop*, Hilton Head, S.C., pp. 256-259, June 1994.

C. Kim and K. D. Wise, "A 64-Site Multiplexed Low-Profile Neural Probe with On-Chip CMOS Circuitry," *Digest 1994 IEEE Symposium on VLSI Circuits*, Honolulu, pp. June 1994.

A. Bragin, J. Hetke, K. Wise, and G. Buzsaki, "Current-source Density Analysis of Hippocampal Discharges in the Intact Rat," *Abstracts of the 24th Meeting of the Society for Neuroscience, Miami Beach*, pg. 399, November 1994.

J. Chen and K. D. Wise, "A High-Resolution Silicon Monolithic Nozzle Array for Inkjet Printing," *Digest Int. Conf. on Solid-State Sensors and Actuators*, Stockholm, pp. 313-324, June 1995.

J. F. Hetke, K. D. Wise, and D. J. Anderson, "Silicon Substrate Microelectrode Arrays: Design Versatility and Fabrication Limits," *Digest 1995 Annual Fall Meeting of the Biomedical Engineering Society*, Boston, October 1995.

J. L. Lund and K. D. Wise, "Multichannel CMOS Intracortical Recording Electrode Arrays," *Digest 1995 Annual Fall Meeting of the Biomedical Engineering Society*, Boston, October 1995.

J. D. Weiland and D. J. Anderson, "Electrical and Histopathological Evaluation of CNS Stimulation using Micromachined, Thin-film Iridium Electrodes," *Digest 1995 Annual Fall Meeting of the Biomedical Engineering Society*, Boston, October 1995.

J. F. Hetke, S. C. Bledsoe, Jr., J. Chen, J. A. Wiler, K. D. Wise, and D. J. Anderson, "Pharmacological Studies of Amino Acid Neurotransmitters using Silicon Substrate Drug Delivery Probes," *1995 Neuroscience Meeting*, San Diego, November 1995.

Papers and Abstracts Submitted by External Probe Users

Z. Horvath, R. Urioste, J. Hetke, K. Wise and G. Buzsaki, "Fine Structure and Cellular Correlates of Hippocampal Sharp-wave Bursts," *1991 Neuroscience Meeting*, New Orleans, Nov. 1991.

R. R. Carter, J. B. Andersen, S. Hansen and J. C. Houk, "Discharge Dynamics of Red Nucleus Neurons in Response to Spinal Cord Stimulation in the *In Vitro* Turtle Brain," *1991 Neuroscience Meeting*, New Orleans, Nov. 1991.

G. Buzsaki, Z. Horvath, R. Urioste, J. Hetke and K. Wise, "High-frequency Network Oscillation in the Hippocampus," *Science*, vol. 256, pp. 1025-1027, May 1992.

J. J. Eggermont, "Neural Interaction in Cat Primary Auditory Cortex. Dependence on Recording Depth, Electrode Separation and Age," *J. Neurophysiology*, vol. 68, pp. 1216-1228, Oct. 1992.

R. R. Carter, Y. Kwon, S. B. Arnold, R. R. Matsumoto and J. C. Houk, "Bistable Discharge Properties of Purkinje Cells in the In Vitro Turtle Brain," *1992 Neuroscience Meeting*, Anaheim, Oct. 1992.

J. C. Prechtl and T. H. Bullock, "Plurality of Visual Mismatch Potentials in a Reptile," *J. Cognitive Neurosci.*, vol. 5, pp. 177-187, 1993.

R. R. Carter and J. C. Houk, "Multiple Single-unit Recordings from the CNS using Thin-film Electrode Arrays," *IEEE Trans. Rehab. Eng.*, vol. 1, pp. 175-184, Sept. 1993.

E. M. Schmidt, W. J. Heetderks and D. M. Camesi, "Chronic Recording from Cortical Areas with Multicontact Silicon Microprobes," *1993 Neuroscience Meeting*, Washington D.C., Nov. 1993.

G. Buzsaki, A. Bragin, J. J. Chrobak, Z. Nadasdy, A. Sik, M. Hsu and A. Ylinen, "Oscillatory and Intermittent Synchrony in the Hippocampus," In: Temporal Coding in the Brain, G. Buzsaki, R. Llinas, A. Berthoz and Y. Christen, eds., Springer, Heidelberg, pp. 146-172, 1994.

M. G. Lee, J. J. Chrobak, A. Sik, R. G. Wiley and G. Buzsaki, "Hippocampal Theta Following Selective Lesion of the Septal Cholinergic System," *Neuroscience*, vol. 62, pp. 1033-1047, Oct. 1994.

A. Bragin, J. Hetke, K. Wise, and G. Buzsaki, "Current-source Density Analysis of Hippocampal Discharges in the Intact Rat," *Abstracts of the 24th Meeting of the Society for Neuroscience, Miami Beach*, pg. 399, November 1994.

E. M. Schmidt, W. J. Heetderks, and D. M. Camesi-Cole, "Chronic Neural Recording with Multicontact Silicon Microprobes: Effects of Electrode Bias," *Abstracts of the 24th Meeting of the Society for Neuroscience*, Miami Beach, pg. 982, November 1994.

A. Ylinen, A. Bragin, Z. Nadasdy, G. Jando, I. Szabo, A. Sik and G. Buzsaki, "Sharp Wave Associated High Frequency Oscillation (200 Hz) in the Intact Hippocampus: Network and Intracellular Mechanisms," *J. Neuroscience*, vol. 15, pp. 30-46, January 1995.

A. Bragin, G. Jando, Z. Nadasdy, J. Hetke, K. Wise and G. Buzsaki, "Gamma (40-100 Hz) Oscillation in the Hippocampus of the Behaving Rat," *J. Neuroscience*, vol. 15, pp. 47-60, January 1995.

T. C. Chimento, J. F. Hetke, D. J. Anderson and M. D. Ross, "Unit Responses from Scarpa's Ganglion in the Rat Recorded with Thin-film Multichannel Passive Electrodes," *Abstr, Association for Research in Otolaryngology*, St. Petersburg, p. 13, February 1995.

A. Bragin, G. Jando, Z. Nadasdy, M. van Landeghem and G. Buzsaki, "Dentate EEG Spikes and Associated Population Bursts in the Hippocampal Hilar Region of the Rat," *J. Neurophysiology*, vol. 73, pp. 1691-1705, April 1995.

B. Brett and D. S. Barth, "Analysis of Laminar Evoked Potentials, Steady-state (40 Hz) Evoked Potentials, and High Frequency (Gamma Band) Oscillating Potentials in Rat Auditory Cortex," *1995 Neuroscience Meeting*, San Diego, November 1995.

Z. Nadasdy, A. Bragnin and G. Buzsaki, "Recognition of Spatially Separated Field Potentials and Unit Activity by "Spatial Clustering" Method" *1995 Neuroscience Meeting*, San Diego, November 1995.

B. Kocsis, A. Bragnin and G. Buzsaki, "Gamma Frequency (30-100 Hz) Patterns in the Hippocampus: Partial Coherence Analysis" *1995 Neuroscience Meeting*, San Diego, November 1995.

G. Buzsaki, A. Bragin, J. J. Chrobak, and Z. Nadasdy, "Memory Consolidation in the "Non-aroused" Brain: a Physiological Perspective," In: Maturational Windows and Cortical Plasticity: is there a Reason for an Optimistic View?, B. Julesz, G. Cowan and I. Kovacs, eds., SFI Studies in the Sciences and Complexity, Addison-Wesley, in press.